TWO-DIMENSIONAL JET-BOUNDARY INTERACTION FOR SUBMERGED THERMAL DISCHARGES

by

Joseph Hoch

A Dissertation Submitted to the Graduate Faculty in Mechanical Engineering in Partial Fulfillment of the Requirements for the Degree of Doctor of Philosophy, The City University of New York

1979

This Manuscript has been read and accepted by the Graduate Faculty in Mechanical Engineering in satisfaction of the dissertation requirements for the degree of Doctor of Philosophy

5/3/1979
date

Chairman of Examining Committee

5/3/79
date

Executive Officer

Dr. Thomas Hewett

Professor Robert Pfeffer

Professor Rishi Raj

Professor James Steven

Professor Sheldon Weinbaum
Supervisory Committee

The City University of New York

ABSTRACT

A comprehensive theoretical and experimental study which investigates the jet-boundary interaction of a heated two-dimensional jet discharging offset from and parallel to a solid wall is presented. The limiting case of a heated wall jet is also considered.

An integral formulation of the conservation equations coupled with appropriate entrainment closure assumptions provide for the solution of both the velocity and temperature fields, while accounting for the effects of ambient motion. The theoretical model is unique in that the base pressure and radius of curvature in the initial region of the jet are retained as variables. Two momentum relationships are introduced to provide closure of the governing equations.

Experimental velocity, pressure and temperature measurements were made to confirm basic assumptions regarding their profiles. Additional data in the pre-attachment region of the offset jet reveals a region of uniform temperature separating the jet and the boundary.

Various comparisons between predicted and measured values of velocity and temperature decay, maximum wall pressure, re-attachment length and recirculation region temperature were made. In general agreement is good.

ACKNOWLEDGMENTS

I wish to acknowledge the guidance and encouragement shown to me by my mentor, Professor Latif Jiji, during my years of study. Appreciation is also extended to Professor Sheldon Weinbaum, who made himself available for numerous helpful discussions and suggestions. I am also grateful to Dr. Ben Tankowski and the M. E. technicians for their help in modifying the wind tunnel, and to Professors Pfeffer and Stevens for making equipment available to me. I would also like to thank Diane Engelhardt and Bryan Palaszewski for their assistance in preparing the final draft of the dissertation.

Finally, I wish to acknowledge the faithful support my wife and family have given me throughout my years of study, especially my parents whose aim it has always been to provide me with the education circumstances denied them.

TABLE OF CONTENTS

LIST OF FIGURES

I. Introduction

A. Background

The free jet has long been of major interest in the study of turbulent shear flows. Besides having many engineering applications, the free turbulent jet provided early investigators with a simple geometry upon which to base various speculative models. Most important among these were the different forms of the mixing length theory developed by Prandtl and Taylor. These early studies provided the framework for much of the later work on more complex turbulent jet problems.

In recent years, considerable attention has been directed toward obtaining an improved theoretical model of turbulent submerged heated flows discharged into quiescent and moving ambients. These efforts have been motivated largely by needs arising from problems of pollution control, such as the dispersion of effluents from industrial chimneys and cooling towers, and the discharge of condenser water and sewage into rivers, lakes, and oceans. These problems introduce such complicating factors as ambient fluid motion, buoyancy, discharge geometry and jet-boundary interaction (see Figure 1).

Most of these studies implicitly account for the turbulent structure and ensuing entraining mechanism of the jet, of which little is known. They thereby avoid the difficulty

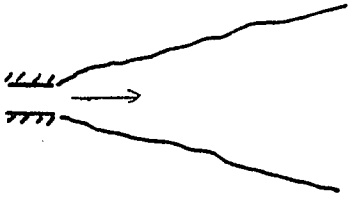

free jet

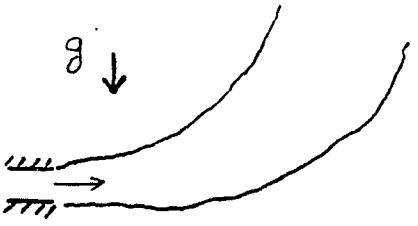

buoyancy effects

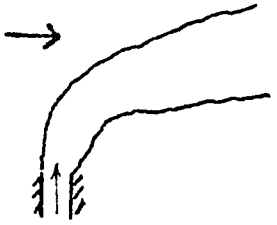

free stream effects

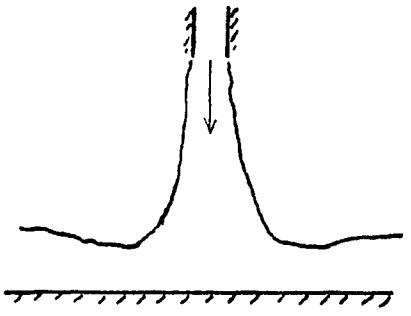

jet-boundary interaction

Figure 1. Illustrations of a Variety of Jet Problems

of directly describing the turbulent nature of the flow. This is achieved by relating the entrainment velocity to the mean characteristics of the jet. This relationship, or entrainment assumption, is usually expressed in terms of at least one empirical unknown which is determined by comparison with experimental data.

Although much attention has been focused on the development of theoretical models to predict the jet characteristics of unbounded flows, the effects of possible jet-boundary interaction have not been fully explored. Three types of jet-boundary interaction are commonly encountered in many engineering applications (see Figure 2): (1) the wall jet, where the fluid is discharged at the boundary, (2) impinging jets, where the discharge is aimed towards the boundary, and (3) the offset jet, where the fluid is discharged at some distance from the boundary and eventually attaches to it due to the bending of the jet by forces acting upon it. The wall jet may be considered a limiting case of the offset jet.

The case of a heated submerged jet in the vicinity of a solid boundary is of special interest because of its application to thermal discharges from power plants which emerge near the bottom of rivers and lakes. The subsequent interaction with the solid surface may significantly alter plume behavior. Furthermore, pressure and shearing forces by the floor-bound jet give rise to scouring and bed erosion resulting in discharge structural problems [1, 2].

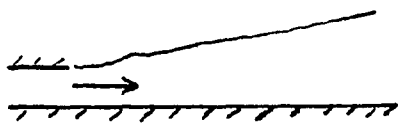

wall jet

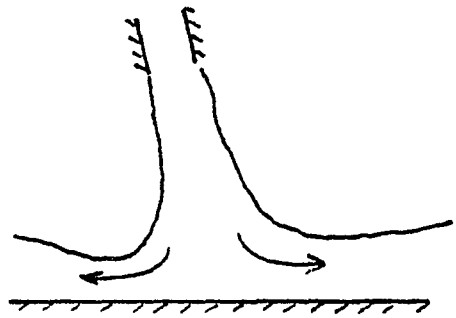

impinging jet

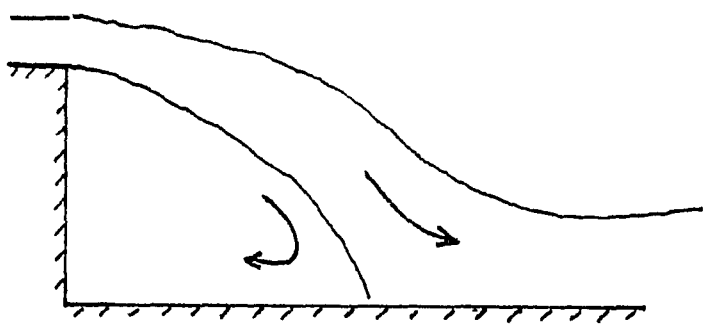

offset jet

Figure 2. Examples of Jet-Boundary Interaction

B. Basic Features of Two-Dimensional Jet-Boundary Interaction

Jet-boundary interaction occurs when a discharge is located in the vicinity of a solid boundary. The presence of this boundary may have a significant effect on the jet characteristics by limiting entrainment between the jet and the boundary. This, in turn, sets up a low-pressure region between the jet and the boundary. Consequently, the jet bends towards the boundary or wall, eventually attaching to it.

In the flow regime prior to jet attachment, known as the pre-attachment region (see Figure 3), pressures are generally lower than hydrostatic levels. As the jet approaches the boundary, pressure levels inside the jet increase, reaching a maximum as the jet attaches.

By attaching to the boundary, the jet encloses a region of eddying motion known as the recirculation region. Fluid entrained from this region by the jet is eventually returned as the jet attaches to the boundary. The recirculation region is bounded by the dividing or re-attaching streamline, across which there is no mass flow. For a heated jet the temperature inside the recirculation region is above ambient levels and therefore may affect the overall jet temperature distribution.

The portion above the dividing streamline is accelerated along the boundary due to the jet's positive pressure.

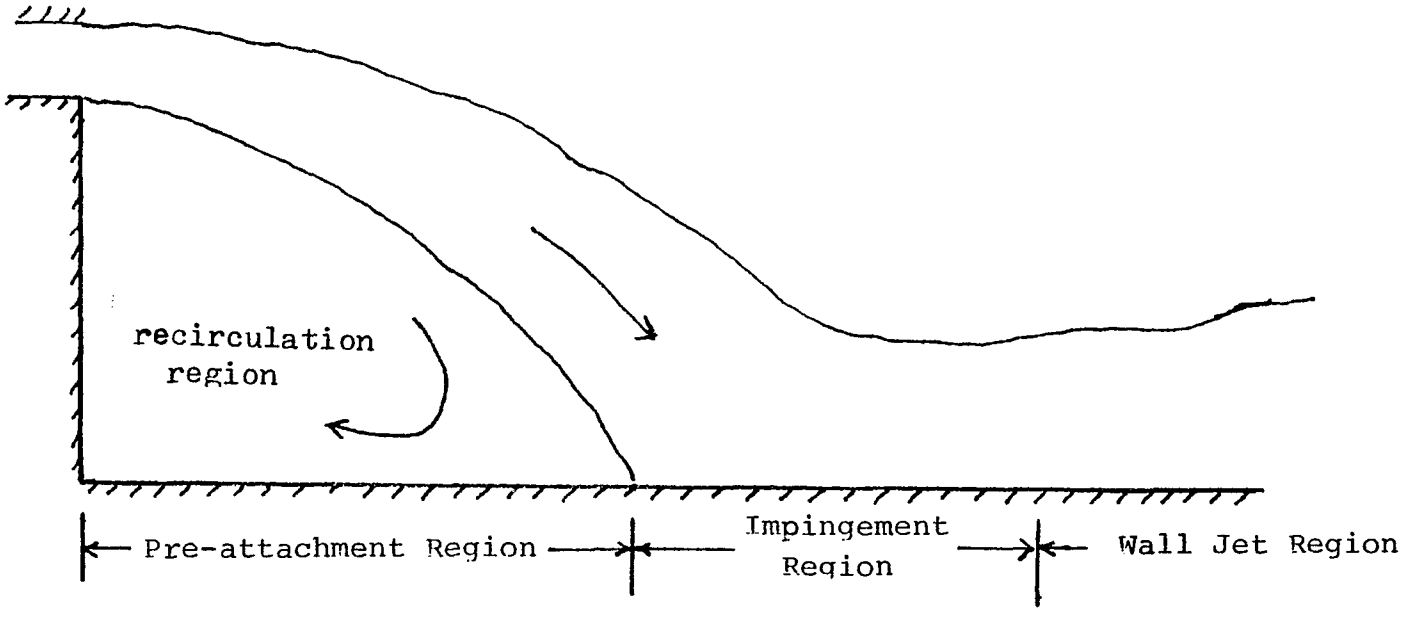

Figure 3. Schematic of a Plane Offset Jet Discharging Parallel to a Solid Boundary

In the second, or impingement region the pressure decreases, eventually reaching hydrostatic levels, and the acceleration ceases. The jet then undergoes turbulent diffusion analagous to that of a plane turbulent wall jet in what is known as the wall jet region.

Prior investigations of two-dimensional jet-boundary interaction were primarily concerned with the pre-attachment region, focusing on the determination of the point of re-attachment. To achieve this, simplifications such as the assumptions of constant negative base pressure in the recirculation region and constant jet-axis radius of curvature were introduced. These assumptions facilitated the use of the free jet velocity distribution, thus bypassing the need to solve for the velocity.

Although these models give reasonable results for the position of the point of jet re-attachment as a function of offset height, the assumptions regarding velocity, pressure and radius of curvature are unrealistic. It is apparent that there is a need for a more substantive model, based on sounder physical reasoning, which could be extended to give the velocity, temperature and pressure distributions in all regions of the jet.

C. Objectives of This Study

It is the aim of this research to investigate both theoretically and experimentally the problem of two-dimen-

sional jet-boundary interaction of a submerged turbulent thermal discharge. In particular, this study focuses on the problem of a two-dimensional jet discharging offset from a solid boundary, and its subsequent dissipation. It is hoped that this study will help provide an understanding of the nature of jet-boundary interaction, and will serve as a useful limiting case of the more prevalent and complex problem of three-dimensional jet-boundary interaction.

Unlike previous models, the theoretical study gives full consideration to the variation of pressure forces in the pre-attachment and impingement regions of the jet. This leads to a more realistic and unique velocity solution. Solutions for velocity, temperature, jet spread and base pressure are obtained for the pre-attachment region and serve as an input into the solution of the impingement and wall jet regions. Effects of free stream on jet characteristics are also considered.

Experiments were performed to provide the necessary data for a better understanding of flow patterns in jet-boundary interaction and for verification of the predictive model.

In addition, because of its importance as a limiting case and the lack of adequate temperature data, the two-dimensional heated wall jet is also examined.

II. LITERATURE SURVEY

Because of the extensive use of jets in engineering applications, their study has long been of interest. Jets have application in film cooling, combustion, sewage disposal, fluidics and heat dissipation from power generation. Recent concern with thermal pollution from power plants has motivated new studies on heated turbulent jets. Theoretical analysis of such jets may be complicated by such factors as the turbulent nature of the flow, ambient fluid motion, buoyancy, discharge geometry and jet-boundary interaction.

Theoretical investigations have been mostly concerned with free jets discharged from round outlets or infinite slots. In a free jet the ambient fluid is assumed infinite in extent and consequently the problem of jet-boundary interaction is bypassed. Round outlets lend themselves to axisymmetrical treatment while infinite slots limit the analysis to two-dimensional jets. Both geometries avoid the complexity of the three-dimensional nature of rectangular outlets.

A. Free Jets: Axisymmetric and Two-Dimensional

Analytic models for complex jet problems rely heavily on methods formulated from the solution of the more simple

momentum turbulent jet. The structure of this jet is broken down into two regions (see Figure 4). The first is the zone of flow establishment, ZFE, in which the mean flow profiles undergo a transition from their internal flow shapes to a free turbulent flow condition, with the centerline velocity remaining constant. The second is the zone of established flow, ZEF, where the turbulent mixing has reached the jet centerline and the core velocity begins to decay. It is in this region where velocity and temperature distributions assume a Gaussian shape.

Two different analytic approaches have been applied to the free momentum jet. The first, is a solution of the governing differential equations making use of experimental evidence regarding the similarity of mean-velocity profiles in successive downstream sections of the jet. Together with this similarity assumption, an adequate hypothesis is introduced relating the eddy viscosity to the mean flow. Tollmien [3] used this approach to solve for the shape of the similarity function, and thus the velocity distribution.

The second approach is to solve the integral form of the conservation equations. This integral approach requires prior specification of the velocity profile. The most frequently used profile is the Gaussian distribution. The integral analysis is then used to solve for the jet

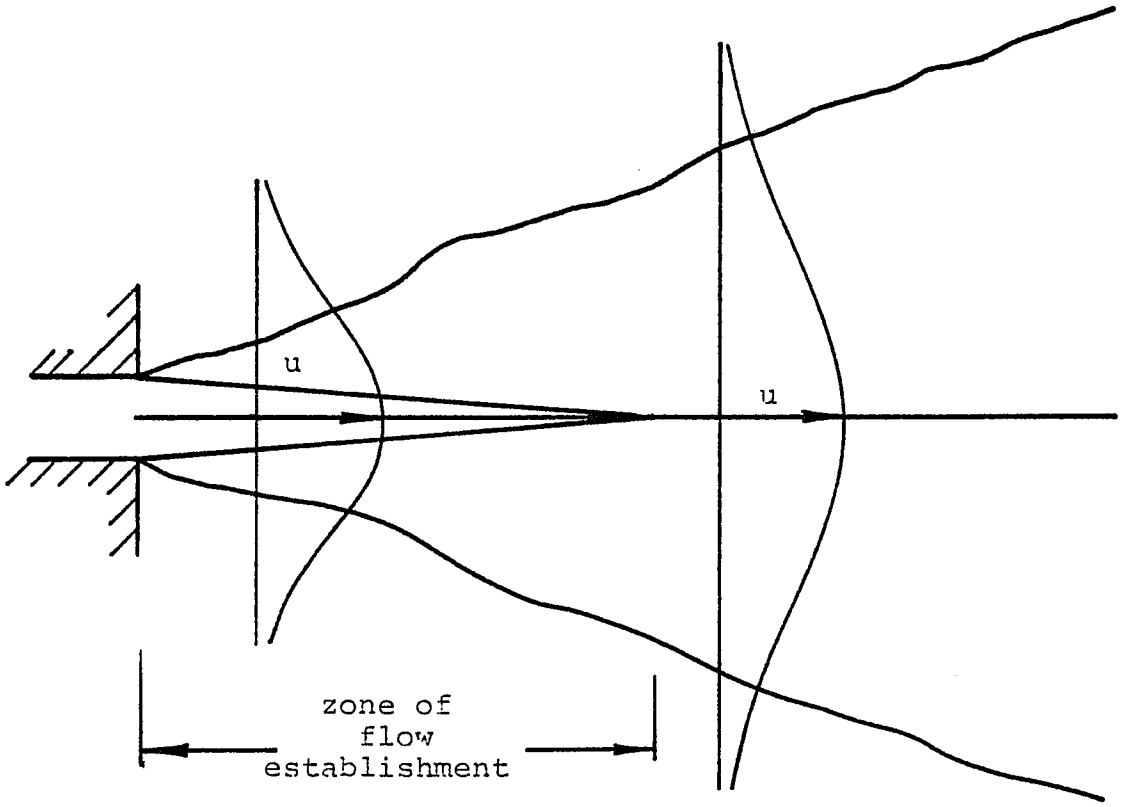

Figure 4. The Zone of Flow Establishment for a Simple Momentum Jet

centerline velocity and jet width.

As with the similarity solution, the integral solution requires an appropriate closure assumption that describes the turbulent nature of the flow. Two possibilities exist: either postulating some geometric relationship (generally linear) for the jet spread, or using the continuity equation with an appropriate entrainment assumption.

Albertson [4] was one of the first to use the integral method to solve for the centerline velocity distribution of both axisymmetric and two-dimensional free momentum jets. Employing a Gaussian-shaped velocity profile, Albertson proposed a linear rate of jet spread as his closure assumption. Theoretical results compared very well with experimental data.

The entrainment concept, first introduced by Morton, Taylor and Turner [5] has dominated most theoretical studies on thermal discharges. Integral equations for the conservation of mass, momentum and density deficit are formulated for instantaneously released or maintained plumes in a uniform or stablely stratified ambient. The entrainment assumption that the lateral velocity of the entrained mass is proportional to the jet centerline velocity is used to provide closure of the governing equations. The constant of proportionality, or the entrainment coefficient, is determined experimentally. For a pure momentum jet or buoyant plume the value of the entrainment coefficient can

be related to the rate of jet spread [6]. This provides a convenient technique for measuring the entrainment coefficient.

The entrainment method was applied by Fan and Brooks [7] and Anwar [8] to buoyant discharges in a stagnant infinite ambient fluid. Fan and Brooks present working charts for both round and two-dimensional outlets. The entrainment coefficient was determined from the experimental data of Rouse, et al. [9].

One of the most common arguments against the use of the entrainment methods in the analysis of buoyant jets is that the entrainment coefficient should be a function of local buoyancy as well as centerline velocity. To account for the effect of buoyancy on the entrainment coefficient, the integrated jet kinetic energy equation, or the first moment of axial momentum, is used. This equation is constructed by multiplying the axial momentum equation by the local axial velocity and then integrating across the jet width. This approach was first used by Priestly and Ball [10] in the analysis of vertically rising plumes. By assuming linear jet spread and similarity of the turbulent shear distribution, the first moment of axial momentum was formulated to obtain closure of the governing equations. With the additional assumption of equality of temperature and velocity profiles, they show that the entrainment coefficient for a buoyant jet can be expressed in terms of the local

Froude number. Fox [11] extended the work of Priestly and Ball and treated the problem of a buoyant plume in a stratified fluid. Here, the entrainment coefficient is presented in terms of the local Froude number and the turbulent Schmidt number. This removes the restriction on the equality of the temperature and velocity profiles imposed by Priestly and Ball. Hirst [12], using the same method, solved the non-vertical round jet problem. However, Hirst did not use the first moment method in the zone of flow establishment. He assumed a form for the entrainment function which is similar to that derived for the zone of established flow using the integrated kinetic energy equation. The corresponding problem of a discharge from a two-dimensional slot was solved by Jirka and Harleman [13].

Jiji and Hoch [14, 15] applied the first moment method in a slightly different manner to solve a variety of free jet problems for both the zone of flow establishment and the zone of established flow.

B. Two-Dimensional Jet-Boundary Interaction (Offset Jets)

Jet-boundary interaction occurs when a discharge is located near a solid boundary. Most previous models on the offset jet are limited to the pre-attachment region. In general, these models are only able to solve for the point of jet re-attachment, and cannot be extended to yield results in the subsequent flow regions. However, they do provide

evidence that the entrainment mechanism of a jet is not altered significantly as it interacts with a boundary.

Bourque and Newman [16] were among the first to investigate the velocity and pressure behavior of a two-dimensional jet in the vicinity of a solid boundary. The problem was greatly simplified by assuming that the presence of the boundary has little effect on the velocity distribution of the jet. Thus, the velocity field is taken from the solution of the two-dimensional free turbulent jet. This assumption implies a zero pressure gradient along the jet trajectory. This is accomplished by assuming that the radius of curvature of the jet centerline and the pressure inside the recirculation region are constant.

With the velocity known, the introduction of an additional equation, or closure assumption, is necessary to determine the only remaining unknown: the radius of curvature. This is achieved by applying the horizontal component of momentum locally at the point of re-attachment while neglecting local pressure variation.

Bourque and Newman applied this solution using the Görtler velocity distribution [17] for a two-dimensional free turbulent jet. This velocity distribution is in terms of a constant jet spread parameter. Some adjustment of this parameter was necessary to obtain satisfactory comparison with experimental data. The value of the jet spread parameter differs from its free jet value owing to the reduced

entrainment on the lower side of the jet.

Though resonable results for the value of the re-attachment point are obtained, the assumption of constant radius of curvature and base pressure is not borne out by experimental data (see Figure 5). This model also fails to account for the rise in pressure and deceleration of the jet as it approaches the point of re-attachment.

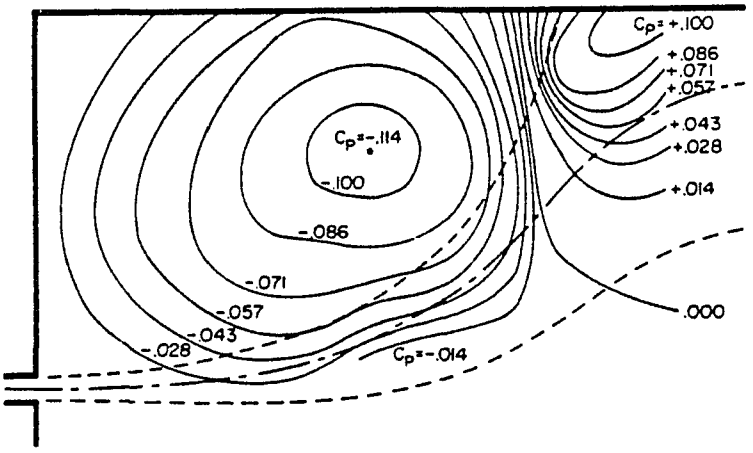

Figure 5. Approximate Pressure Contours Inside the Pre-attachment Region [16]

In a later model, Bourque [18] relaxed the constant radius of curvature restriction by assuming a sinusoidal shape for the re-attachment streamline, and jet centerline. He obtained reasonable agreement with experimental data using a single fixed value for the spread parameter. Bourque points out that this assumption offsets the unrealistic model of constant recirculation region pressure. He still, however, failed to detail the pressure distribution and relate it to the velocity field.

The constant radius of curvature assumption has dominated subsequent jet-boundary interaction models. Sawyer [19], using a control volume approach together with the constant radius of curvature assumption, obtained a solution for the re-attachment point as a function of discharge offset distance using a single value for the spread parameter. In addition, he found that the velocity profiles of the jet as it curved towards the boundary exhibited no obvious asymmetry. This observation was in apparent disagreement with the arguments put forward by Prandtl [20], which indicated that there should be enhanced entrainment in the outer portion of a curved jet, and reduced mixing in the inner portion, due to the influence of centrifugal forces on parcels of fluid which transfer momentum from layer to layer. Experiments on the effects of curvature upon wall jets blowing around circular cylinders [21] were in agreement with Prandtl's momentum-transfer arguments.

In a later paper, Sawyer [22] resolved this discrepancy by postulating that there must be a flow of fluid across the jet centerline for the observed symmetry of the velocity profiles to be compatible with different entrainment rates on the two sides of the jet. A first-order mixing length theory was used to show that the effects of different entrainment rates on the two sides of the jet does not substantially alter the velocity profiles from their free jet shapes. Therefore, the total entrainment to the jet will remain unchanged. This finding has substantial importance for any integral solution of the jet-boundary interaction problem, in that it enables the use of free jet entrainment theory in the solution of the jet-boundary interaction problem.

In a study related to jet-boundary interaction, Marsters [23] investigated the interaction of two parallel two-dimensional jets issuing into a stagnant surrounding. Because of reduced entrainment between the jets, they will bend towards each other and eventually merge. The problem is unique in that the area between the jets is open, enabling entrainment of ambient fluid into the low pressure region. If the jets are far enough apart, the entrainment may prevent the jets from merging. Marsters' analysis is based on the constant radius of curvature assumption used by Bourque and Newman. Although the theory predicts the merging of the jets reasonably well, it does not predict

accurately the secondary flow entrained into the unobstructed space between the nozzles.

Bourque and Rougier [24] examined the problem of jet-reattachment for a round discharge. They based the solution to this problem on the corresponding solution of the two-dimensional jet [16]. Comparison between theoretical results and experimental data was found to be good over a wide range of geometries.

Rajaratman and Subramanya[25] experimentally investigated the velocity and pressure fields of a two-dimensional jet initially offset from a parallel bottom surface. In particular, attention was focused on the transition of the jet from the pre-attachment region to the re-attached wall jet region (see Figure 3). Detailed measurements of the velocity field, wall pressure and shear stress are presented for small values of the offset parameter.

C. Two-Dimensional Wall Jets (Zero Offset)

A special case of the offset jet is the wall jet where the discharge is issued along the surface (see Figure 6). Although considerable research has been done on this problem, little attention has been given to the temperature field.

An experimental study of a two-dimensional wall jet was undertaken by Forthmann[26]. Using a very wide nozzle, he observed that the velocity distribution for a wall jet

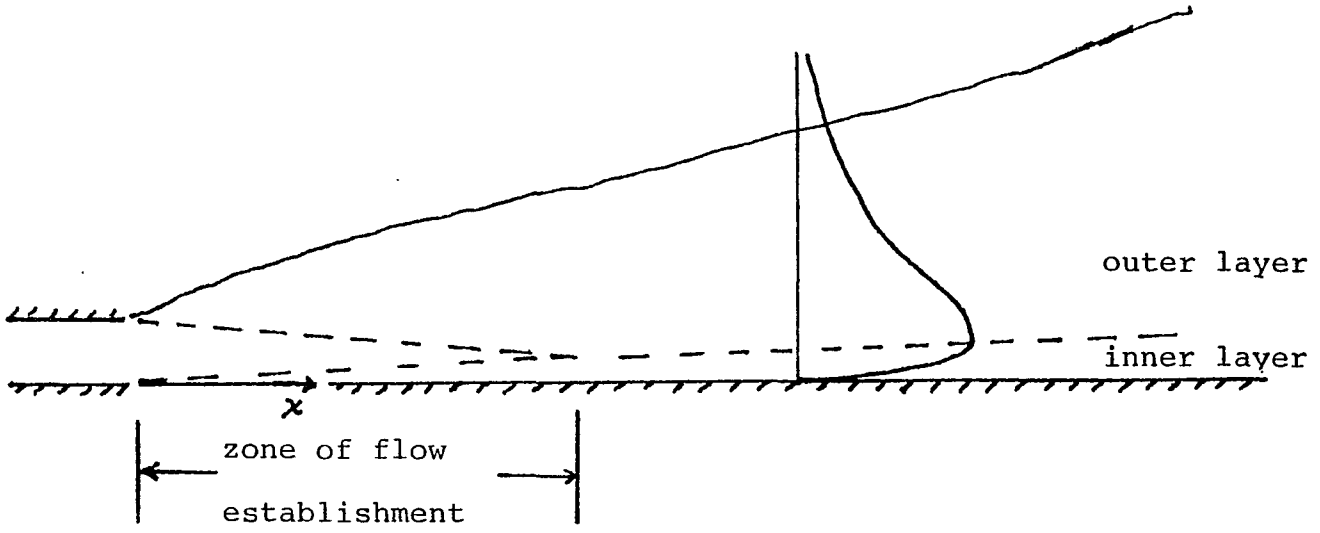

Figure 6. The Two-Dimensional Wall Jet

becomes nearly self similar after approximately 25 diameters downstream.

Glauert [27] studied both radial and two-dimensional wall jets for laminar and turbulent flows. He pointed out that the turbulent wall jet has features in common with both the free jet and the boundary layer. The spreading fluid is retarded by the frictional resistance of the wall and the inner part of the flow is expected to show a structural similarity to a boundary layer, whereas entrainment of ambient fluid occurs near the outer edge of the flow. Based on this assumption, Glauert divided the flow into two regions by introducing an eddy viscosity near the wall consistent with the Blasius 1/7th power-law profile, and a constant eddy viscosity in the outer portion of the flow. The division of these two flow layers was assumed to occur at the point of maximum velocity. Although complete similarity is not possible, Glauert assumed that variations in the Reynolds number within the inner layer are small. These two layers were then treated separately and matched at the point of maximum velocity. The similarity exponents were then determined by comparison with experimental data.

Sigalla [28] measured the skin friction and velocity distribution in a plane turbulent wall jet. He demonstrated that it is possible to describe the variation of the skin friction coefficient using a formula with the same Reynolds number dependency as the Blasius empirical formula for pipe

flow. This formula is also used to calculate the skin friction for turbulent flow over a flat plate for a wide range of Reynolds numbers. Sigalla also measured maximum velocities and jet spread for the wall jet. Although the jet spread rate is constant downstream of the outlet, the value of that constant was found to be lower than that for free jets.

Myers, Schauer and Eustis [29] studied the two-dimensional turbulent wall jet in a stationary ambient. An integral method was used to solve for the maximum velocity and jet width. Closure was provided by making use of the first moment of momentum equation in the outer layer of the wall jet. The shear stress in the outer layer was obtained using Prandtl's hypothesis. The free jet value of the empirical constant in Prandtl's hypothesis, k, was used for the outer layer. Experiments were run for values of the Reynolds number ranging between 7,000 and 25,000. Theoretical results for maximum velocity and jet width compared well with experiment and did not show significant Reynolds number dependency. Myers et al. claim that the solution for maximum velocity and jet width is also not sensitive to the value of k. This is not the case for free jets. It is also surprising that the free jet value of k gave good results for the jet width of a wall jet. The lower value of the jet spread rate of a wall jet would imply a lower value of k.

By assuming that the wall jet is a self-preserving flow, Schwarz and Cosart [30] were able to show that the jet width of the two-dimensional wall jet is a linear function of the axial distance from the jet outlet. Furthermore, the maximum axial velocity decays exponentially over a wide range of Reynolds numbers. Experimental measurements of jet spread and velocity agree closely with Sigalla's data. Their measured value of the skin friction showed very little dependence on the Reynolds number, but was approximately twice the average values measured by Sigalla.

A two-dimensional turbulent wall jet discharging parallel to a free stream was investigated by Kruka and Eskinazi [31]. A similarity transformation was introduced for both the inner and outer layers of the jet. The width of the inner layer was shown to be a linear function of the axial distance, and is independent of the free stream to jet velocity ratio. They demonstrated that the maximum axial velocity decays exponentially, however the value of the exponent varies with the velocity ratio. The variation of the exponent as well as a scaling constant were taken from experimental data. Measurements of maximum axial velocity and jet spread for low velocity ratios approach the results of previous investigators for zero free stream. Kruka and Eskinazi also measured the skin friction for different velocity ratios. Results for low velocity ratio seem to confirm Sigalla's findings for zero free stream.

Using a velocity distribution that is consistent with existing universal turbulent boundary layer and free jet profiles, Spalding [32] obtained an expression for the entrained mass in a wall jet discharging into a co-axial free stream. His results showed the entrained mass for a wall jet to be lower that the free jet value. This resulted in a lower entrainment coefficient for wall jets. Measurements by Escudier and Nicol [33] confirm his postulation.

Using the results of previous investigators for axial velocity decay and jet spread, Rajaratnam [34] obtained a value for the entrainment coefficient for wall jets which is approximately half the free jet value. This is in agreement with Spalding's findings. Townsend [35] postulated that the reduction in entrainment is due to two factors. First, the presence of a solid boundary, in contrast to a plane of symmetry, would restrict eddies of the outer layer to sizes somewhat smaller than those found in a free jet of the same width causing a reduction in the dissipation length scale. In addition, a smaller entrainment constant would imply a larger effective stain of the turbulence and a somewhat smaller ratio of Reynolds stress to the turbulent intensity.

In the only study on heated two-dimensional adiabatic wall jets Seban and Back [36] carried out experiments on a wall jet discharged below a surface at low values of free stream to jet velocity ratio. It should be noted that the

configuration used in this study differs from a wall jet discharged over a surface. Buoyancy action in these two arrangements of heated wall jets may differ substantially. Seban and Back made velocity measurements and observed a correspondence to turbulent wall jets in stationary ambients. They point out that Glauert's similarity assumptions are still valid in the presence of a small free stream. Based on this assumption, a semi-empirical formula is presented for maximum axial velocity which is independent of the velocity ratio. By adjusting the eddy diffusivity Seban and Back were able to predict temperature profiles for an adiabatic wall jet. Their experiments showed that temperature profiles are nearly linear throughout the jet even in the small region near the wall where the temperature is constant. They were unable, however, to find this region of constant temperature experimentally. Seban and Back did not take into account variations in velocity and temperature as a function of the free stream velocity ratio. Their predictions for velocity and adiabatic wall temperature do not agree well with experimental data. Apparently the velocity ratio does affect the temperature distribution in a wall jet even for small value of the velocity ratio.

D. Related Studies - Three-Dimensional Jets

Although considerable work has been done on free two-dimensional and axisymmetric jets, little attention has been

given to discharges from rectangular outlets. This is due to the geometrical complexity and possible asymmetry introduced. Furthermore, studies on the problem of three-dimensional jet-boundary interaction are extremely limited.

An experimental and theoretical study of the three-dimensional flow characteristics of a long slender discharge in the vicinity of a solid boundary was presented by Sacks, et al. [37]. Although experiments showed that for such discharge configurations, the velocity distribution in the near field could be approximated by the velocity distribution of a two-dimensional free jet, the pre-attachment interaction regions between the jet and the boundary exhibit totally different characteristics. For a three-dimensional jet, this region was dominated by significant crossflow from the sides, in contrast to a two-dimensional jet where a reverse flow vortex is formed. This entrainment from the sides of the jet inhibits the jet from bending towards the boundary.

Assuming that the crossflow in the sides of the jet due to entrainment is perpendicular to the direction of the jet flow, Sacks et al. were able to model the influence of the nearby boundary on the jet. A dynamic equation in terms of the pressure difference across the jet is used to obtain the jet displacement.

The limiting case of a three-dimensional rectangular turbulent wall jet (zero offset) was investigated by

Sforza and Herbst [38]. They experimentally examined the velocity field and found it to be characterized by three distinct regions of axial velocity decay. The decay rate in the near field was found to depend on the aspect ratio, whereas far downstream, the velocity decays at the same rate as a radial wall jet. For low aspect ratios, decay rates seem to be near those of two-dimensional wall jet, although some spanwise irregularities were evident in the measured velocity profiles.

Another limiting case which is of interest is the free rectangular jet (infinite offset). Trentacoste and Sforza [39]. carried out an experimental investigation on a rectangular three-dimensional free jet. They observed that, unlike the axisymmetric jet, the rectangular discharge is characterized by three distinct flow field regions: (i) The potential core zone in which the centerline axial velocity corresponds to the jet discharge velocity. (ii) The characteristic decay zone where the velocity profiles in the plane of the minor axis are found to be "similar," whereas those in the plane of the major axis are "nonsimilar." (iii) The axisymmetric decay region, where the velocity profile is developed along both axes. The length of both the potential core and the distance where the axisymmetric decay begins is shown to be dependent on the aspect ratio. The entrainment rate is shown to vary linearly with axial distance. Corresponding data on the temperature field was

recently obtained by Sforza and Stasi [40].

An experimental investigation of rectangular jets was also carried out by Yevdjevich [41], who found that in the characteristic decay region, the centerline velocity decays at the same rate as a two-dimensional jet, regardless of aspect ratio. Therefore, the centerline velocity decay of rectangular jets of different aspect ratios was represented by a single curve throughout the characteristic decay region. According to Yevdjevich, only the length of the characteristic decay region, after which axisymmetric decay begins, varied with aspect ratio. His recorded values of this length were also in disagreement with Trentacoste and Sforza.

Sfier [42] measured the mean velocity and temperature profiles of non-buoyant rectangular jets having different aspect ratios. He observed that the temperature fields for rectangular discharges can be divided into three regions of temperature decay. This is analogous to what Trentacoste and Sforza found for the velocity field. He also found that the temperature spread along the major axis was approximately equal to the velocity spread, up to the point where axisymmetric decay begins.

Narian [43] presented a solution for the velocity distribution of a three-dimensional rectangular jet. He considers the discharge as being made up a distribution of elemental sources of equal strength. The summation of the sources gives the three-dimensional velocity distribution. The final

velocity solution is given in terms of a number of empirical constants that vary with aspect ratio.

A comprehensive review of both wall jets and three-dimensional jets is contained in a recent text by Rajaratman [34].

III. Scope of Work

The survey of previous literature reveals that there are several important jet-boundary interaction problems that have yet to be studied experimentally or theoretically. Most studies on wall jets have been limited to the velocity field. Some experimental data is available on the temperature field of a wall jet in a moving ambient (film cooling) with an adiabatic wall boundary condition. However, there has yet to be a comprehensive study detailing the effects of free stream on the temperature distribution of a wall jet.

The majority of previous experimental and theoretical studies of the two-dimensional offset jet were limited to the pre-attachment region and the determination of the point of re-attachment. Variation of the pressure inside the recirculation region was not taken into account in the theoretical models. Instead, the radius of curvature of the jet trjectory was assumed constant, thereby yielding a uniform base pressure [16, 19, 23]. This was coupled with the assumption that the jet velocity distribution was similar to that of a free jet. These assumptions are not borne out by experimental data. To date, no theoretical model has predicted the velocity or pressure variation of a two-dimensional offset jet.

Only one experimental study [25] considered the velocity distribution of an offset jet (for small offset heights).

This study was also the only one to investigate the transition from a detached to a re-attached jet. However, there is still a need for more experimental data on jet trajectory and velocity decay over a wide range of offset heights. Furthermore, the effects of free stream on jet characteristics has yet to be studied either experimentally or theoretically.

Finally, there has been no work on the temperature distribution of a heated two-dimensional offset jet. There is a need for both analytical and experimental studies of the temperature distribution.

A. Statement of Problem

This study was undertaken as part of a wider research project examining the multi-dimensional effects of jet-boundary interaction. This investigation will be limited to the problem of two-dimensional jet-boundary interaction. The research is both experimental and theoretical. Both the velocity and temperature field will be considered. The purpose of this study is to help fill the gap in present knowledge on two-dimensional jet-boundary interaction.

The discharge geometry considered is that of a heated two-dimensional (slot) jet whose orientation is horizontal, and which is discharging offset from, and parallel to an adiabatic boundary. The jet is assumed to be fully turbulent. Free stream effects will also be considered. The free stream

is parallel to the discharge direction. Ambient turbulence effects are not considered. The trajectory, dilution and spread will be examined for all the flow regions of the heated jet.

1. Theoretical Study

The theoretical analysis considers the effect of the offset parameter and free stream motion on the velocity and temperature distribution of a two-dimensional discharge parallel to a solid boundary. The limiting case of the wall jet (zero offset) is also considered.

The analysis is based on the integral formulation of the basic conservation laws. This approach yields a set of governing ordinary differential equations instead of the more complicated partial differential equations.

The flow field is divided into three main flow regimes: (i) the pre-attachment region, where the jet bends towards the boundary due to the reduced pressure below, (ii) the impingement region which immediately follows jet attachment and where pressures are higher than hydrostatic levels, and (iii) the wall jet region where the jet behaves like an ordinary wall jet. The integral equations are derived for each region. Appropriate velocity and temperature profiles are introduced for each flow region.

Due to the turbulent nature of the flow, a closure scheme

for the governing equations is necessary. Previous studies of two-dimensional offset jets [19,22] have shown that the entrainment closure model for free jets can be used for the first region of the offset jet. Therefore, in all cases, closure will be provided through use of an appropriate entrainment assumption.

Unlike previous studies, the present model will not assume that the base pressure or jet axis radius of curvature are constant in the pre-attachment region. These will be left as dependent variables to be determined by the solution. Because these variables are left as unknowns, two additional conditions are necessary to complete the solution. These equations are obtained through an iterative procedure by uniquely applying conservation of momentum at the point of re-attachment. Wall jet theory is used to determine the velocity distribution in the re-attached jet.

Once the velocity field is established, the temperature distribution in each region is obtained using the appropriate integral energy equation. Both the energy equation and temperature profile in the pre-attachment region are derived so as to reflect the higher than ambient temperature inside the recirculation region.

Details of the theoretical model are provided in chapters IV and V.

2. Experimental Study

To aid in the modeling of the various flow regions and to provide verification for theoretical solutions, an experimental study of two-dimensional jet-boundary interaction was undertaken. Experiments were conducted in a low-speed wind tunnel primarily designed for environmental studies. Velocity and temperature distributions as well as surface pressure measurements were obtained throughout the flow field, at various offset heights. Particular emphasis was placed upon the temperature field inside the recirculation region. Flow visualization using smoke tracers were also studied. Details of the experimental setup are provided in chapter VI.

IV. MATHEMATICAL FORMULATION

In this section we present the integral form of the conservation equations for the interaction of a heated jet discharging parallel to and offset from a solid boundary. The limiting case of zero offset, or a wall jet, is considered first.

A. Two-Dimensional Wall Jet

In a two-dimensional discharge from a slot situated along a wall two flow regions exist. The first zone, which immediately follows the outlet , is characterized by a core region of uniform velocity. In this zone the outer layer of the jet mixes with the ambient fluid setting up a free jet boundary while a boundary layer is formed in the region between the core and the wall (see Figure 7). The second zone begins at the point where these two mixing regions meet. In this zone, which is analogous to the zone of established flow for a free jet, the outer region has a structural similarity to a two-dimensional free jet, whereas the inner region behaves somewhat like a boundary layer flow over a flat plate. The velocity and temperature profiles differ from one region to another, however the basic governing integral equations are the same.

For constant fluid properties, hydrostatic pressure distribution and negligible buoyancy effects (see page 154), the two-dimensional integral equations are:

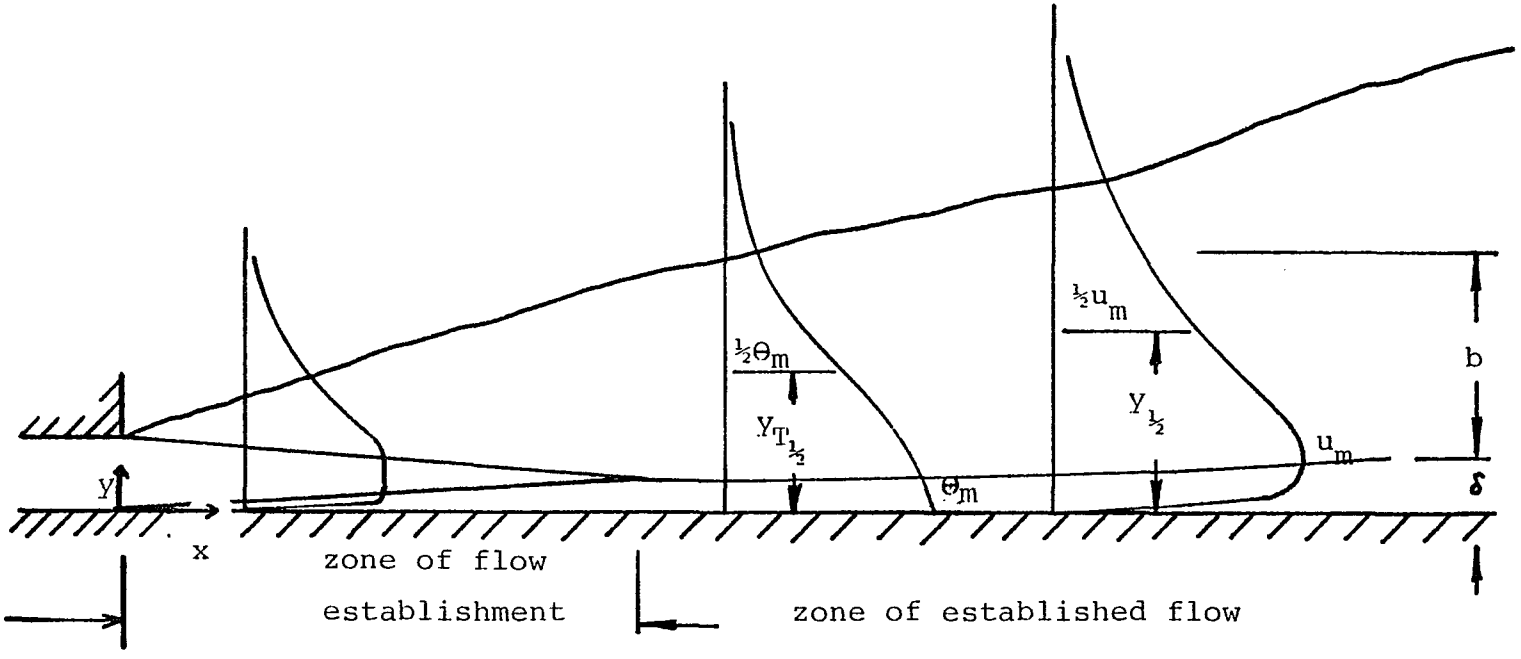

Figure 7. Schematic of the Two-Dimensional Heated Wall Jet

Conservation of Mass:

$$\frac{d}{dx^*}\int_0^{w^*} u^* dy^* = \frac{dQ_e^*}{dx^*} \tag{1}$$

where u^* is the axial velocity, w^* the jet's outer limit, $\frac{dQ_e^*}{dx^*}$ the volumetric rate of entrained mass, x^* and y^* the axial and normal distances respectively.

Conservation of Momentum:

Conservation of momentum for both the inner layer, where the flow behaves like a boundary layer, and the outer layer, where the flow behaves like a two-dimensional free jet, gives:

$$\frac{d}{dx^*}\int_0^{\delta^*} u^{*2} dy^* - u_m^* \frac{d}{dx^*}\int_0^{\delta^*} u^* dy^* = -\tau_0/\rho \tag{2}$$

and

$$\frac{d}{dx^*}\int_{\delta^*}^{w^*} u^{*2} dy^* + u_m^* \frac{d}{dx^*}\int_0^{\delta^*} u^* dy^* = u_\infty^* \frac{dQ_e^*}{dx^*} \tag{3}$$

where u_m^* is the maximum axial velocity, u_∞^* the free stream velocity, δ^* the boundary layer thickness, ρ the jet density and τ_0 the shear stress at the wall.

In writing separate momentum equations for the inner and outer regions, it is assumed that the shear stress at the point of maximum velocity is zero. Although this is

not precisely the case it should not be critical in an integral solution [29].

Conservation of Energy:

The integral form of conservation of energy for a wall jet is:

$$\frac{d}{dx^*}\int_0^{w^*}(T^*-T_\infty^*)\,u^*\,dy^* = 0 \qquad (4)$$

where T^* and T_∞^* are the jet and ambient temperatures respectively.

Equations (1)-(4) may be non-dimensionalized by introducing the following non-dimensional quantities:

$$u = u^*/u_d^* \qquad y = y^*/d$$
$$u_m = u_m^*/u_d^* \qquad x = x^*/d$$
$$u_\infty = u_\infty^*/u_d^* \qquad Q_e = Q_e^*/u_d^* d \qquad (5)$$
$$\theta = \frac{T^*-T_\infty^*}{T_d^*-T_\infty^*} \qquad w = w^*/d$$

where d, u_d^* and T_d^* are the discharge width, velocity and temperature respectively and u_∞ the free stream to discharge velocity ratio. Substituting the above non-dimensional quantities into equations (1)-(4) the integral conservation equations become:

Conservation of Mass:

$$\frac{d}{dx}\int_0^w u\,dy = \frac{dQ_e}{dx} \tag{6}$$

Conservation of Momentum:

$$\frac{d}{dx}\int_0^\delta u^2\,dy - u_m\frac{d}{dx}\int_0^\delta u\,dy = -\frac{1}{2}u_m^2 c_f \tag{7}$$

and

$$\frac{d}{dx}\int_\delta^w u^2\,dy + u_m\frac{d}{dx}\int_0^\delta u\,dy = u_\infty\frac{dQ_e}{dx} \tag{8}$$

where c_f is the skin friction and, is defined as:

$$c_f = \frac{\tau_o}{\frac{1}{2}\rho u_d^{*2}}$$

Conservation of Energy:

$$\frac{d}{dx}\int_0^w u\theta\,dy = 0 \tag{9}$$

B. Two-Dimensional Jet-Boundary Interaction

The discharge of a two-dimensional jet in the vicinity of a boundary is characterized by three distinct flow regions (see Figure 8). In the first, or pre-attachment region, the jet closely resembles a two-dimensional free jet. However, because of limited entrainment between the jet and the boundary an area of reduced pressure is established. This causes the jet to bend and eventually impinge onto the boundary enclosing a region of separated flow. In the second zone, or the impingement region, the wall pressure is higher than the hydrostatic pressure causing the fluid to accelerate. After a short distance the jet reaches hydrostatic pressure and the flow behaves as if it were a wall jet. This last region is referred to as the wall jet region.

The presence of a free stream, for low values of u_∞, should have little direct influence on the pressure distribution in the pre-attachment region. The free stream will reduce entrainment into the jet. This will cause the jet momentum to be more concentrated thus delaying jet attachment and causing slightly higher wall pressure in the impingement region.

To adequately model two-dimensional jet-boundary interaction, consideration must be given to the variation of pressure forces in the pre-attachment and impingement regions.

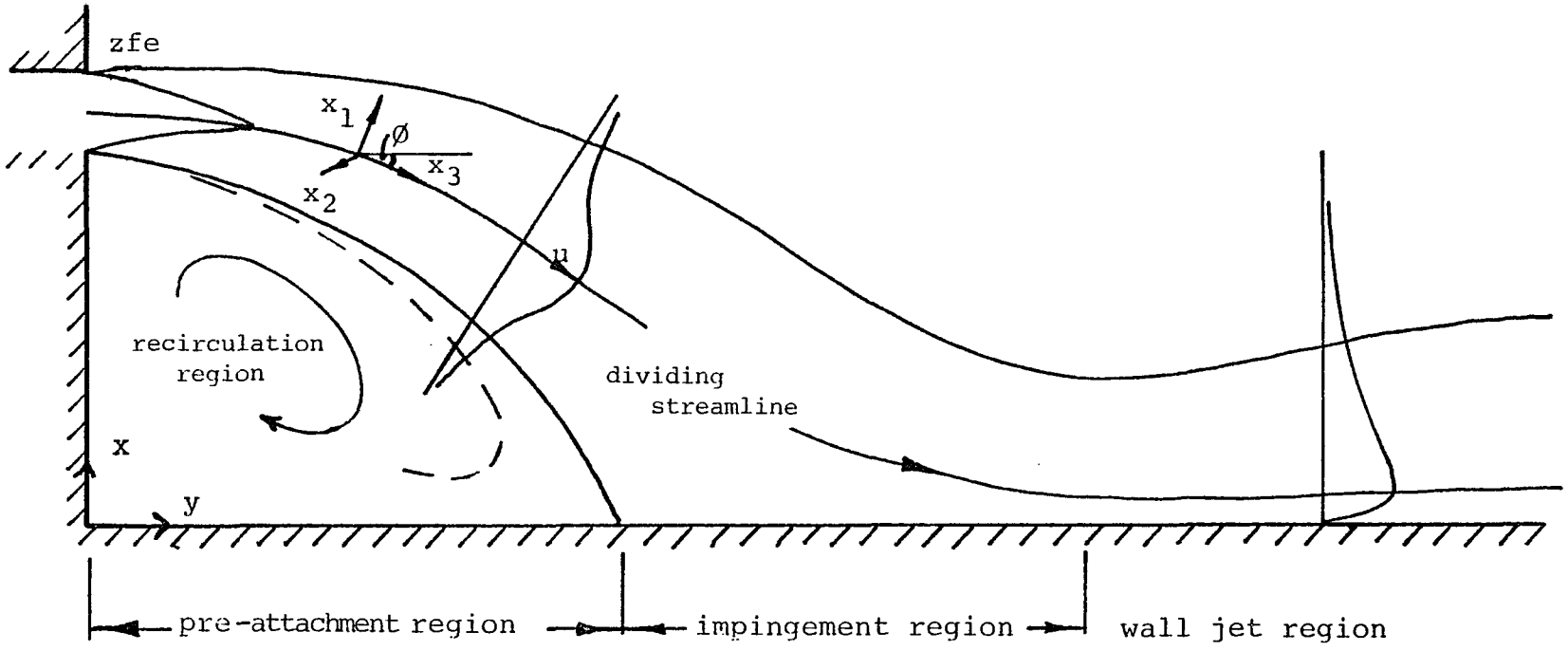

Figure 8. Schematic of Two-Dimensional Jet-Boundary Interaction

A new approach which adequately accounts for the pressure variations is presented. The unique characteristics of each of the flow regions necessitate different sets of integral conservation equations. We therefore present the derivation of the governing equations for each of the flow regions individually.

1. Pre-attachment Region

For constant fluid properties and negligible buoyancy (see page 154) the integral conservation equations written in the jet coordinate system shown in Figure 8 are:

Conservation of Mass:

$$\frac{d}{dx_3^*}\int_{-w^*}^{w^*} u^* \, dx_1^* = \frac{dQ_e^*}{dx_3^*} \tag{10}$$

where x_1^* and x_3^* are the transverse and axial directions respectively.

Conservation of Axial Momentum:

$$\frac{d}{dx_3^*}\int_{-w^*}^{w^*} u^{*2}\, dx_1^* = u_\infty^* \int_0^{w^*} u^* dx_1^* - \int_{-w^*}^{w^*} \frac{1}{\rho}\frac{dp^*}{dx_3^*}\, dx_1^* \tag{11}$$

Conservation of Transverse Momentum:

$$\frac{1}{r^*}\int_{-w^*}^{w^*} u^{*2}\, dx_1^* = \frac{1}{\rho}\left[P_\infty^* - P_b^*(x_3^*)\right] \tag{12}$$

where P^* is the pressure acting on the integral control volume, P_b^* the effective base pressure bordering the jet and r^* the local radius of curvature. $(P_\infty^*-P_b^*)$ in the transverse equation (12) is the effective pressure gradient normal to the jet which causes the jet to bend towards the boundary.

Conservation of Energy:

The conservation of energy equation for the pre-attachment region has to reflect the fact that the temperature of the fluid inside the recirculation region is greater than that of the ambient. Although this temperature is unknown, efficient mixing inside the recirculation region allows us to assume it to be constant. This assumption will be verified experimentally (see page 130). Conservation of energy applied to a control volume bounded on one side by the ambient temperature T_∞^* and the other side by T_R^*, the temperature inside the recirculation region, gives (see Figure 9):

$$\frac{d}{dx_3^*}\int_{-w^*}^{w^*} u^* T^* dx_1^* = T_\infty^* \frac{d}{dx_3^*}\int_0^{w^*} u^* dx_1^* + T_R^* \frac{d}{dx_3^*}\int_{-w^*}^{0} u^* dx_1^* \qquad (13)$$

or:

$$\frac{d}{dx_3^*}\int_{-w^*}^{w^*} u^*(T^*-T_\infty^*)\,dx_1^* - \frac{d}{dx_3^*}\int_{-w^*}^{0} u^*(T_R^*-T_\infty^*)\,dx_1^* = 0 \qquad (14)$$

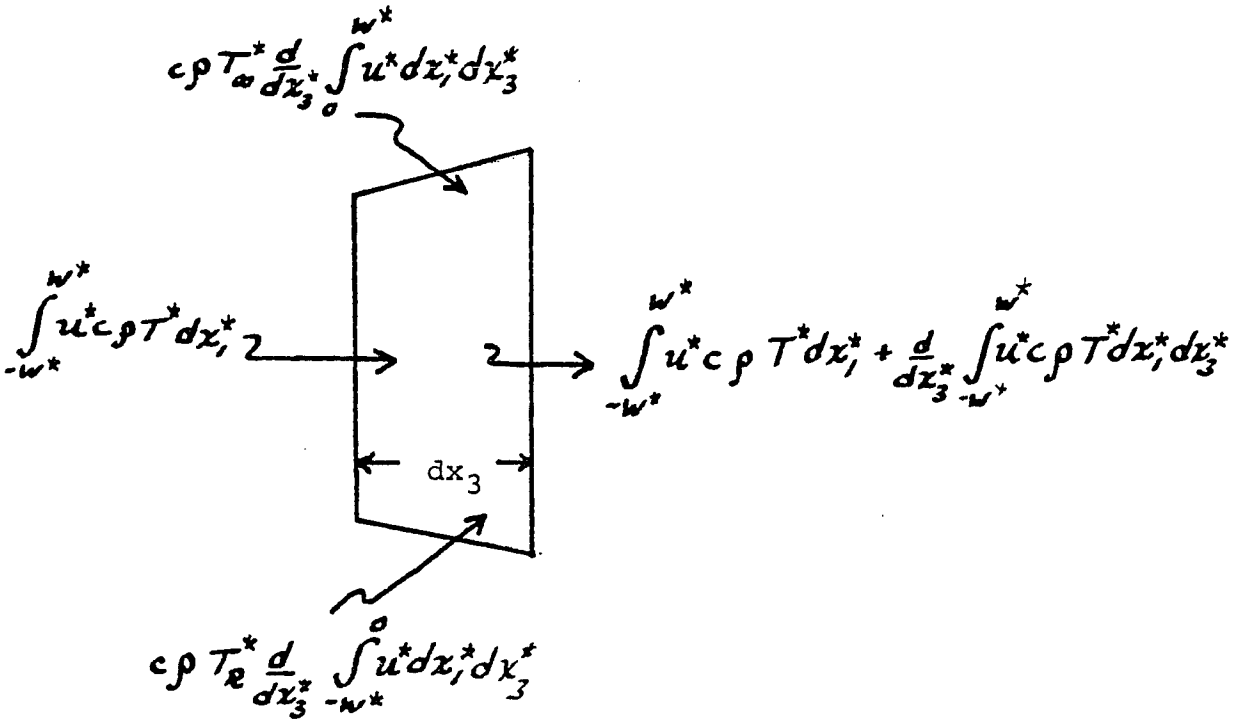

Figure 9. Conservation of Energy on an Integral Control Volume in the Pre-attachment Region

Introducing the non-dimensional variables in equation (5), the governing integral equations in the pre-attachment region become:

Conservation of Mass:

$$\frac{d}{dx_3}\int_{-w}^{w} u\,dx_1 = \frac{dQ_e}{dx_3} \tag{15}$$

Conservation of Axial Momentum:

$$\frac{d}{dx_3}\int_{-w}^{w} u^2\,dx_1 = u_\infty \frac{dQ_e}{dx_3} - \int_{-w}^{w} \frac{dP}{dx_3}\,dx_1 \tag{16}$$

Conservation of Transverse Momentum:

$$\frac{1}{r}\int_{-w}^{w} u^2\,dx_1 = -P_b(x_3) \tag{17}$$

Conservation of Energy:

$$\frac{d}{dx_3}\int_{-w}^{w} u\theta\,dx_1 - \frac{d}{dx_3}\int_{-w}^{0} u\theta_R\,dx_1 = 0 \tag{18}$$

where:

$$P = \frac{P^* - P_\infty^*}{\rho U_j^{*2}}$$

$$P_b = \frac{P_b^* - P_\infty^*}{\rho U_j^{*2}}$$

$$r = r^*/d$$

and

$$\theta_R = \frac{T_R^* - T_\infty^*}{T_j^* - T_\infty^*}$$

Equations (15)-(18) represent the governing integral equations for the pre-attachment region. An additional relationship is necessary to fix the extent of the pre-attachment region. Assuming that there exists a re-attachment (dividing) streamline extending from the edge of the discharge to the point of re-attachment across which there is no mass flow, all the mass entrained in the inner part of the jet will eventually be returned to the recirculation region at jet impingement. The equation for this dividing streamline is therefore given by:

$$\int_{-b_R}^{0} u \, dx_1 = \frac{1}{2} \tag{19}$$

where b_R is the distance from the jet axis to the dividing

streamline. The pre-attachment region ends as the dividing streamline intersects the boundary (see Appendix A).

2. Impingement Region

This region begins at the point of re-attachment. We assume, that the jet has completely bent and is parallel to the boundary. The high pressure associated with jet impingement causes a slight acceleration of the jet. Otherwise, there is little difference in comparison to the behavior of a wall jet. The wall jet momentum equations must be modified to account for the excess pressure in this region. Equations (7)and(8) may be rewritten as follows:

Conservation of Axial Momentum:

Inner Region:

$$\frac{d}{dx}\int_0^\delta u^2 dy - u_m \frac{d}{dx}\int_0^\delta u\, dy = -\frac{1}{2}u_m^2 c_f - \frac{d}{dx}\int_0^\delta P\, dy \qquad (20)$$

Outer Region:

$$\frac{d}{dx}\int_\delta^W u^2 dy + u_m \frac{d}{dx}\int_0^\delta u\, dy = u_\infty \frac{dQ_e}{dx} - \frac{d}{dx}\int_\delta^W P\, dy \qquad (21)$$

The integral form of conservation of mass and energy are the same as for a wall jet, and are given by equations (6) and (9).

3. Wall Jet Region

This region begins once the jet pressure drops to hydrostatic level. Equations (6)-(9) which govern a wall jet, are used to predict the velocity and temperature distributions in this region.

V. Solutions

In this chapter the governing integral equations for the wall jet and jet-boundary interaction problems are solved. To complete the integral solution, appropriate velocity and temperature profiles, boundary conditions and closure assumptions are made, and outlined for the various flow regimes under consideration.

A. Wall Jet

1. Assumed Profiles: Zone of Established Flow

To evaluate the integrals in equations (6) - (9), velocity and temperature profiles must be introduced. For the inner layer, which resembles boundary layer flow over a flat plate, a 1/7th power law applies, therefore:

$$u = u_m \left(y/\delta\right)^{1/7} \quad , \quad 0 \le y \le \delta \tag{22a}$$

In the outer region where the flow is similar in nature to a free jet, we will assume a Gaussian-shaped velocity profile:

$$u = (u_m - u_\infty)\, e^{-\left(\frac{y-\delta}{b}\right)^2} + u_\infty \quad , \quad y > \delta \tag{22b}$$

where b is a measure of the jet spread.

For an adiabatic boundary condition at the wall, our experimental results (see Chapter VII) reveal that the temperature profile of a wall jet can be represented by a

Gaussian profile of the following form:

$$\theta = \theta_m e^{-(y/b_T)^2} \quad , y > 0 \tag{23}$$

where θ_m is the maximum axial temperature, and b_T a measure of the thermal spread of the jet.

We should point out that equation (23) does not agree with the results of Seban and Back (46), who concluded that the temperature profile was linear in shape. This, however, does not satisfy the adiabatic wall condition, whereas a Gaussian profile would.

For two-dimensional free jets, the thermal half-width is related to the jet half-width as follows:

$$y_{T_{1/2}} = \lambda \, y_{1/2} \tag{24}$$

where λ is the turbulent Schmidt number. Reported values of the turbulent Schmidt number vary from 1.12 to 1.41 [44, 45]. In terms of spread parameters equation (24) can be rewritten for a wall jet as follows:

$$b_T = \lambda \, (\delta + .833 \, b) / .833 \tag{25}$$

where (δ + .833 b) represent the velocity half-width $y_{1/2}$. The temperature profile can then be rewritten as:

$$\theta = \theta_m e^{-\left[\frac{.833\, y}{\lambda(\delta + .833 b)}\right]^2} \tag{26}$$

2. Evaluation of Integrals

Using the assumed profiles (22) and (23), integrating all Gaussian integrals to infinity, and setting $w = \sqrt{2}\, b + \delta$, equations (6) - (9) become:

Conservation of Mass:

$$\left[\tfrac{7}{8}\delta + \frac{\sqrt{\pi}}{2} b\right]\frac{du_m}{dx} + \left[\frac{\sqrt{\pi}}{2}(u_m - u_\infty) + \sqrt{2}\, u_\infty\right]\frac{db}{dx_3} + \left[\tfrac{7}{8} u_m - u_\infty\right]\frac{d\delta}{dx} = \frac{dQ_e}{dx} \tag{27}$$

Conservation of Momentum:

$$\frac{7}{72} u_m^2 \frac{d\delta}{dx} - \frac{49}{72} u_m \delta \frac{du_m}{dx} = \frac{1}{2} u_m^2 c_f \tag{28}$$

and:

$$\left[\frac{\sqrt{\pi}}{\sqrt{2}}(u_m - u_\infty) b + \sqrt{\pi}\, b u_\infty + \tfrac{7}{8} u_m \delta\right]\frac{du_m}{dx} + \left[\tfrac{7}{8} u_m^2 - u_\infty^2\right]\frac{d\delta}{dx} + \left[\frac{1}{2}\sqrt{\frac{\pi}{2}}(u_m - u_\infty) + \sqrt{\pi}\, u_\infty (u_m - u_\infty) + \sqrt{2}\, u_\infty^2\right]\frac{db}{dx} = u_\infty \frac{dQ_e}{dx} \tag{29}$$

Conservation of Energy:

Equation (9) can first be integrated with respect to x, yielding:

$$\int_0^\infty u\, \theta\, dy = \text{constant} \tag{30}$$

The constant of integration is obtained by evaluating the above integral at the discharge, where:

$$u = \theta = 1 \quad , \qquad 0 \leq y \leq 1$$

Using the above boundary condition, we obtain:

$$\int_0^\infty u\,\theta\,dy = 1$$

Substituting velocity and temperature profiles into the above we obtain:

$$\theta_m = \frac{1}{\int_0^\delta u_m \left(\frac{y}{\delta}\right)^{1/7} e^{-(y/b_T)^2} dy + \int_\delta^\infty \left[(u_m - u_\infty) e^{-\left(\frac{y-\delta}{b}\right)^2} + u_\infty\right] e^{-(y/b_T)^2} dy} \qquad (31)$$

The three simultaneous equations (27) - (29) governing the velocity distribution have three dependent variables δ, b, and u_m. However, they cannot be solved until appropriate assumptions describing the rate of entrainment, dQ_e/dx, and the skin friction, c_f, are introduced. In addition, boundary conditions on b and u_m must also be specified.

3. Entrainment Assumption

In order to obtain closure of the governing equations, an entrainment assumption will be used to describe Q_e. For two-dimensional free jets Morton, et al., [5] introduced the following hypothesis:

$$\frac{dQ_e}{dx} = 2\alpha u_c$$

where the entrainment coefficient α is determined empirically and is equal to .069 for two-dimensional free jets, and u_c refers to the centerline velocity. For a wall jet this is rewritten as:

$$\frac{dQ_e}{dx} = \alpha u_m$$

where the maximum velocity u_m replaces the centerline velocity u_c of the free jet. Based on an average of most existing data for the wall jet spread and velocity decay rates, Rajaratman [19] found the value of α to be .035. For a co-axial wall jet, the above equation can be modified to:

$$\frac{dQ_e}{dx} = \alpha (u_m - u_\infty) \qquad (32)$$

4. Skin Friction

The skin friction, c_f, in equation (28) can be determined using the Blasius law, which calculates the skin friction for turbulent flow through pipes and over flat plates. For boundary layer flow over a flat plate the Blasius law gives [46]:

$$c_f = 0.045 \left(\frac{\nu}{V_\infty \delta^*} \right)^{1/4} \tag{33}$$

where V_∞ is the free stream velocity, ν the kinematic viscosity and δ^* the boundary layer thickness. By substituting the dimensional maximum velocity u_m^* for the free stream velocity, and redefining δ^* as the thickness of the inner layer, equation (33) can be rewritten for a wall jet as follows:

$$c_f = 0.045 \left(\frac{\nu}{u_m^* \delta^*} \right)^{1/4}$$

Sigalla's [32] measurements showed that the constant 0.045 should be adjusted upwards for a wall jet. He determined that:

$$c_f = 0.056 \left(\frac{\nu}{u_m^* \delta^*} \right)^{1/4} \tag{34}$$

In terms of non-dimensional quantities equation (34) can be rewitten as:

$$c_f = 0.056 \left(Re_d \, u_m \, \delta \right)^{-1/4} \tag{35}$$

where Re_d is the discharge Reynolds number and is defined as:

$$Re_d = \frac{u_d^* \, d}{\nu}$$

5. Boundary Conditions: Zone of Flow Establishment

The system of equations (27) - (29) can now be solved for $u_m(x)$, $b(x)$, $\delta(x)$, $\theta_m(x)$, given their appropriate boundary conditions. These boundary conditions, b_o, u_{mo} and δ_o are obtained from the solution of the zone of flow establishment.

The flow in the zone of flow establishment is characterized by a potential core of constant velocity, whose width decreases downstream of the discharge. This is due to the increasing width of the boundary layer near the wall, and the turbulent mixing, or free jet boundary, in the outer layer of the jet. The zone of flow establishment ends when the boundary layer and the free jet boundary meet (see Figure 7). Further turbulent mixing causes the maximum axial velocity to decay.

The governing integral conservation equations (6) - (8) are still valid for the zone of flow establishment. However, they can be simplified, since the maximum axial velocity, u_m, is constant in this region. Integrating equations (6) -(9) along x between the discharge and the end of the zone of flow establishment, $x = x_o$, and setting $u_m = 1$, we obtain:

Conservation of Mass:

$$\int_0^w u(x_o)\,dy = \alpha(1-u_\infty)x_o + 1 \qquad (36)$$

Conservation of Momentum:

Inner layer:

$$\int_0^{\delta} u(x_o)\,[u(x_o)-1]\,dy = -\int_0^{x_o} \tfrac{1}{2} c_f\,dx \qquad (37)$$

Outer layer:

$$(1-u_\infty)\int_0^{\delta} u(x_o)\,dy + \int_{\delta}^{\infty} u(x_o)\,[u(x_o)-u_\infty]\,dy = 0 \qquad (38)$$

where the rate of entrainment is determined using equation (32) with $u_m = 1$, and the skin friction c_f is given by equation (35). It should be noted that the value of the entrainment coefficient α is different in the zone of flow establishment.

The integrals in equations (36) - (38) are evaluated at $x = x_o$, where the width of the potential core is zero. Substituting velocity profile (22) into equations (36) - (38), we obtain:

$$x_o = \frac{\frac{7}{8}\delta_o + \frac{\sqrt{\pi}}{2} b(x_o)(1-u_\infty) + \sqrt{2}\, b(x_o)\, u_\infty - 1}{\alpha(1-u_\infty)} \qquad (39)$$

$$b(x_o) = \frac{2\sqrt{2/\pi}\,(1-\frac{7}{8}\delta)}{(1-u_\infty)+\sqrt{2}\,u_\infty} \qquad (40)$$

and

$$\delta(x_o) = 0.442\,(Re_d)^{-1/5}\,x_o^{4/5} \qquad (41)$$

Equations (39) - (41) give the three necessary boundary conditions $b(x_o)$, $\delta(x_o)$ and x_o.

6. Numerical Solution

The system of equations (27) - (29) are solved numerically for $u_m(x)$, $b(x)$ and $\delta(x)$. A Runga-Kutta procedure is programmed to carry out step-wise integration for each of these unknown variables. The maximum temperature can be determined from equation (31) at any axial distance x, once the local values of u_m, δ and b are determined. The integrals in equation (31) are evaluated numerically using the Adaptive Simpson Quadrature Method.

B. Jet-Boundary Interaction

1. Pre-attachment Region - Velocity Distribution

Equations (15) - (18) represent the conservation equations for the pre-attachment region of a jet discharging offset from and parallel to a solid boundary. In order to evaluate the integral equations it is necessary to introduce appropriate velocity and temperature profiles.

a. Velocity Profiles

For a stationary ambient, since the velocity inside the recirculation region is very small, we will follow previous studies in assuming that the bending of the jet does not influence the shape of the velocity profile. Therefore, the velocity profile is given by:

$$u = u_m e^{-(x_1/b)^2} \tag{42}$$

For small values of free stream, we will assume the velocity inside the recirculation region to be very small. Therefore, in the presence of free stream, the velocity profile is given by:

$$u = (u_m - u_\infty) e^{-(x_1/b)^2} + u_\infty \quad , x_1 > 0 \tag{43a}$$

$$u = u_m e^{-(x_1/b)^2} \quad , \qquad x_1 < 0 \tag{43b}$$

Hot wire anemometer measurements inside the recirculation region generally confirm this assumption (see Chapter VII).

b. Evaluation of Integrals

Substituting velocity profiles (43) into the integral equations for the pre-attachment region (15) - (17), integrating all Gaussian integrals to infinity, and setting

$w = \sqrt{2}\, b$, we obtain:

Conservation of Mass:

$$\left[(2u_m - u_\infty) + 2\sqrt{\frac{2}{\pi}}\, u_\infty\right]\frac{db}{dx_3} + 2b\frac{du_m}{dx_3} = \frac{2}{\sqrt{\pi}}\frac{dQ_e}{dx_3} \tag{45}$$

Conservation of Axial Momentum:

$$\left[(u_m - u_\infty)^2 + \sqrt{2}\, u_\infty (u_m - u_\infty) + u_m^2\right]\frac{db}{dx_3} + \left[2(u_m - u_\infty) + \sqrt{2}\, u_\infty + 2u_\infty\right] b\frac{du_m}{dx_3} = -\frac{2\sqrt{2}}{\sqrt{\pi}}\int_{-w}^{w}\frac{dP}{dx_3}\, dx_1 \tag{46}$$

Conservation of Transverse Momentum:

$$P_b = \frac{\pi}{4}\frac{b}{r}\left[u_m^2 + (u_m - u_\infty)^2 + 2\sqrt{2}\, u_\infty (u_m - u_\infty) + \frac{4}{\sqrt{\pi}} u_\infty^2\right] \tag{47}$$

c. Entrainment Assumption

Sawyer [22] showed that a jet discharging offset to a parallel plate does not maintain an even spread due to the different rate of entrainment on either side of the jet. However, this small difference does not affect overall entrainment rates. We will therefore assume that the entrainment rate in the pre-attachment region is similar in nature to that of the free jet, or:

$$\frac{dQ_e}{dx_3} = 2\alpha u_m \tag{48}$$

This is in accordance with our assumed velocity profile. In the presence of free stream, the entrainment rate must be adjusted for the outer portion of the jet where free stream effects occur. Therefore:

$$\frac{dQ_e}{dx_3} = \alpha u_m + \alpha(u_m - u_\infty) \tag{49}$$

The value of the entrainment coefficient is expected to lie between the two limiting cases of the free jet and the wall jet. For a two-dimensional free jet, the value of the entrainment coefficient is approximately .036 in the zone of flow establishment (based on Albertson's [4] data), and .069 in the zone of established flow. The value of α for a wall jet is approximately .031 in the zone of flow establishment, and .035 in the zone of established flow. Therefore, the value of α in the pre-attachment region will most likely vary between these two extremes, depending on the initial offset height.

The solution should not be too sensitive to the value of α, since pressure effects are predominant in this region, especially prior to jet impingement. It therefore seems reasonable to use an average of the two limiting values of α for the pre-attachment region. Therefore, α is set at 0.033 and 0.052 for the zone of flow establishment and the zone of established flow respectively.

d. Pressure Variation

Two different pressure terms appear in equations (45) - (47): the base pressure P_b, which represents the pressure difference normal to the jet axis, and dP/dx_3, the axial pressure gradient. Based on an analysis of pressure contours within the pre-attachment region (see Figure 5), it seems reasonable to assume that P varies linearly across the jet, so:

$$\bar{P}(x_3) = \frac{1}{2} P_b(x_3) \qquad (50)$$

Where $\bar{P}$ is the average pressure inside the jet and is a function of x_3. The axial pressure gradient can then be evaluated in a numerical step-wise solution, using previous values of P_b.

e. Closure of the Governing Equations

Even after making appropriate assumptions to evaluate $\frac{dQ_e}{dx_3}$ and $\frac{d\bar{P}}{dx_3}$, we are still left with a system of three equations, (45) - (47), and four unknowns: u_m,b,r, and $\bar{P}$. In order to obtain closure of the governing equations without introducing any additional empirical data, we will independently solve for the approximate jet trajectory. This will in effect give us the value of the radius of curvature, leaving only three unknowns: u_m, b and $\bar{P}$.

We begin by postulating an arbitrary polynomial shape for the jet trajectory. Using a fifth order polynomial for the assumed jet trajectory, we have:

$$y = a_0 + a_1 x + a_2 x^2 + a_3 x^3 + a_4 x^4 + a_5 x^5 \qquad (51)$$

where x and y are the Cartesian coordinates, and a_1 through a_5 are constants to be determined from boundary conditions. This is the minimum order polynomial that can be expected to adequately represent the axis trajectory.

At the discharge, assuming the jet axis is horizontal and higher order derivatives are zero (i.e. $\bar{P}(0)=0$), we have:

$$x = 0 \qquad y = h + \tfrac{1}{2}$$

$$x = 0 \qquad \frac{dy}{dx} = \frac{d^2y}{dx^2} = \frac{d^3y}{dx^3} = 0$$

It should be noted that for small offset heights ($h < 2$), the higher order derivatives may not be zero.

Substituting these four boundary conditions into equation (51), we obtain:

$$y = (h + \tfrac{1}{2}) + a_4 x^4 + a_5 x^5 \qquad (52)$$

Two more boundary conditions, which describe the effect of the boundary on the jet trajectory, are still necessary.

The remaining boundary conditions are obtained by applying horizontal and vertical momentum principles at re-attachment. Bourque and Newman (15) applied the horizontal momentum principle locally at the point of re-attachment.

Following their method, which neglects local pressure variation, we have:

$$\cos\gamma \int_{-w}^{w} u^2 dx_1 = J_a - J_b \tag{53}$$

where γ is the angle at which the dividing streamline hits the boundary (see Figure 10), J_a the momentum that proceeds downstream along the wall, and J_b the momentum of the jet below the dividing streamline returned into the recirculation region.

Basically, this equation balances the momentum that continues downstream with that which is reversed into the recirculation region. Assuming that at the re-attachment point the jet flow divides in such a way that the momentum of the initial reversed flow and flow downstream are similar to the parts of the jet profile (43) above and below the dividing streamline, we have:

$$J_a = \int_{-b_R}^{w} u^2 dx_1 \tag{54a}$$

and

$$J_b = \int_{-w}^{-b_R} u^2 dx_1$$

where b_R, the position of the dividing streamline is given by equation (19). Although a Gaussian profile may not accurately represent the velocity at the point of re-attach-

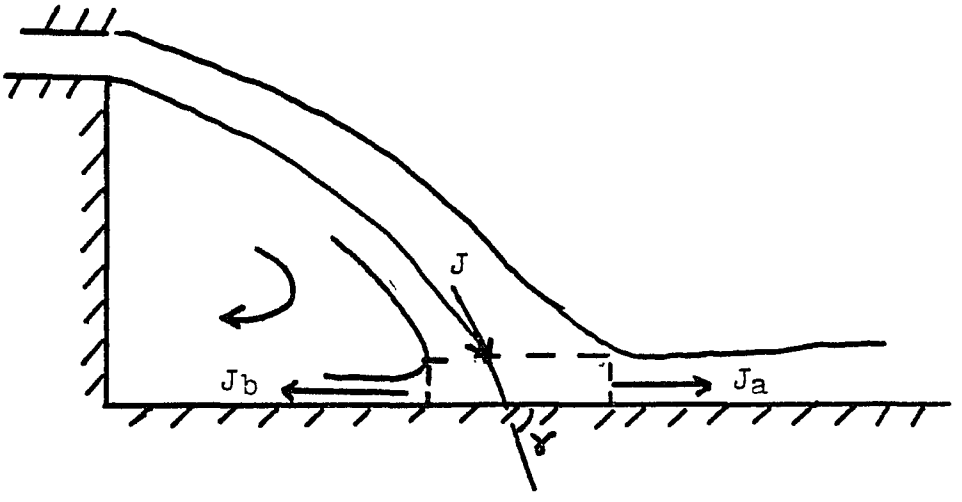

Figure 10. Horizontal Momentum Condition

ment its use in equation (54) is reasonable as far as the overall volume and momentum are concerned.

Although this last assumption may be inaccurate it should not have much of an effect on the final shape of the assumed trajectory profile (see Appendix C). Using equation (43) and integrating equation (53) is rewritten as:

$$\cos\gamma = \frac{2u_m^2\, erf\left(\sqrt{2}\,\frac{b_2}{b}\right) + (u_m-u_\infty)^2 - u_m^2 + 2\sqrt{2}\,u_\infty(u_m-u_\infty) + \frac{4}{\sqrt{\pi}}u_\infty^2}{u_m^2 + (u_m-u_\infty)^2 + 2\sqrt{2}\,u_\infty(u_m-u_\infty) + \frac{4}{\sqrt{\pi}}u_\infty^2} \qquad (55)$$

The only additional unknown introduced here is the angle γ which is the angle the dividing streamline makes with the boundary and can be determined knowing the position of the dividing streamline (see Appendix A).

The final boundary condition can be obtained by applying conservation of momentum in the vertical direction for a control volume enclosing the portion of the jet that continues downstream following re-attachment. The vertical component of the momentum above the dividing streamline just prior to re-attachment, J_c, must be balanced by the pressure force necessary to move this portion of the jet away from the wall. With reference to Figure 11, we can write the vertical momentum equation as:

$$J_c|\sin\phi| = F_w - F_p|\sin\phi| \qquad (56)$$

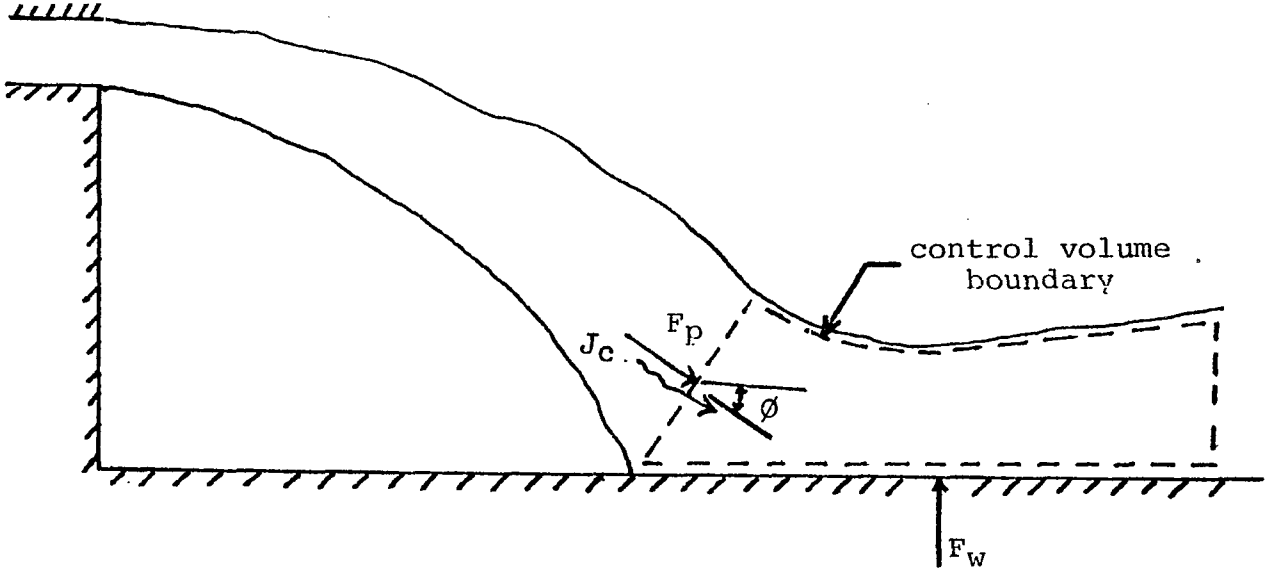

Figure 11. Vertical Momentum Condition

where F_w is the total pressure force along the boundary, F_p the pressure force acting on the control volume surface normal to the impinging jet, and ϕ the local angle of inclination of the jet axis, given by:

$$\phi = \tan^{-1}\left(dy/dx\right)$$

The value of J_c is determined using equation (54). Both J_c and F_p are functions of tne velocity and pressure at the point of re-attachment, while F_w is determined from the pressure distribution in the impingement region (see Section 3). Using equations (43) and (54), we have:

$$\left[u_m^2\, erf\left(\frac{\sqrt{2}\,b_R}{b}\right) + (u_m - u_\infty)^2 + 2\sqrt{2}(u_m - u_\infty)u_\infty + \frac{4}{\sqrt{\pi}}u^2\right]\frac{b}{2}\sqrt{\frac{\pi}{2}}\,|\sin\phi| = F_w - F_p|\sin\phi| \tag{57}$$

where F_p is given by:

$$F_p = \int_{-b_\ell}^{w} \overline{P}\, dx_1 \tag{58}$$

and is evaluated at the point of re-attachment.

Although equations (55) and (57) represent two independent boundary conditions that should be sufficient for solving for the remaining constants in the trajectory profile, they cannot be directly applied. This is because the conditions are on the dependent variables u_m, b and $\overline{P}$ rather than the independent variables x and y. Equations (55) and (57)

cannot be evaluated until equations (45) - (47) are solved for u_m, b and $\bar{P}$, while this system of equations cannot be integrated until we have described the shape of the trajectory.

In order to resolve this dilemma, we introduce two substitute boundary conditions on the independent variables x and y. These boundary conditions amount to little more than a guess on the trajectory shape, to be verified using equations (55) and (57). This guess makes use of the fact that there is an inflection point in the trajectory upstream of re-attachment. At the point of inflection, the following conditions apply:

$$x = x_i \qquad y = y_i \tag{59a}$$

and

$$x = x_i \qquad \frac{d^2y}{dx^2} = 0 \tag{59b}$$

where x_i and y_i refer to the coordinates of the inflection point.

Substituting these conditions into equation (52), we obtain:

$$y = (h+1/2) + 5/2\,(h+1/2-y_i)\left[(x/x_i)^4 - 3/5\,(x/x_i)^5\right] \tag{60}$$

With suitable values of x_i and y_i, the radius of curvature of the jet axis can be determined from [47]:

$$r = \frac{\left[1 + \left(dy/dx\right)^2\right]^{3/2}}{d^2y/dx^2} \tag{61}$$

where the derivatives dy/dx and d^2y/dx^2 are obtained using equation (60).

For a given value of x_i and y_i the radius of curvature is determined and we are left with only three unknowns: u_m, b and $\overline{P}$, and three equations, (45) - (47). This system of simultaneous equations can then be solved for the velocity and pressure field in the pre-attachment region. After the solution is completed, we check to see if conditions (55) and (57) are satisfied. If not, we alter the values of either x_i and y_i until both conditions are met. This iterative procedure is carried out by first fixing x_i and determining the value of y_i that satisfies condition (55). Condition (57) is then applied to determine the correct value of x_i.

f. Boundary Conditions: Zone of Flow Establishment

The solution for the two-dimensional jet boundary interaction problem in the pre-attachment region is not complete until adequate boundary conditions for u_m, b and $\overline{P}$ are

specified. These boundary conditions are obtained from the solution of the zone of flow establishment in which a transition of the relatively uniform discharge conditions to a Gaussian distribution takes place.

Only the boundary conditions at the start of the zone of established flow are needed. Therefore, we can integrate the continuity and momentum equations (15) - (16) between $x_3=0$ and x_o, using entrainment relationship (49), noting that $u_m = 1$ and assuming $P_b = 0$ at the discharge. Equations (45) - (47) become:

Conservation of Mass:

$$\int_{-w}^{w} u(x_o)\, dx_1 = 1 + \alpha(2-u_\infty)\, x_o \tag{62}$$

Conservation of Axial Momentum:

$$\int_{-w}^{w} u^2(x_o)\, dx_1 - u_\infty \left[\alpha(2-u_\infty)\, x_o\right] + \int_{-w}^{w} P\, dx_1 = 1 \tag{63}$$

Using equations (47) and (50), the pressure integral in equation (63) can be related to the radius of curvature. Therefore:

$$\left(1 + b/r\right) \int_{-w}^{w} u^2(x_o)\, dx_1 - \alpha(2-u_\infty)\, u_\infty = 1 \tag{64}$$

where the radius of curvature is evaluated using equation (61). Integrating equations (62) and (63), and using equation (64), we obtain:

$$b(x_o) = \frac{r}{\sqrt{2}} \left\{ \sqrt{\frac{4\sqrt{2}\left[1+2\alpha u_\infty (1-u_\infty) x_o\right]}{r\left[(1-u_\infty)^2\sqrt{\pi/2} + 2u_\infty(1-u_\infty)\sqrt{\pi} + 2\sqrt{2}\,u_\infty^2\right]} + 1} - 1 \right\} \tag{65}$$

and:

$$x_o = \frac{\left[(1-u_\infty)\sqrt{\pi} + 2\sqrt{2}\,u_\infty\right] b - 1}{2\alpha(1-u_\infty)} \tag{66}$$

A numerical solution of equations (65) and (66) will give the values of $b(x_o)$ and x_o for a given jet trajectory and radius of of curvature.

2. Pre-attachment Region - Temperature Distribution

The conservation of energy equation (18) can be integrated along the jet axis x_3, yielding:

$$\int_{-w}^{w} u\theta\, dx_1 - \int_{-w}^{o} u\,\theta_R\, dx_1 = \text{constant} \tag{67}$$

The constant of integration is evaluated by applying equation (67) at the discharge ($x_3=0$), where both u and θ are equal to unity.

Substituting these conditions into equation (67), we have:

$$\int_{-w}^{w} u\,\theta\,dx_1 - \int_{-w}^{0} u\,\theta_R\,dx_1 = 1 - \frac{\theta_R}{2} \tag{68}$$

a. Temperature Profile

The temperature profile of a two-dimensional jet discharging near a boundary will differ significantly from that of a heated free jet. This is due to the temperature inside the recirculation region, θ_R, which is above ambient levels. Assuming the temperature inside the recirculation region is constant, the temperature profile for the pre-attachment region may be given as:

$$\theta = \theta_m e^{-(x_1/\lambda b)^2}, \quad x_1 > 0$$

$$\theta = (\theta_m - \theta_R) e^{-(x_1/\lambda b)^2} + \theta_R, \quad x_1 < 0 \tag{69}$$

where θ_m is the temperature along the jet axis. Note that θ_m is not necessarily the maximum axial temperature. When θ_m becomes less than θ_R, the maximum axial temperature will occur within the recirculation region, and not along the jet axis.

Introducing profiles (43) and (69) into equation (68), and integrating, we obtain:

$$\theta_m = \frac{1 + \frac{\theta_a}{2}\left[u_m b\Lambda - 1\right]}{\frac{b\Lambda}{2}\left[(u_m - u_\infty) + u_m\right] + \frac{\sqrt{\pi}}{2}\lambda b u_\infty} \tag{70}$$

where

$$\Lambda = \sqrt{\frac{2\lambda^2}{1+\lambda^2}} \tag{71}$$

b. Recirculation Temperature, θ_R

The value of θ_R , though constant, still has not been determined. Because the recirculation region is well mixed and uniform, its temperature can be approximated by the value of the maximum temperature near the point of re-attachment, where the fluid is returned into the recirculation region.

Assuming that the jet begins to divide at the axis inflection point (x_i , y_i), we have:

$$\theta_R = \frac{2}{b(x_i)\Lambda\left\{\left[u_m(x_i) - u_\infty\right] + u_m(x_i)\right\} + b(x_i)\left[\sqrt{\pi}\lambda u_\infty - u_m(x_i)\Lambda\right] + 1} \tag{72}$$

where $u_m(x_i)$ and $b(x_i)$ are the values of u_m and b at the inflection point.

3. Impingement Region

This region is characterized by its excess pressure. Except for this, the impingement region resembles a wall jet. Therefore, the velocity profile is given by equation (22). Introducing equation (22) into the conservation of momentum equations (20) and (21) for the impingement region, we obtain:

Inner layer:

$$\frac{7}{72}u_m^2\frac{d\delta}{dx}-\frac{49}{72}u_m\delta\frac{du_m}{dx}=\frac{1}{2}u_m^2c_f+\int_0^{\delta}\frac{dP}{dx}dy \tag{73}$$

Outer layer:

$$\left[\sqrt{\frac{\pi}{2}}(u_m-u_\infty)b+\pi b u_\infty+\frac{7}{8}u_m\delta\right]\frac{du_m}{dx}+\left(\frac{7}{8}u_m^2-u_\infty^2\right)\frac{d\delta}{dx}$$
$$+\left[\frac{1}{2}\sqrt{\frac{\pi}{2}}(u_m-u_\infty)^2+\pi u(u_m-u_\infty)+\sqrt{2}u_\infty^2\right]\frac{db}{dx}=u_\infty\frac{dQ_e}{dx}-\int_{\delta}^{\infty}\frac{dP}{dx}dy \tag{74}$$

where $\frac{dQ_e}{dx_3}$ and c_f can be approximated by their wall jet values.

a. Wall Pressure

The surface pressure variation in the impingement region is shown for h=5.7 in Figure 12. The pressure at the beginning

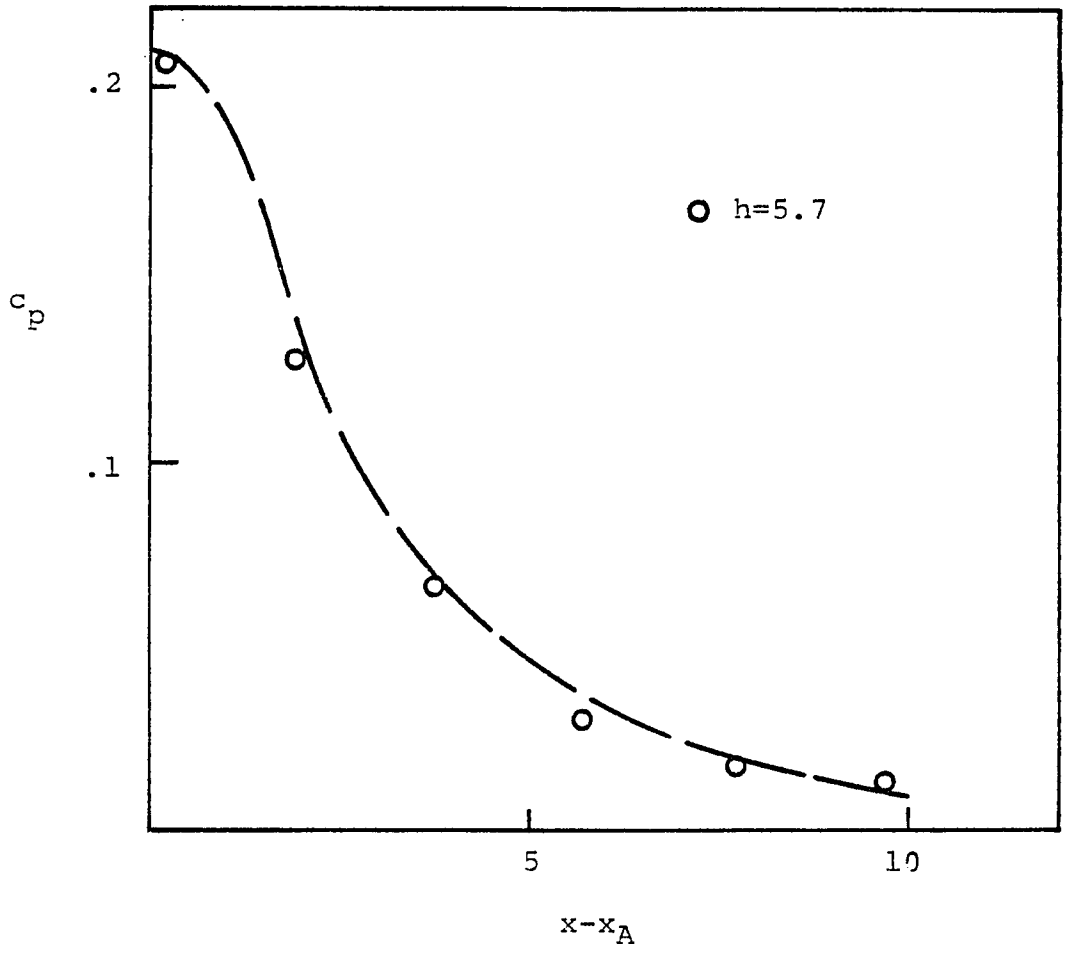

Figure 12. Experimental Wall Pressure in the Impingement Region of an Offset Jet

of the region is maximum and then eventually drops down to ambient levels. If P_w is the wall pressure in this region, we could write:

$$P_w = f(P_m, h, Re_d; x-x_A) \tag{75}$$

where P_m is the maximum wall pressure, h the offset height and Re_d the discharge Reynolds number and x_A is the value of x at jet re-attachment.

For turbulent jets, we do not expect any significant variation in flow properties with Reynolds number; therefore, we have:

$$P_w = f(P_m, h; x-x_A)$$

or normalizing the above, we have:

$$\frac{P_w}{P_m} = f(h; x-x_A)$$

This is analogous to the case of free impinging jets onto solid surfaces, where it has been found [48-50] that:

$$\frac{P_w}{P_m} = F(H, X) = e^{-\beta(X/H)^2}$$

Where H is the distance from the jet discharge to the boundary (see Figure 13), X is the distance along the surface measured

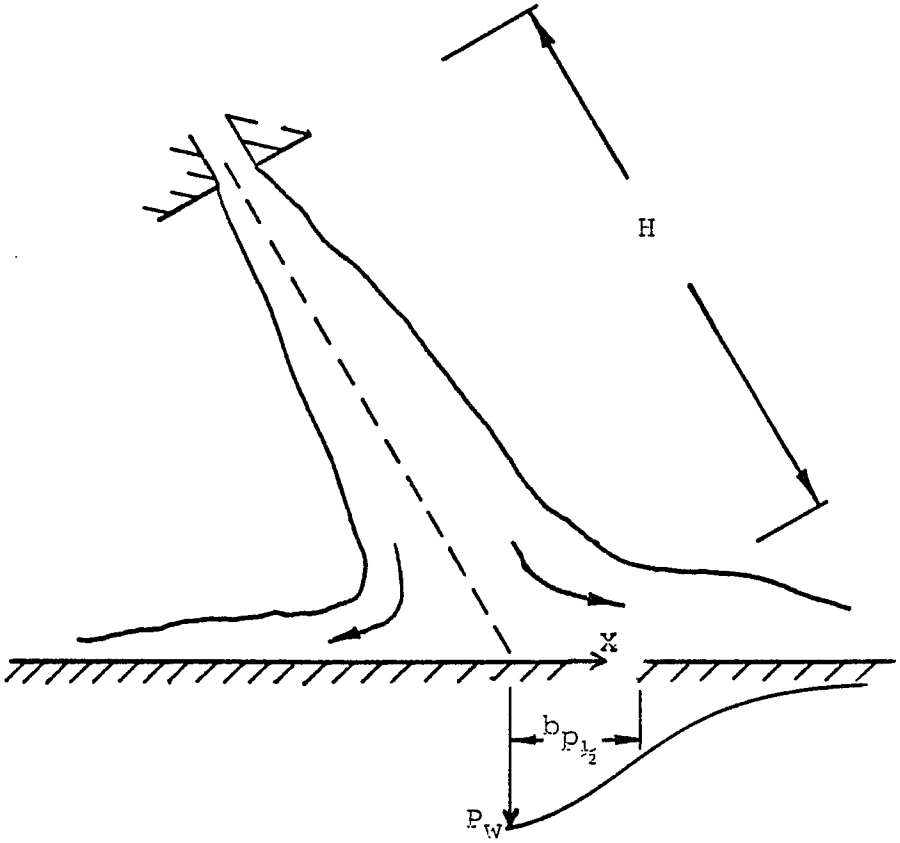

Figure 13. Schematic of a Plane Impinging Jet

from the stagnation point, and β is an empirical constant. This constant is, in effect, a pressure spread parameter, which is independent of H.

The value of β was found to be 38.5 for two-dimensional jets [48]. Figure 14 compares the pressure distribution along the wall for an offset jet in the impingement region, and an impinging jet, where $b_{P1/2}$ is the distance along the surface where the pressure is half the stagnation pressure. It is apparent that the pressure distribution for these two cases are similar in nature. Therefore we will assume:

$$\frac{P_w}{P_m} = e^{-\beta\left[\frac{x-x_A}{h}\right]^2} \tag{76}$$

The value of β is determined by comparison to experimental data. Taking the derivative of equation (76), we obtain:

$$\frac{dP_w}{dx} = -2\beta\,\frac{P_m}{h^2}\,(x-x_A)\,e^{-\beta\left[\frac{x-x_A}{h}\right]^2} \tag{77}$$

Assuming the pressure varies linearly across the jet, the pressure terms in equations (73) and (74) become:

$$\int_0^{\delta}\frac{dP}{dx}\,dy \approx \delta\,\frac{dP_w}{dx}\left[1-\frac{1}{2(1+\sqrt{2}\,b/\delta)}\right]$$

$$\int_{\delta}^{w}\frac{dP}{dx}\,dy \approx \frac{1}{2}\,\frac{dP_w}{dx}\left[\sqrt{2}\,b+\delta-\frac{\delta^2}{\sqrt{2}\,b+\delta}\right] \tag{78}$$

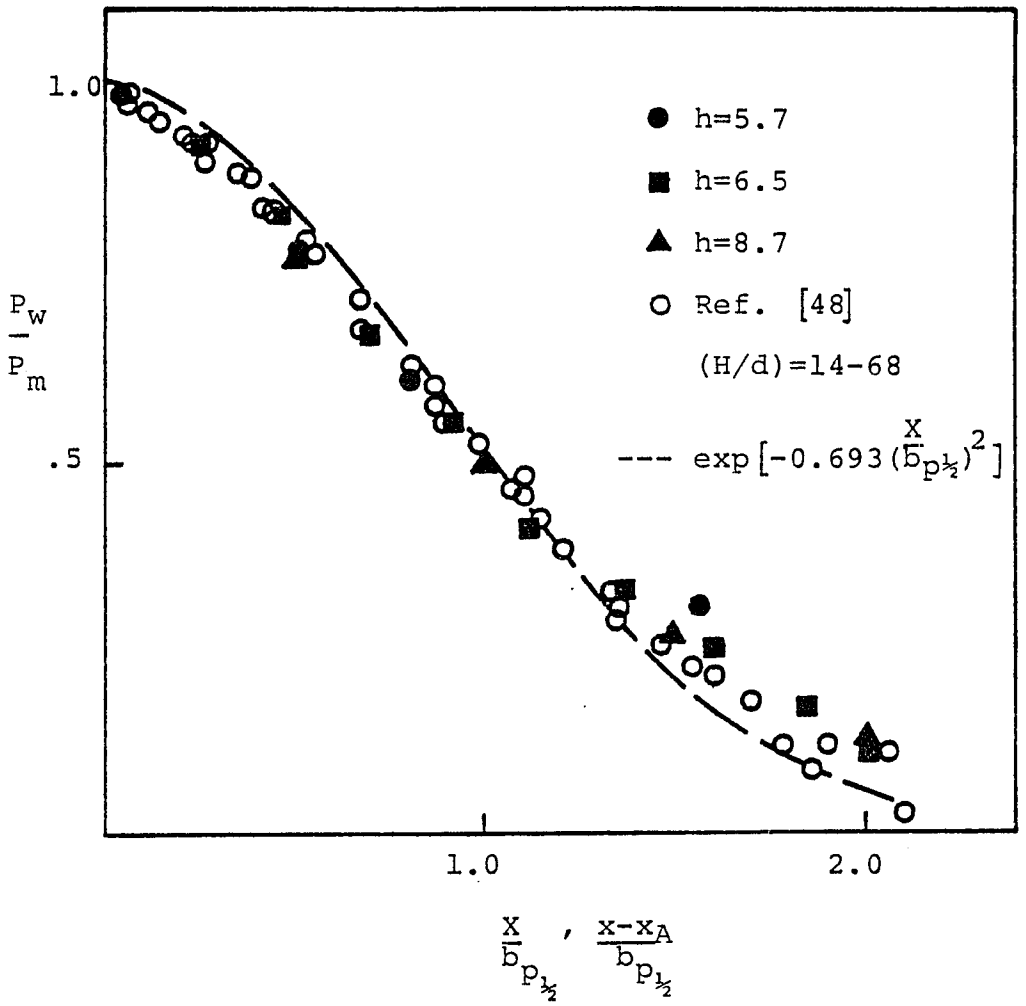

Figure 14. Comparison of Wall Pressure Profiles of Impinging and Offset Jets

Having determined the wall pressure profile in the impingement region we can also evaluate F_p in equation (57). The wall pressure force, F_p, is given by:

$$F_p = \int_{x_A}^{\infty} P_w \, dx \tag{79}$$

or using equation (76) we have:

$$F_p = \frac{\sqrt{\pi}}{2} \frac{h^2}{\beta} \rho_m$$

b. Boundary Conditions

The boundary conditions for the impingement region are obtained by matching with the pre-attachment region at the point of re-attachment. The values of u_m and b are taken directly from the velocity profile just prior to the point of impingement, whereas δ is set equal to the distance between the boundary and the jet axis.

4. Impingement Region: Temperature Distribution

As with the velocity distribution, the temperature distribution is expected to be similar in nature to the wall jet. The excess pressure does not affect the conservation of energy equation or the temperature profile. The

value of Θ_m in the impingement region is therefore obtained from equations (26) and (30).

5. Wall Jet Region

Two-dimensional wall jet theory can be used to describe the jet behavior in this region. As x becomes sufficiently large, $\frac{d\bar{P}}{dx}$ in equations (68) and (69) becomes zerc, and the governing equations become exactly identical to the wall jet equations. The solution to these equations has already been described in Section A.

6. Numerical Solution

The equations governing the jet-boundary solution are sclved numerically for each of the regions. Figure 15 shows a schematic flow diagram of the computer program. The only input to the program is the offset parameter h plus a suitable guess for x_i and y_i. If h=0, the program gives the wall jet solution outlined in Section A. Otherwise, it first calculates the jet trajectory based on the initial guess of x_i and y_i, and then calculates the appropriate zone of flow establishment boundary conditions. Equations (45) to (47) are then solved numerically for u_m, b and $\bar{P}$ until the jet attaches (see section B, part 1). Once the jet hits the boundary, the program checks to see if the reattachment boundary conditions (56) and (58) are satisfied.

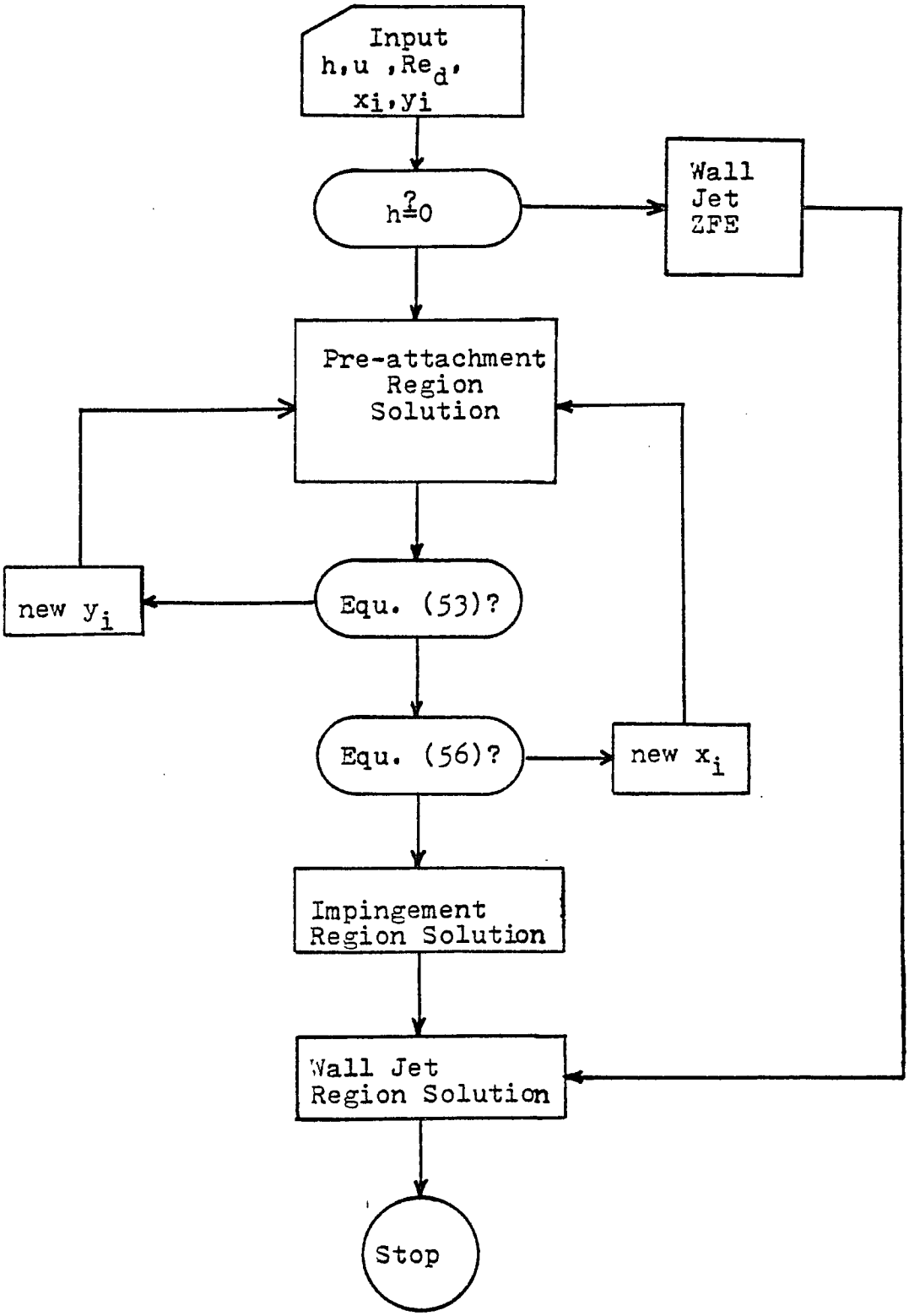

Figure 15 Flow Chart of the Numerical Solution

If they are not satisfied, the program chooses a new value foe either x_i and y_i, depending on which condition the program is iterating. This procedure continues until both equations (53) and (56) are satisfied. Once the velocity field is known, equation (65) is used to solve for the temperature along the jet axis.

Using the values of b, u_m and δ from the pre-attachment solution as boundary conditions, the program then solves equations (23), (73), (74) and (30) for u_m, b, δ and θ_m in the impingement and wall jet regions.

VI. EXPERIMENTAL SETUP

Experimental investigation of the two-dimensional jet-boundary interaction problem was conducted in the low speed wind tunnel facility of the Mechanical Engineering Laboratory of the City College of New York.

A. Wind Tunnel

The wind tunnel is shown schematically in Figure 16. The design is similar to one built by Sexton [51] for Building Research Station and was used previously by Tandowski [52] to model street level pollution due to short stack emissions. The tunnel has a test section measuring 42 in. wide by 30 in. high by 90 in. long. The working section is enclosed in a large pressure tight chamber.

Air flow through the wind tunnel, which simulates free stream motion is produced by a 7.5 horsepower centrifugal blower which exhausts air from the observation chamber. The flow is drawn through a bellmouth entry constructed of flexible 1/8" plywood molded over a rib and spar framework. The smooth curves of the bellmouth accelerate the flow smoothly and avoid separation problems associated with sharp edged entrances. After passing through a short settling length the flow passes through a 3-inch section of honeycomb with 1/4-inch cells, which breaks up any large scale turbulent eddies and produces unidirectional flow. Immediately

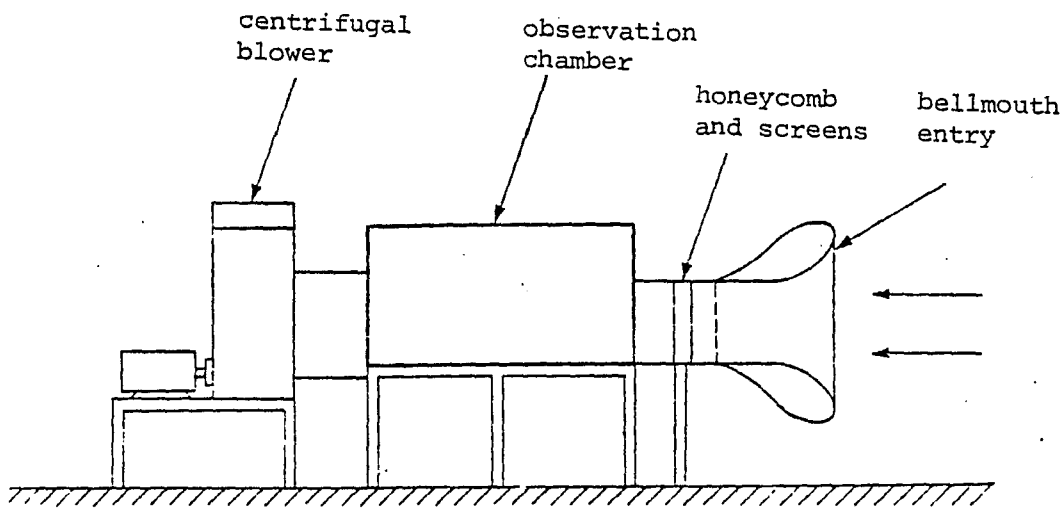

elevation

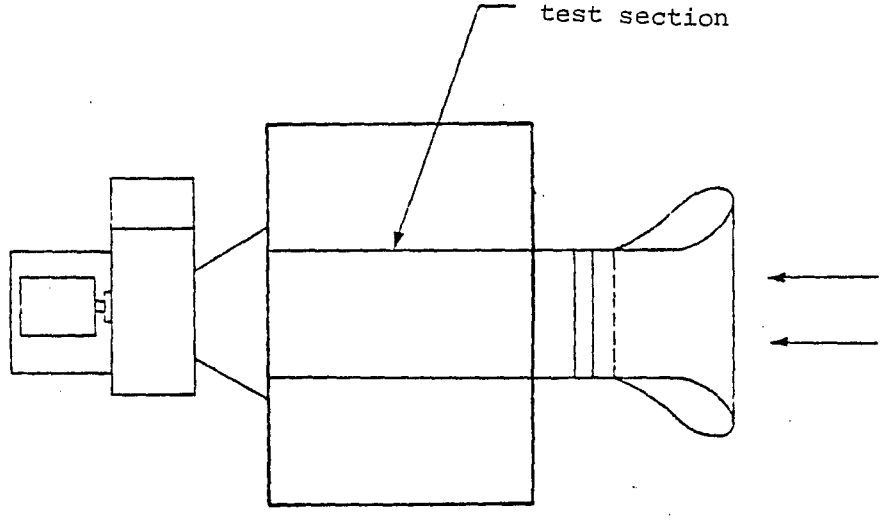

plan view

Figure 16. Schematic Drawing of the Low Speed Wind Tunnel

following the honeycomb there is screening composed of Scott Filter Foam sandwiched between wire screens. The uniform distribution of flow resistance over the entrance area produces a flow with uniform velocity when the chamber is evacuated by the blower. The maximum velocity that can be obtained under this arrangement with the blower operating at full capacity is approximately 13 ft/sec. Any velocity below that can be produced by adjusting baffles at the blower's exhaust, by adjusting a variable speed belt drive on the blower motor, or by the amount of screening across the entry.

B. Heated Air Supply

The heated jet supply system, shown in Figure 17, was designed to provide a wide range of discharge velocity and temperature. A centrifugal blower with a capacity of 70 scfm was used to supply air to a 4.5 kw Chromolox electric circulation heater. The air flow rate to the heater was controlled by a valve located upstream of the discharge. A calibrated venturi-meter was used to measure the flow rate.

The electric heater was equipped with a thermostat for maintaining a supply of constant temperature air. Because of the long distance between the heater and the tunnel, there was considerable heat loss through the pipe. However, this length of pipe helped dampen small temperature fluctuations not picked up by the thermostat. Maximum temperatures up to

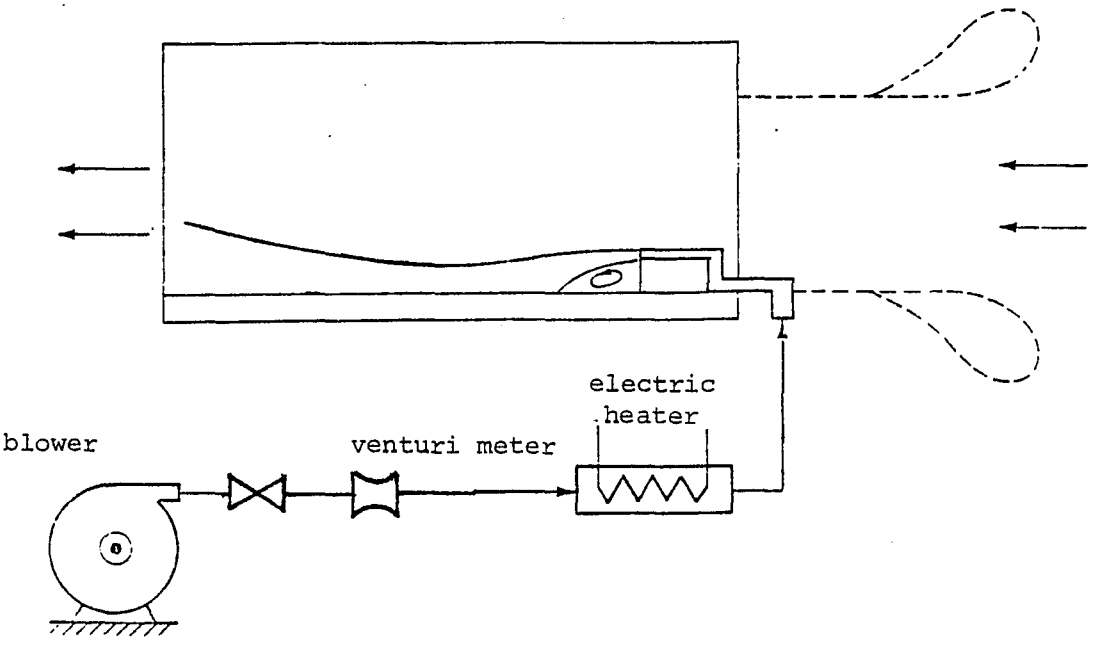

Figure 17. Heated Air Supply System

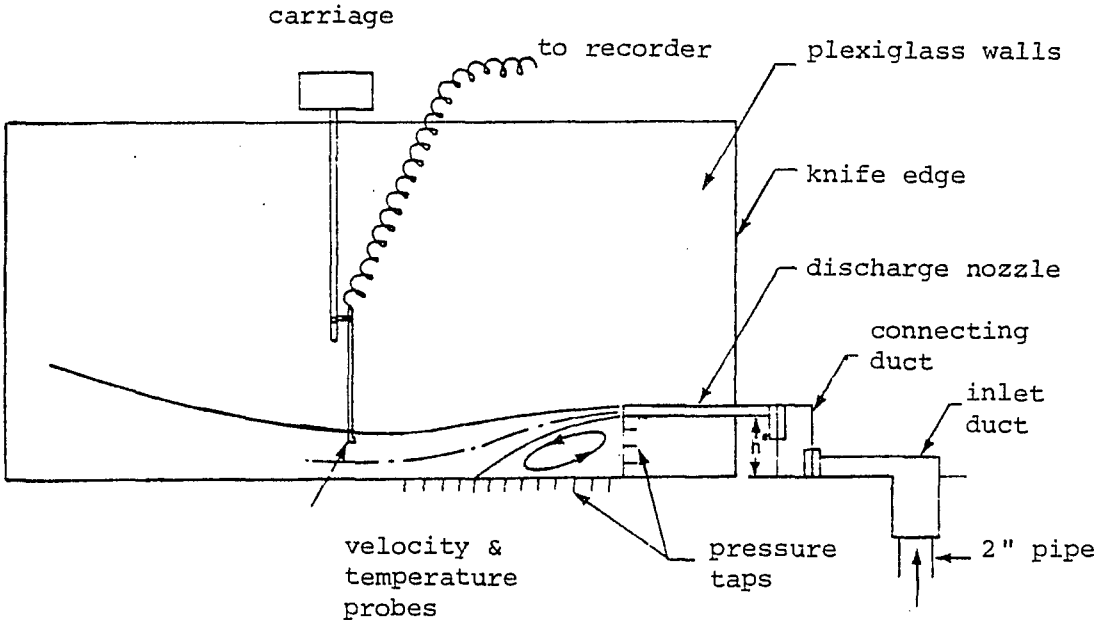

Figure 18. Test Section Elevation

250°F were maintained to ±1°F.

C. Test Section

Observations and measurements on two-dimensional jet-boundary interaction were made in the test section shown in Figure 18. The free stream velocity through the test section was designed to be steady and uniform with recorded turbulence intensity levels below .1%. The heated air was supplied to the test section through an insulated rectangular inlet duct which was connected to a horizontally oriented rectangular nozzle. Two different nozzles were used, one with a nozzle height of 0.26 in. and the other of 0.46 in. Both had a nozzle width of approximately 4 7/8 in. A calibrated venturi-meter was used to calculate the value of the flow rate. The discharge jet velocity for these nozzles could be varied from approximately 10 to 120 ft/sec, depending on nozzle height. Discharge Reynolds numbers were well within the turbulent range. The Froude number based on nozzle height d and the available capacity of the electric heater can be varied from approximately 10 to infinity. Sample discharge velocity and temperature measurements are shown in Figure 19.

The offset distance h* between the jet and the bottom plate was varied using removable connecting ducts of different dimensions (see Figure 20). The offset parameter, $h=h^*/d$, was also varied using different nozzle heights d* at a fixed

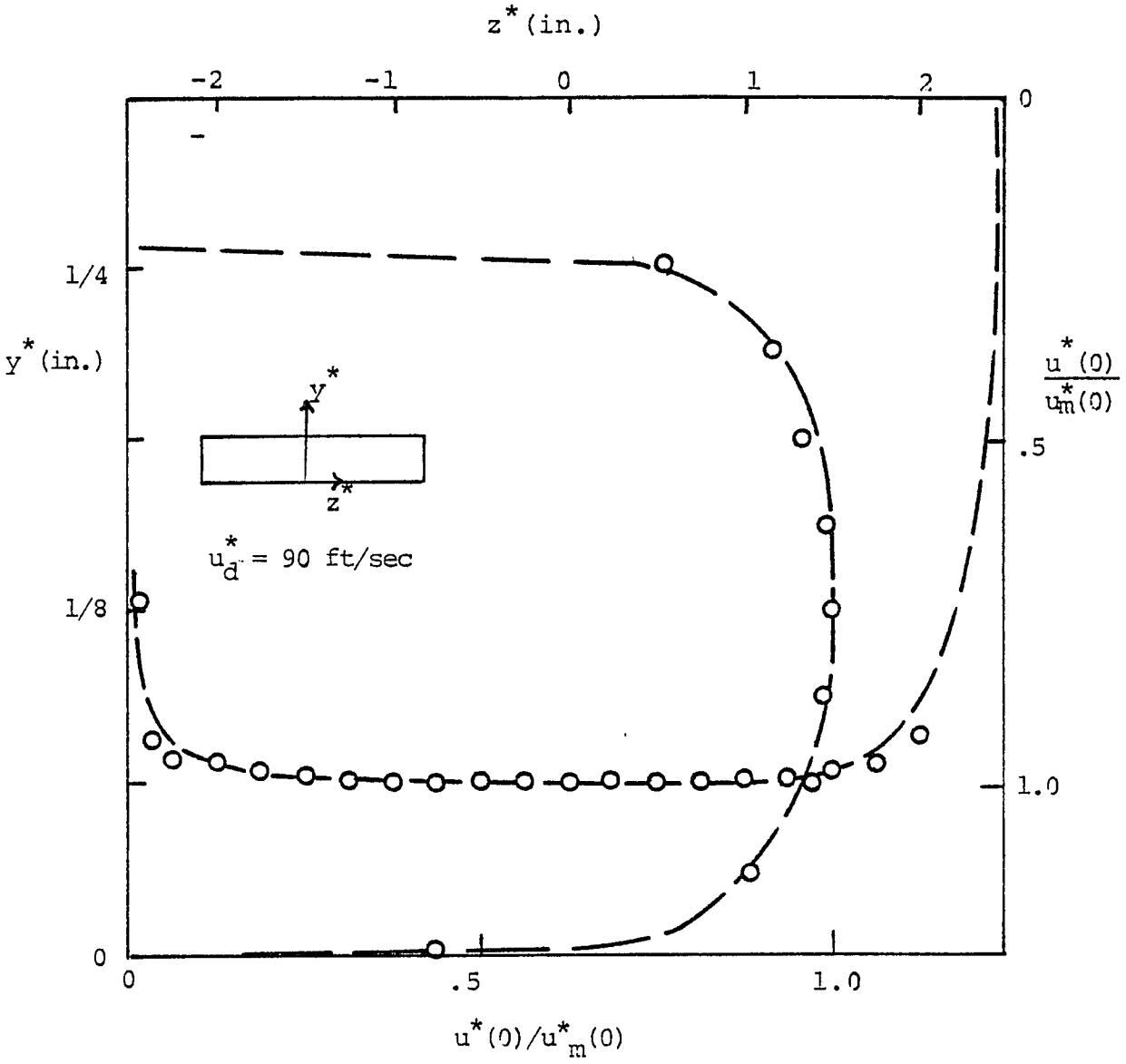

Figure 19a. Velocity Profile at Jet Discharge Nozzle

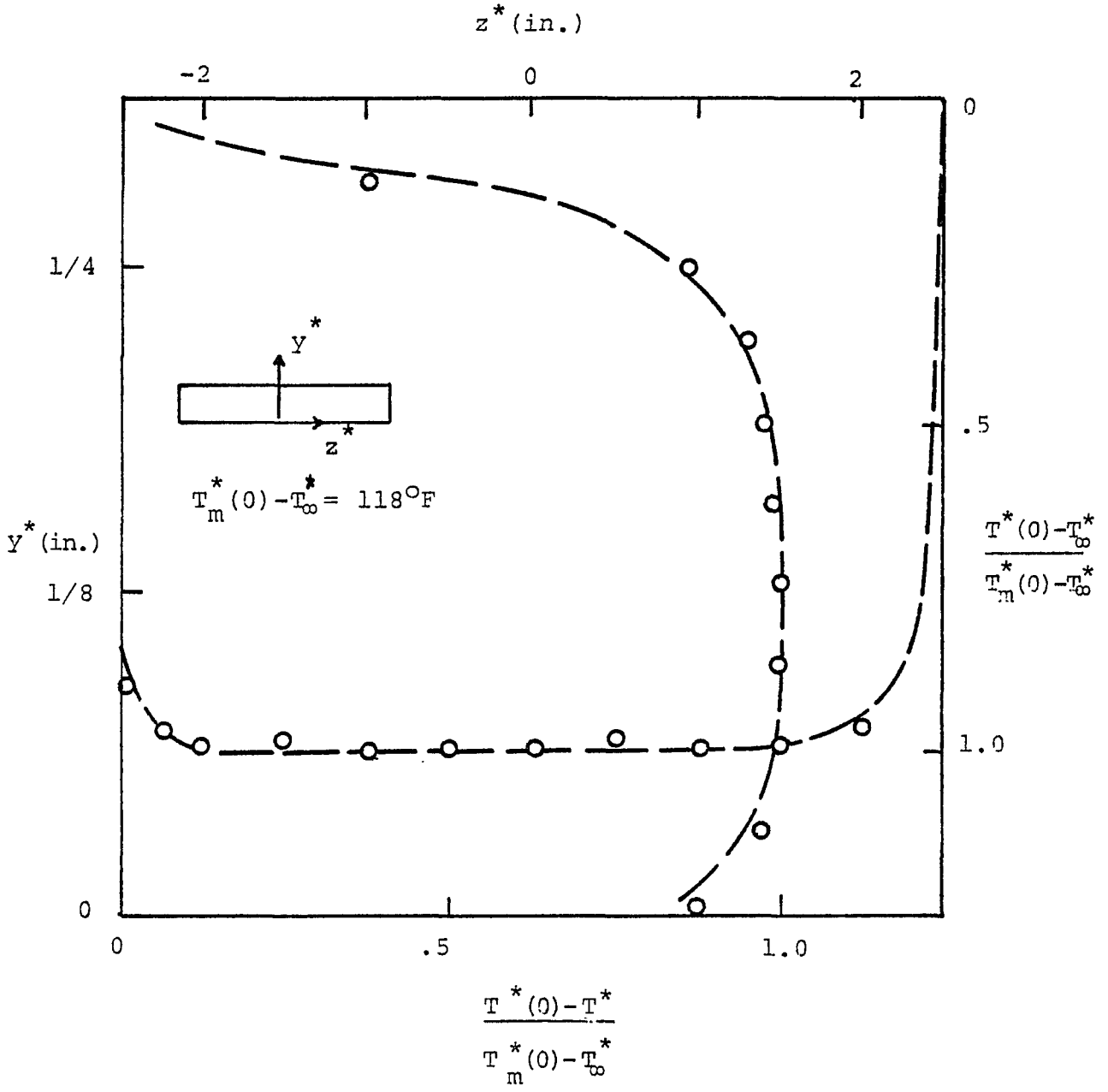

Figure 19b. Temperature Profile at Jet Discharge Nozzle

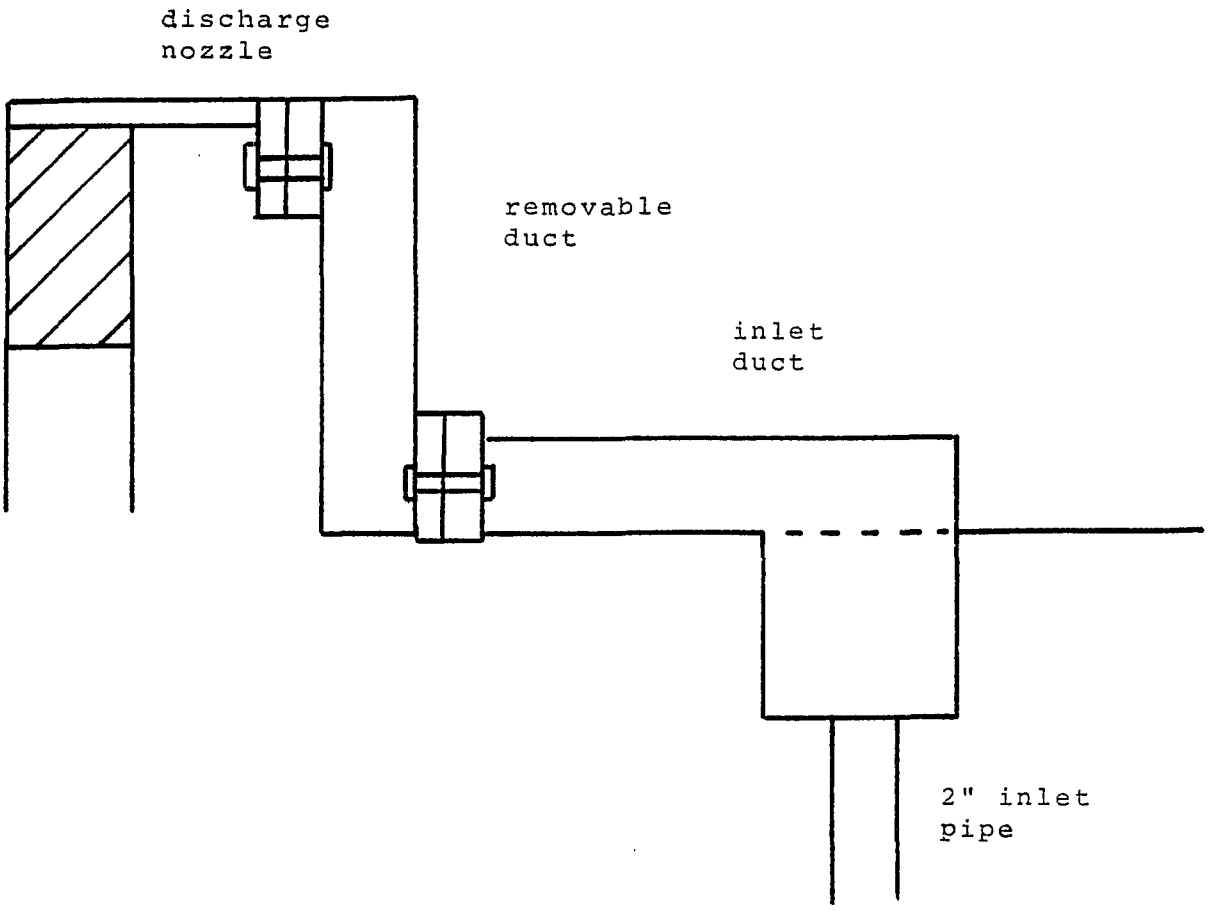

Figure 20. Schematic Drawing of Removable Duct

location h*. This arrangement gave a range of h from zero (wall jet) to 13.8.

In order to insure the jet remains two-dimensional, two plexiglass plates were placed vertically on each side of the jet nozzle, forming a channel with a spacing equal to the nozzle width. Each plate is 72 in. long, 20 in. high and 3/8 in. thick with a tapered upstream leading edge designed to prevent separation of the free stream. A horizontal plate was inserted at the bottom of the channel with which jet interaction took place.

D. Instrumentation

Probes for measuring jet velocity, temperature and pressure were mounted on a uniquely designed three-dimensional traversing mechanism [52]. The traversing mechanism consists of a probe carriage mounted on ball bushings which ride two horizontal rails, and a feed screw that moves the carriage across the working section. The probes were suspended well below the probe carriage so that the flow in the vicinity of the probes was not affected by the presence of the carriage. The horizontal traversing mechanism was mounted on vertical rails and feed screws to the probes could be moved to any position on a cross-section plane of the test section. The feed screws were turned by Minarik variable speed motors and controls.

To measure mean velocities, a TSI (Thermo-Systems Inc.) 1050 series constant temperature hot wire anemometer system with DISA 55A22 (Danske Instruments Inc.) hot wire probe aligned perpendicular to the mean flow direction was used. The hot wire calibration was done on a TSI model 1125 Calibrator which is, in essence, a precision orifice meter where the pressure drop across the orifice is related to the velocity. The pressure drop was measured using a Furness Controls Ltd. micromonometer capable of measuring down to 0.1 mm. of water full scale, with 3% accuracy full scale.

Velocity measurements of heated wall jets were also made using a total pressure pitot tube connected to the micromonometer at small velocities or a Valadine model 3300 pressure transducer for higher velocities.

Temperature measurements were made using copper-constantan thermocouples coupled with either an Omega Engineering Inc. electronic ice point, or an Omega Engineering Inc. model 175 Digital Temperature Indicator. Micimonometer, pressure transducer and thermocouple readings were fed into a Hewlett-Packard HP 3480 Data Logger (digital voltmeter and recorder) for further data reduction. Mean velocities for the heated wall jet were computed using the measured dynamic pressure and temperature at any given point. Mean velocities measured with the hot-wire anemometer or the pitot tube probe were found to be nearly identical.

RMS turbulence measurements were made using a DISA 55D35 RMS meter. The RMS values are read off the face meter

on the unit. The time constant was chosen such that the the meter's needle remained on a fixed position. RMS readings were used to locate the boundary of the recirculation region (the dividing streamline) which is characterized by the locus of peak RMS values [52].

To determine the pressure distribution at the bottom surface, pressure taps were used to obtain measurements with the micromonometer. Pressure taps at the step face of offset jets were also used to examine streamline separation in the recirculation region.

To examine the basic features of the flow field, a smoke visualization scheme was used. An opaque white smoke is produced by vaporizing light oil [53] in a modified Preston-Sweeting type smoke generator [54]. The smoke produced in this manner differs in density by less than 5% from the density of air at the same temperature [55]. This means that the smoke follows the streamlines of the flow without appreciable settling over the length of the test section. A schematic diagram of the smoke generator is shown in Figure 21.

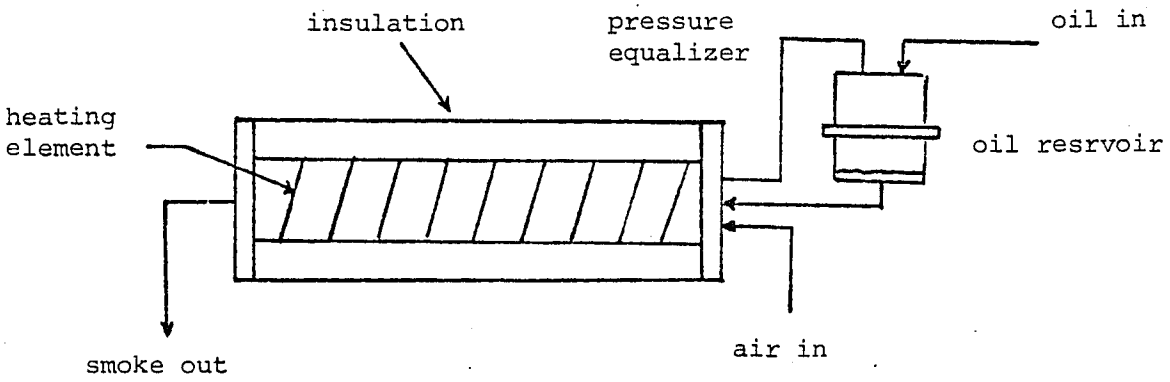

Figure 21. Schematic Diagram of the Smoke Generator

E. Verification of Experimental Data

To establish confidence in our experimental setup, and measuring techniques we compared our own experimental results with previously published experimental data for the wall jet. Figure 22 shows our experimental results for the maximum axial velocity decay of a wall jet at various Reynolds numbers. Also shown are the experimental results of Myers et al [29]. The broken line represents an approximate average of previous data compiled by Rajaratnam [34]. Agreement with previous experimental data is good. We also see that, as expected, variation of axial velocity decay with Reynolds number is small. This is because the effect on the velocity of the boundary layer is small compared to the turbulent mixing in the outer layer.

Figure 23 shows the velocity profile of a wall jet at various axial distances. As we can see, the jet profiles are nearly similar, and comparison with previous experimental data [28] is good.

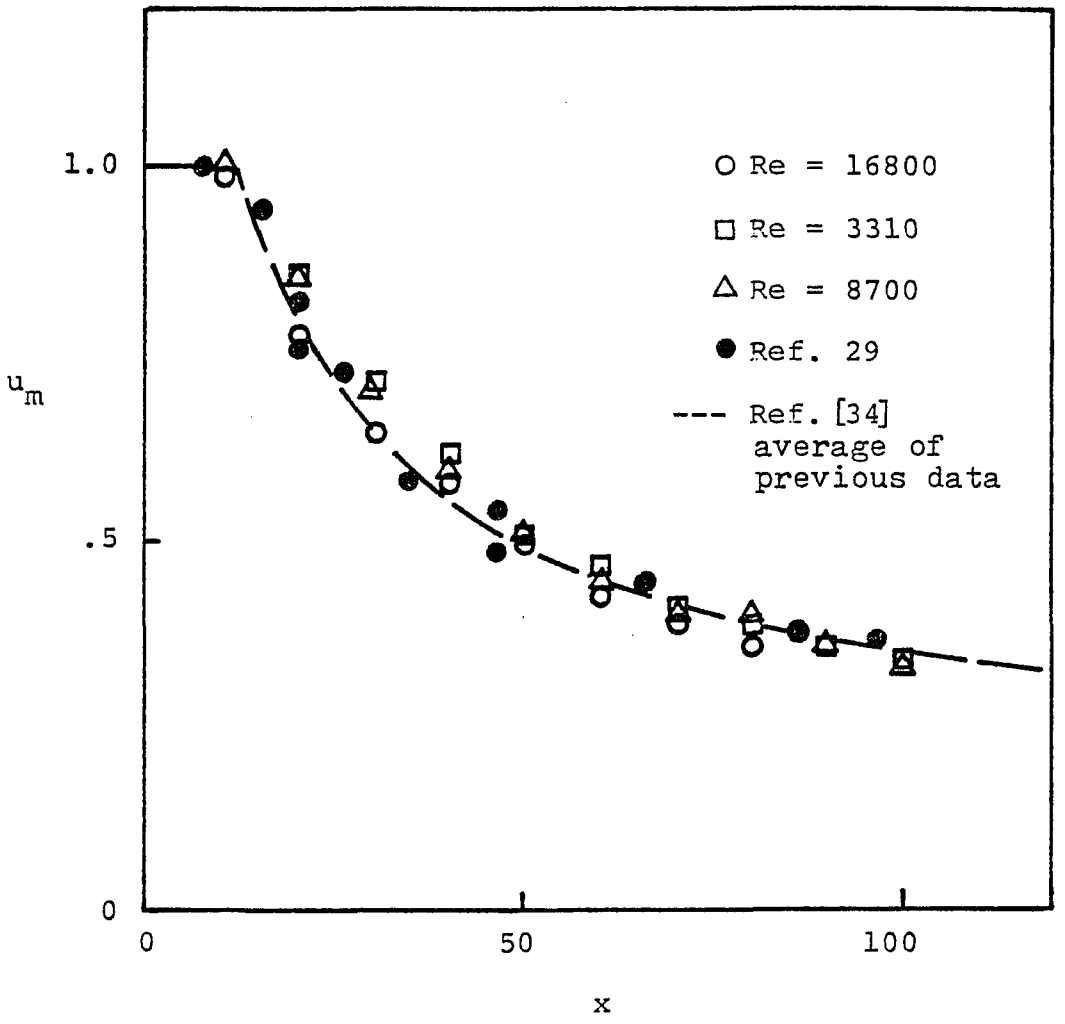

Figure 22. Experimental Axial Velocity Decay for a Plane Wall Jet

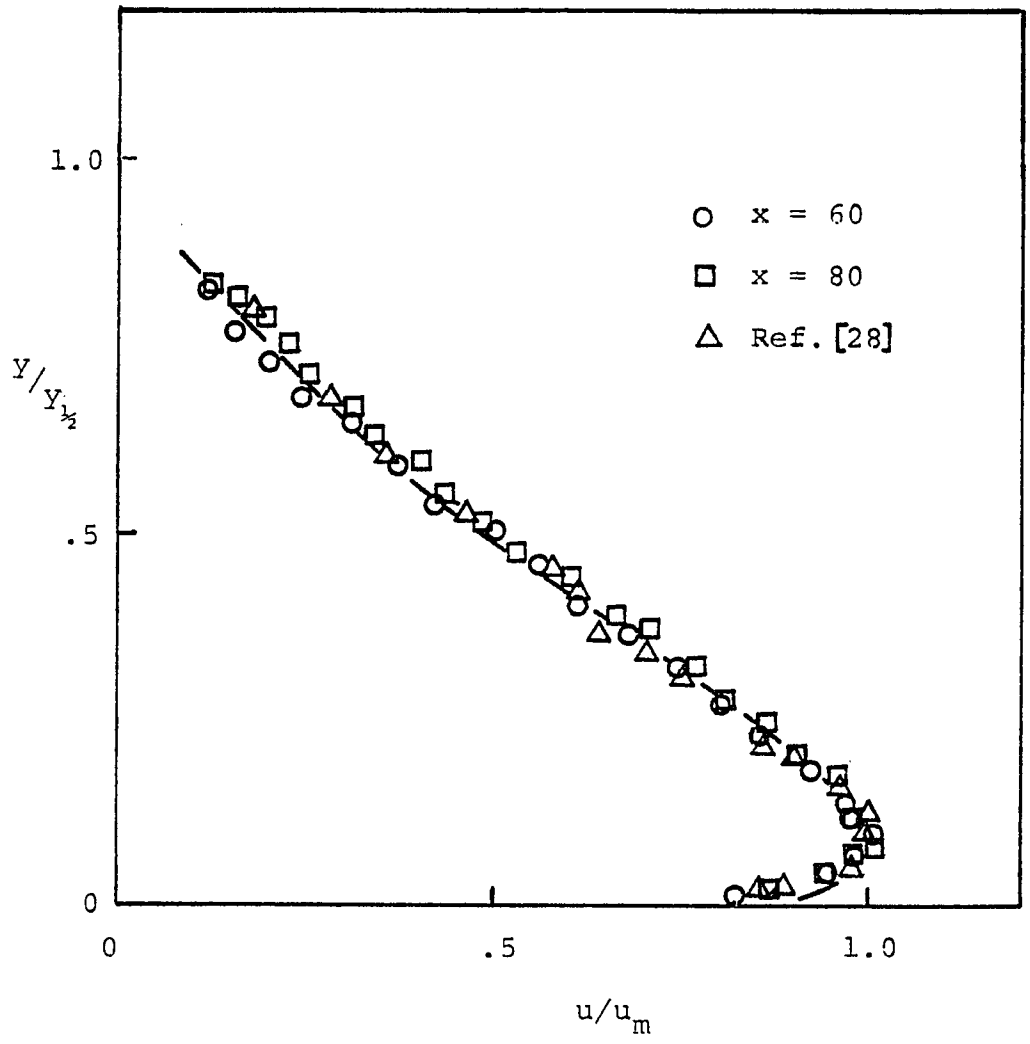

Figure 23. Experimental Velocity Profile for a Plane Wall Jet

VII. Presentation and Discussion of Results

The method of solution outlined in chapters IV and V has been used to solve for the velocity and temperature field of the two-dimensional jet-boundary interaction problem. Comparisons are made wherever possible with experimental data, in order to verify the accuracy of our solution. Additional experimental results that substantiate the basic assumptions used in the formulation of our model are also presented.

We will begin by examining the heated wall jet, and proceed to the more complex case of a jet discharging offset from, and parallel to, a solid boundary.

A. Wall Jet

1. Velocity Distribution

Equations (27) - (29) were solved, using boundary conditions (39) - (41) to obtain the solution for the wall jet. Figures 24 and 25 show the comparison between theoretical predictions and experimental data for the maximum axial velocity u_m and jet half-width $y_{\frac{1}{2}}$ at various values of the free stream velocity ratio. As can be seen, agreement is very good.

The value of the entrainment coefficient, α, used was 0.035. This was taken from Rajaratnam [34] and is based on

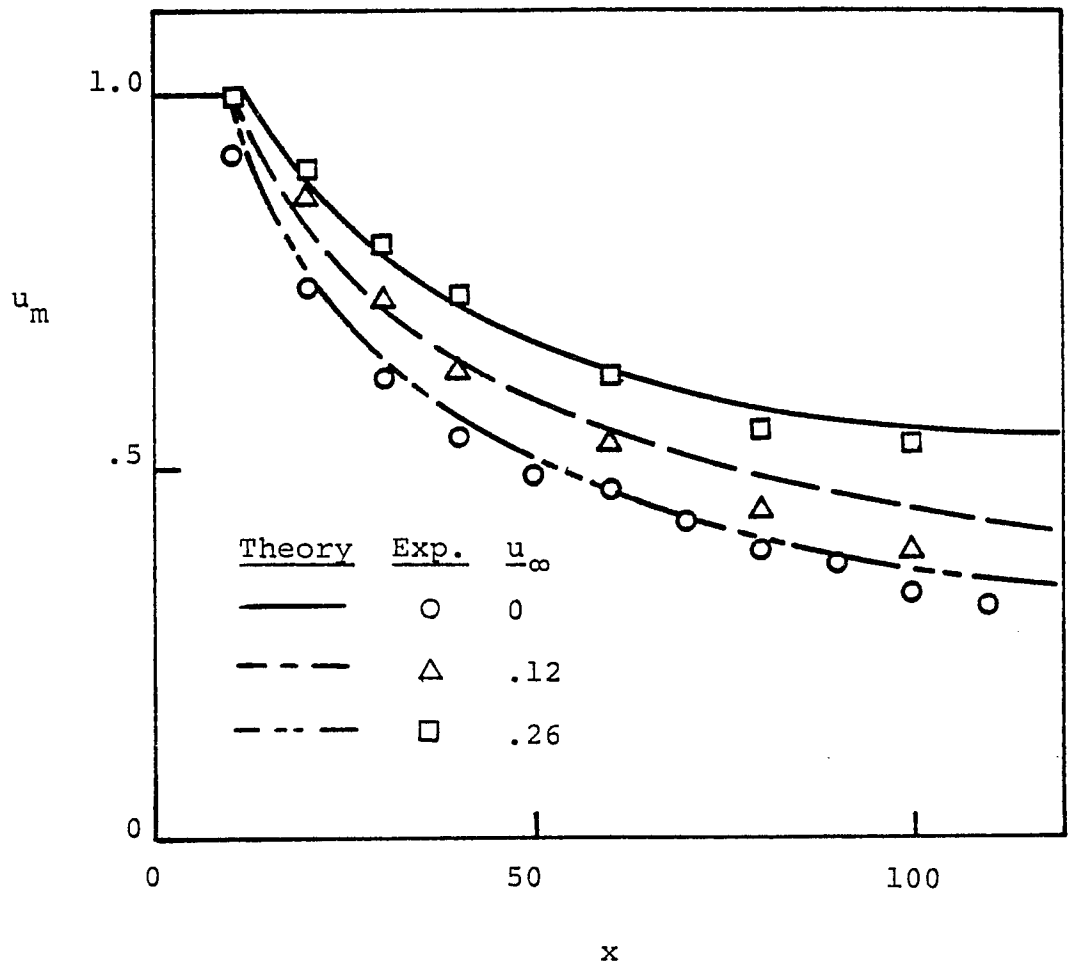

Figure 24. Axial Maximum Velocity Decay for a Two-Dimensional Wall Jet in a Coaxial Free Stream

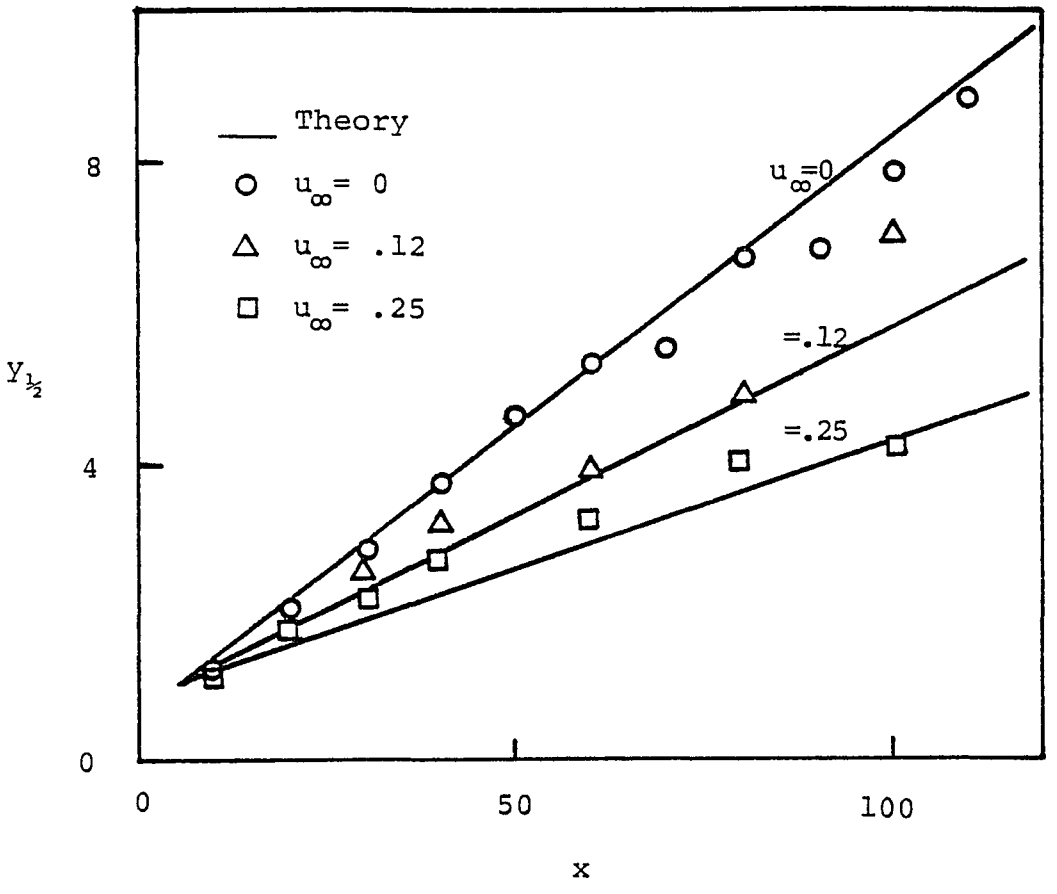

Figure 25. Jet Half-Width for a Two-Dimensional Wall Jet in a Coaxial Free Stream

the average of a number of experimental studies on the wall jet. This value was also used in the re-attached portion of the jet-boundary interaction problem where the entrainment mechanism is identical with that of a wall jet.

In the zone of flow establishment, Rajaratnam found that the value of the entrainment coefficient was somewhat lower and hence α was set at 0.031.

2. Temperature Distribution

The solution for the maximum axial temperature of a wall jet is obtained from equaticn (31), which is in terms of the turbulent Schmidt number.

Before fixing the value of the Schmidt number, we must ascertain the validity of our assumed Gaussian temperature profile. Figure 26, which shows measured temperature profiles for a wall jet, demonstrates that the Gaussian shaped temperature profile is indeed valid. Previous investigators [36] were unable to measure a region of constant temperature near the wall, and therefore assumed a linear-shaped temperature profile.

a. Turbulent Schmidt Number

Reported values of the turbulent Schmidt number for a two-dimensional free jet vary from 1.12 to 1.41 [44,45]. The value should not differ significantly for a wall jet, although it is defined differently. Experimental velocity

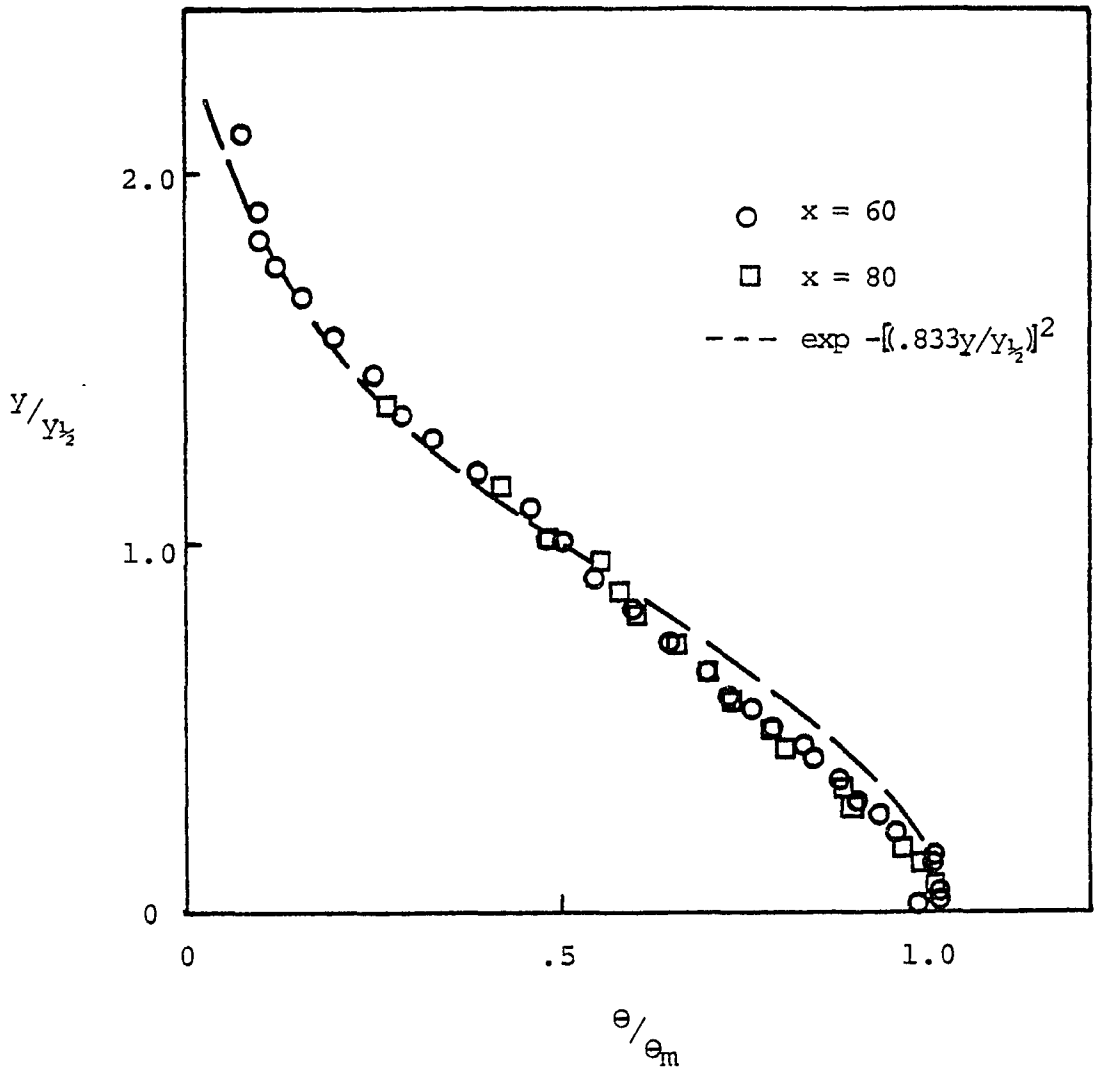

Figure 26. Temperature Profile for a Two-Dimensional Heated Wall Jet

and temperature half-widths for a two-dimensional wall jet are shown in Figure 27. A least squares fit of both curves yields a value of 1.15 for the turbulent Schmidt number.

Using this value of the turbulent Schmidt number, Figure 28 shows the solution of equation (31) for the maximum axial temperature at various values of u_∞ . Agreement with experimental data is good.

B. Jet Boundary Interaction (Offset Jet)

Theoretical results for velocity, temperature and pressure distributions of the two-dimensional jet boundary interaction problem are presented and compared with appropriate experimental data. In addition, experimental data is presented that helps describe the general flow field.

1. Flow Field - Smoke Visualization

The flow pattern of a two-dimensional heated offset jet was examined by injecting small quantities of smoke into the recirculation region from two ports in the rearward-facing step. The smoke was observed to remain trapped under the dividing streamline while moving in a vortex-like motion in the recirculation region. The outline of the dividing streamline can be approximated from photographic studies. Figure 29 shows a typical photograph of the recirculation region.

The location of the dividing streamline can also be obtained by taking measurements with an RMS voltmeter. The

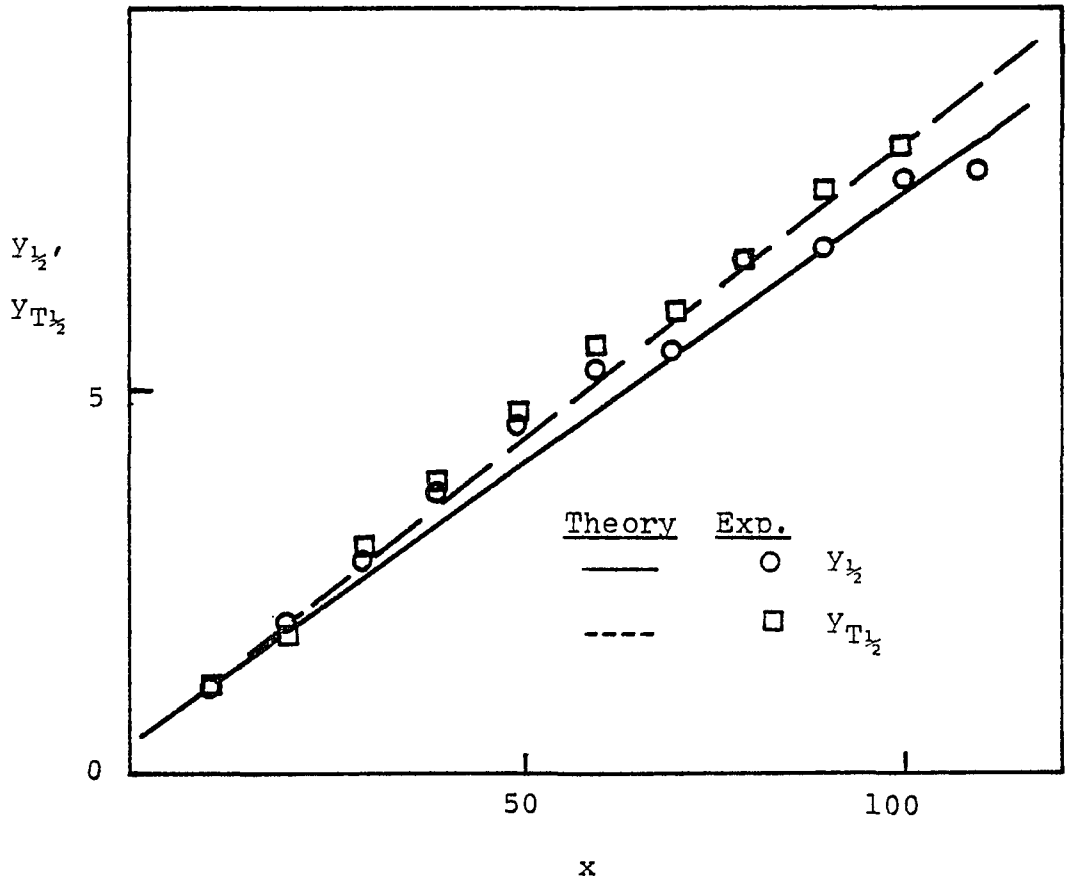

Figure 27. Velocity and Temperature Half-Widths of a Two-Dimensional Heated Wall Jet

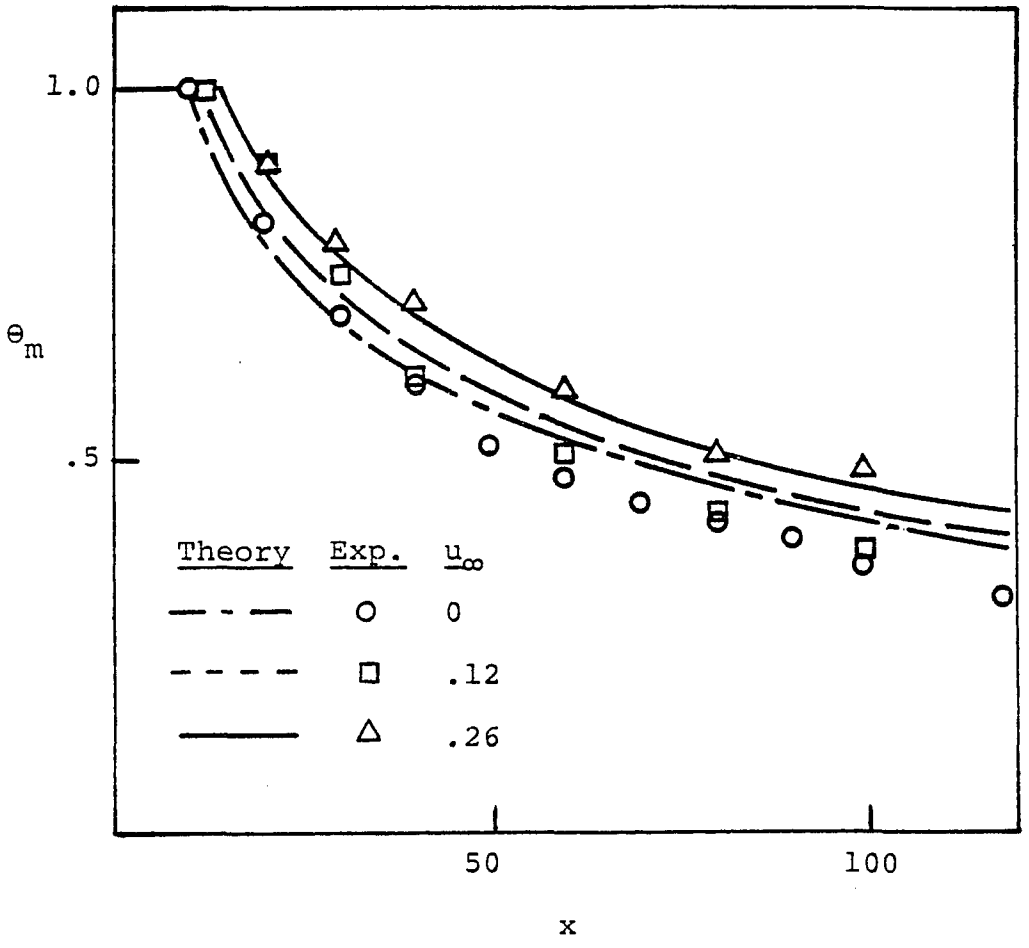

Figure 28. Axial Maximum Temperature Decay for a Heated Two-Dimensional Wall Jet in a Coaxial Free Stream

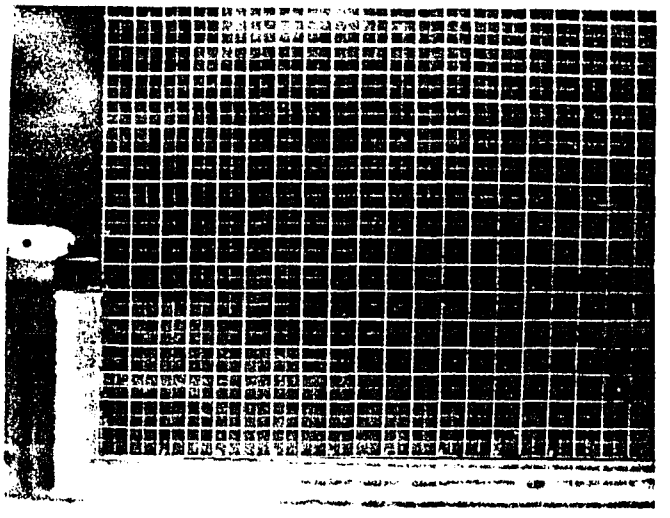

h = 6.5

White Dots:
Locus of Maximum
RMS

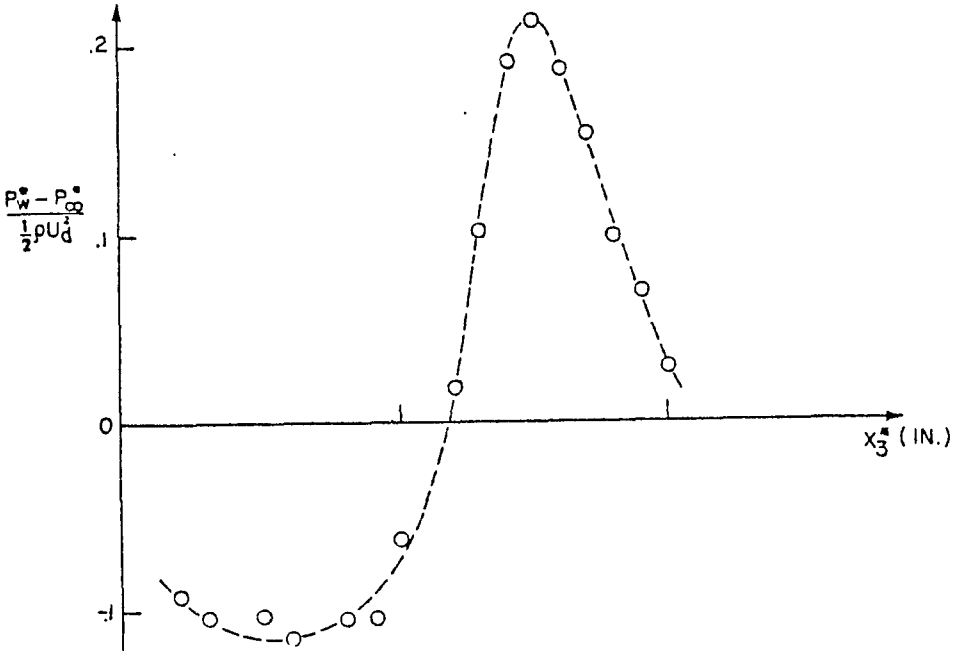

Figure 29. Smoke Photograph, Maximum RMS and Wall Pressure of the Pre-attachment Region of a Two-Dimensional Offset Jet

locus of peak RMS values roughly corresponds to the position of the dividing streamline. Peak RMS values are superimposed on the smoke photograph in Figure 29 to demostrate their correlation with the dividing streamline. In addition, surface pressure measurements are also shown to illustrate the fact that the wall pressure was found to peak near the end of the recirculation region where the dividing streamline intersects the surface. Therefore, the beginning of the impingement region can be characterized by the maximum wall pressure.

Figure 30 shows wall pressure measurements for jet-boundary interaction at various offset heights h. The effect of free stream velocity u_∞ on the wall pressure is illustrated in Figure 31. Apparently, the free stream's only effect is to delay jet-attachment and slightly increase the maximum value of the wall pressure. Otherwise, the pressure distribution appears unchanged. This is in agreement with our model assumption that for small values, the free stream will have no other effect than limiting entrainment on the outer portion of the jet, thereby restricting the spreading of the jet.

Surface pressure measurements were also obtained along the step face of the jet in order to examine the possibility of any streamline separation. The pressure on the step was found to be uniform.

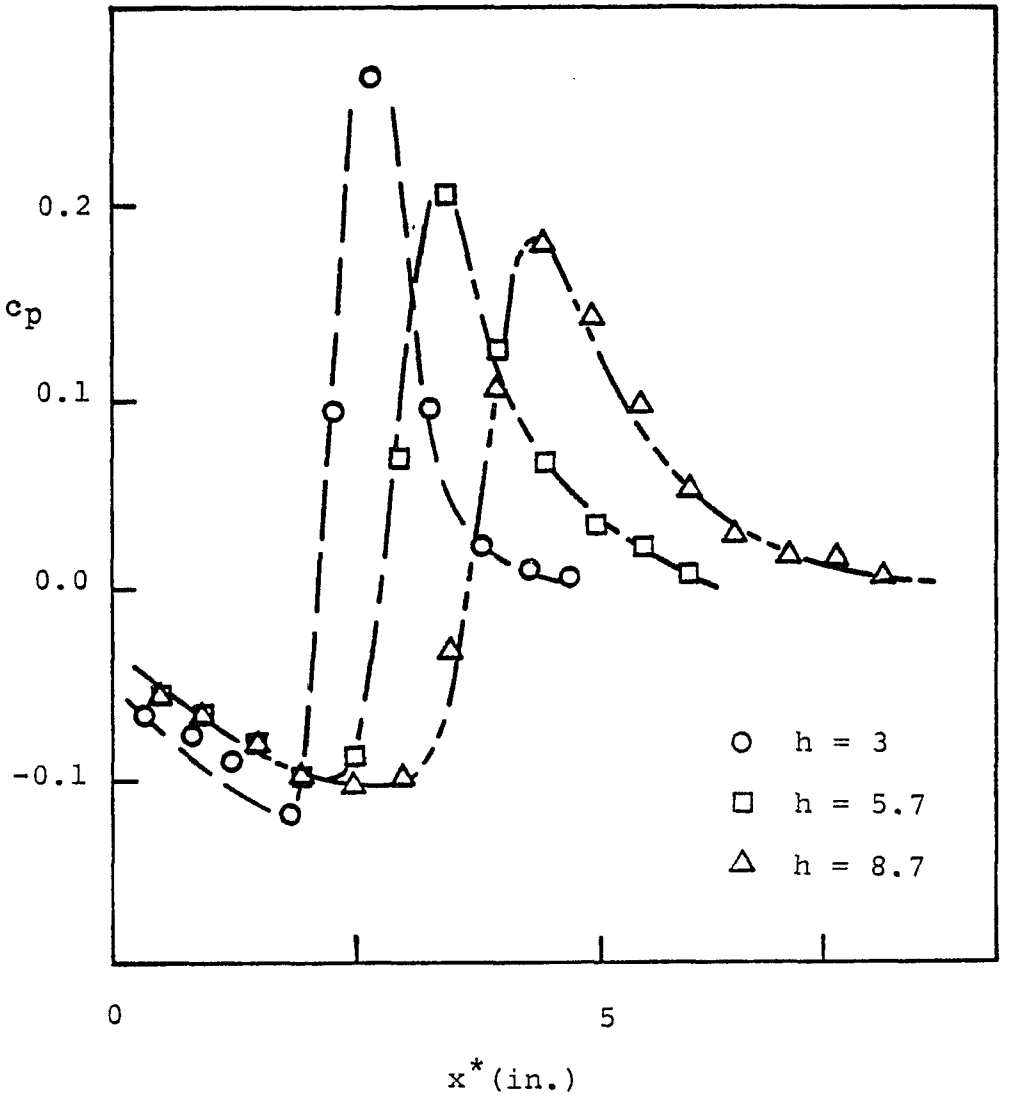

Figure 30. Wall Pressure Measurements for a Two-Dimensional Offset Jet

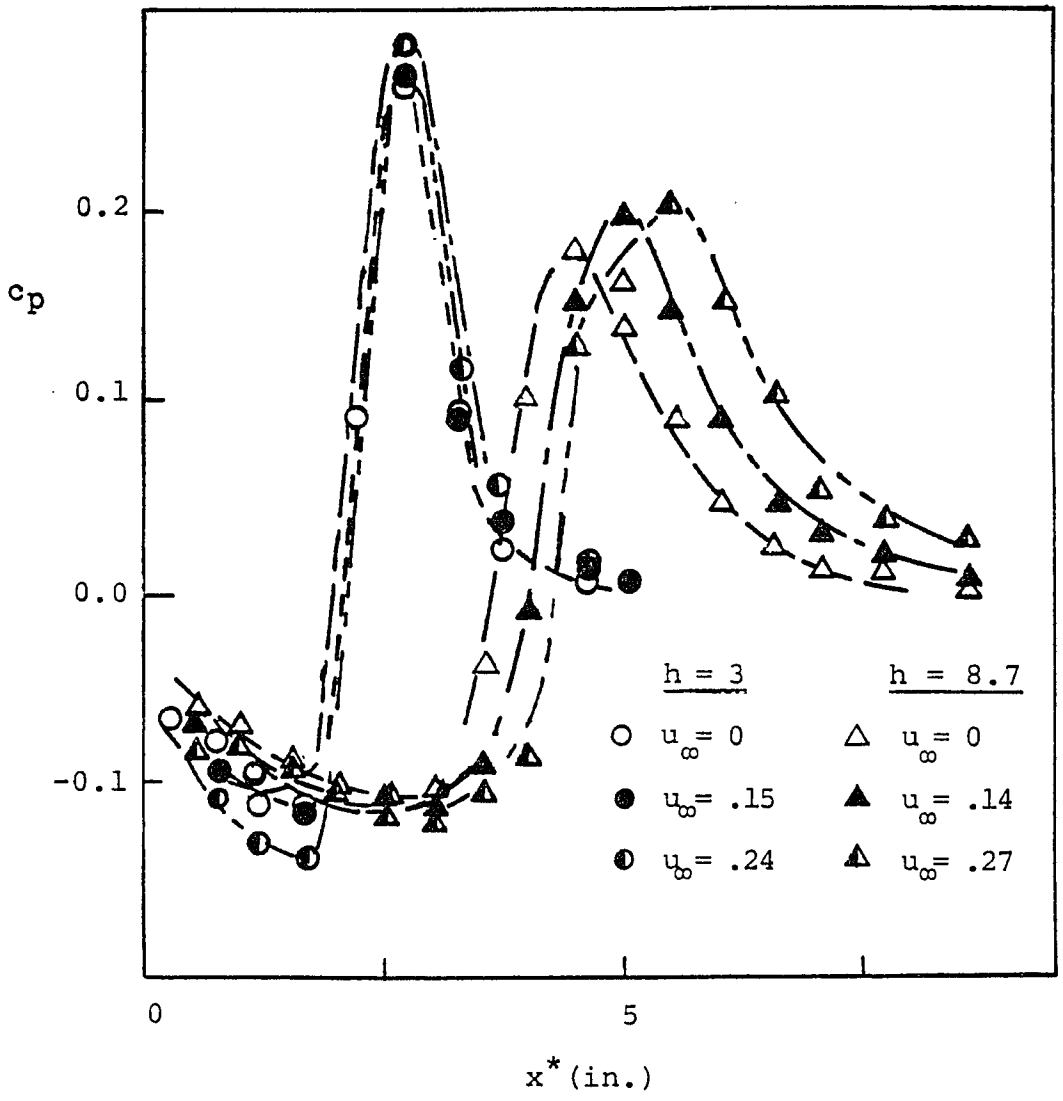

Figure 31. Free Stream Effects on the Wall Pressure of a Two-Dimensional Offset Jet

The delay in attachment is due to the fact that the jet momentum is slightly more concentrated. This also causes the increase in maximum wall pressure levels.

2. Pressure Spread Parameter

In arriving at our theoretical solution of the velocity field, one semi-empirical constant was left undetermined: the pressure spread parameter β that appears in the impingement region wall pressure profile, equation (76). This profile is employed in both the momentum equations of the impingement region (73) - (74) and in the vertical momentum boundary condition used to determine the jet trajectory in the pre-attachment region. Because of the importance of this pressure profile in the determination of the velocity field, we must substantiate its validity and show that the spread parameter β is unaffected by variations in either offset heights or free stream velocity u_∞ .

Figure 32 shows the variation of normalized wall pressure in the impingement region for various values of h and u_∞ . As can be seen, there is good agreement between the assumed wall pressure profile and experimental data with β set equal to 3.4. This appears to be true over a wide range of offset heights and free-stream velocity ratios. The spread in the data at the end of the impingement region is most likely due to the extremely small pressures being measured in some cases.

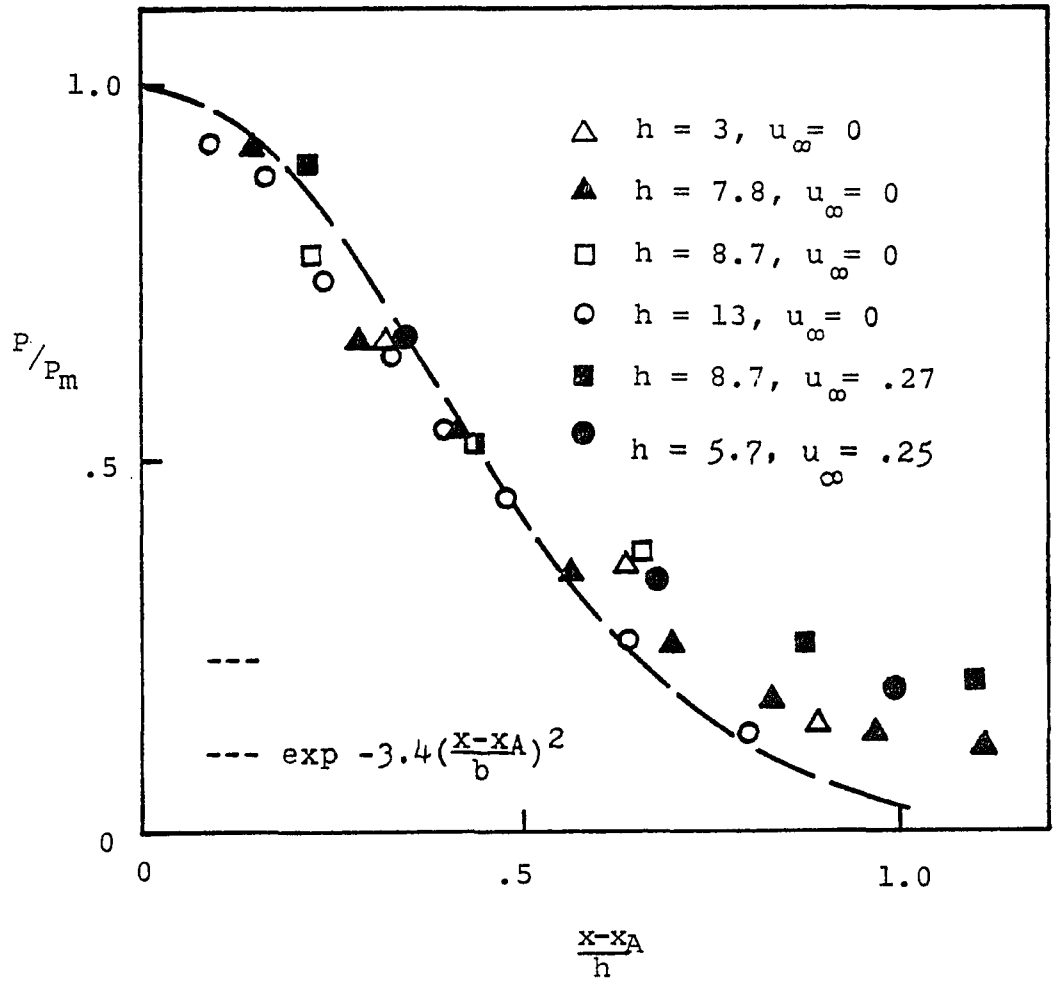

Figure 32. Normalized Wall Pressure in the Impingement Region of an Offset Jet

Having thus established the value of the pressure spread parameter, we can proceed to apply our theoretical model. We begin by looking at the pre-attachment region.

3. Pre-attachment Region

a. Jet Trajectory

By allowing the pressure to vary in the pre-attachment region, we were not forced to assume a constant jet trajectory radius of curvature. Figure 33 shows the predicted jet trajectory for various offset heights and values of u_∞ compared with experimental data. Agreement is very good. The fifth order polynomial profile seems to adequately describe the jet trajectory for this range of h. At high values of h, the predicted trajectory does not agree as well with experimental data. Figure 34 shows the jet trajectory for h = 13.8. Poor agreement between theory and experiment is perhaps due to the fact that a fifth order polynomial is of too low an order for large values of h. The prescribed trajectory, therefore, does not have a high enough number of zero derivatives at the discharge and is forced to bend down towards the boundary too early. At higher values of h, the model could be modified by using a higher order polynomial.

Figure 35 shows the variation of the re-attachment length x_A with offset height and free stream velocity ratio. Here,

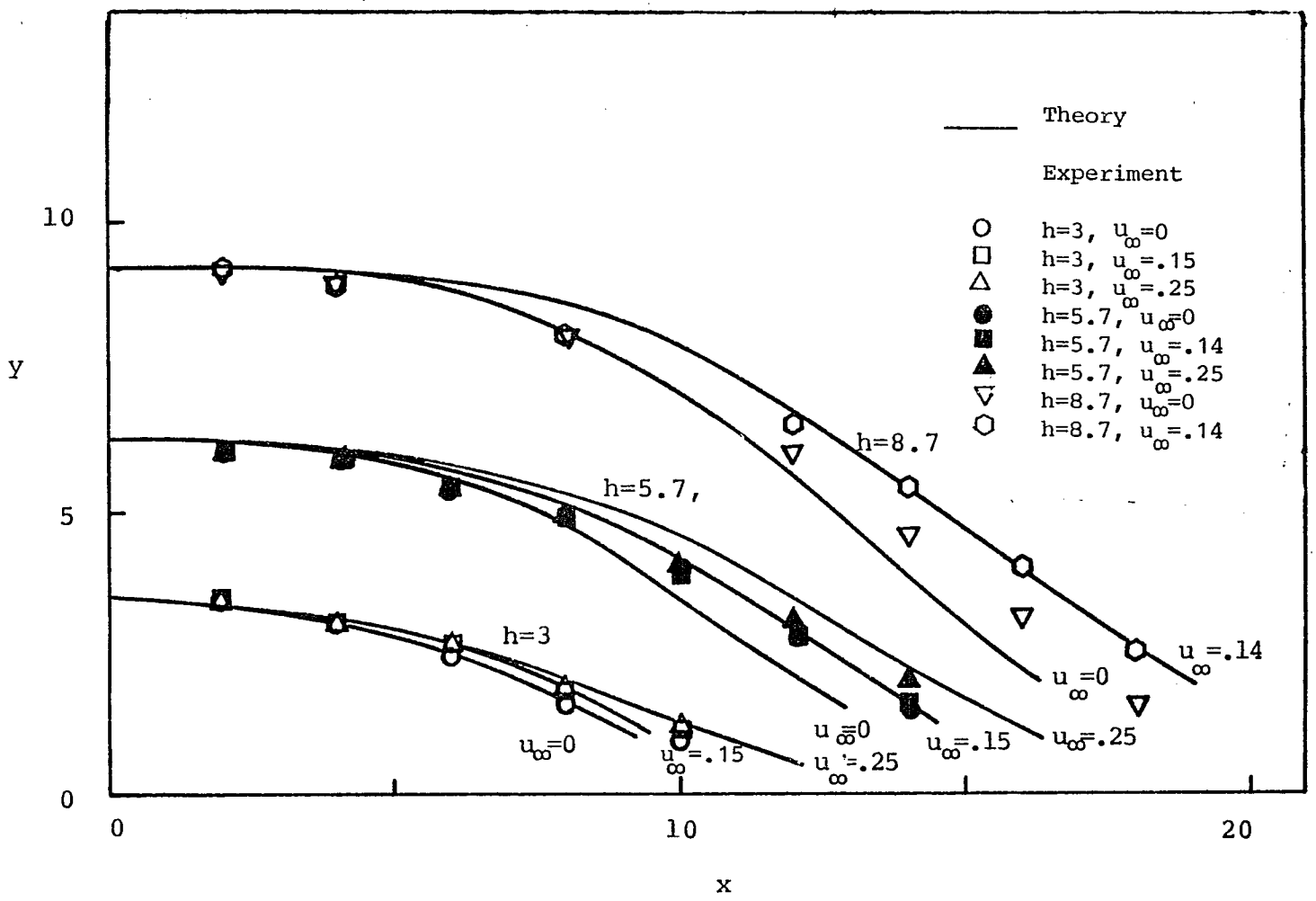

Figure 33. Jet Trajectory in the Pre-attacment Region of a Two-Dimensional Offset Jet

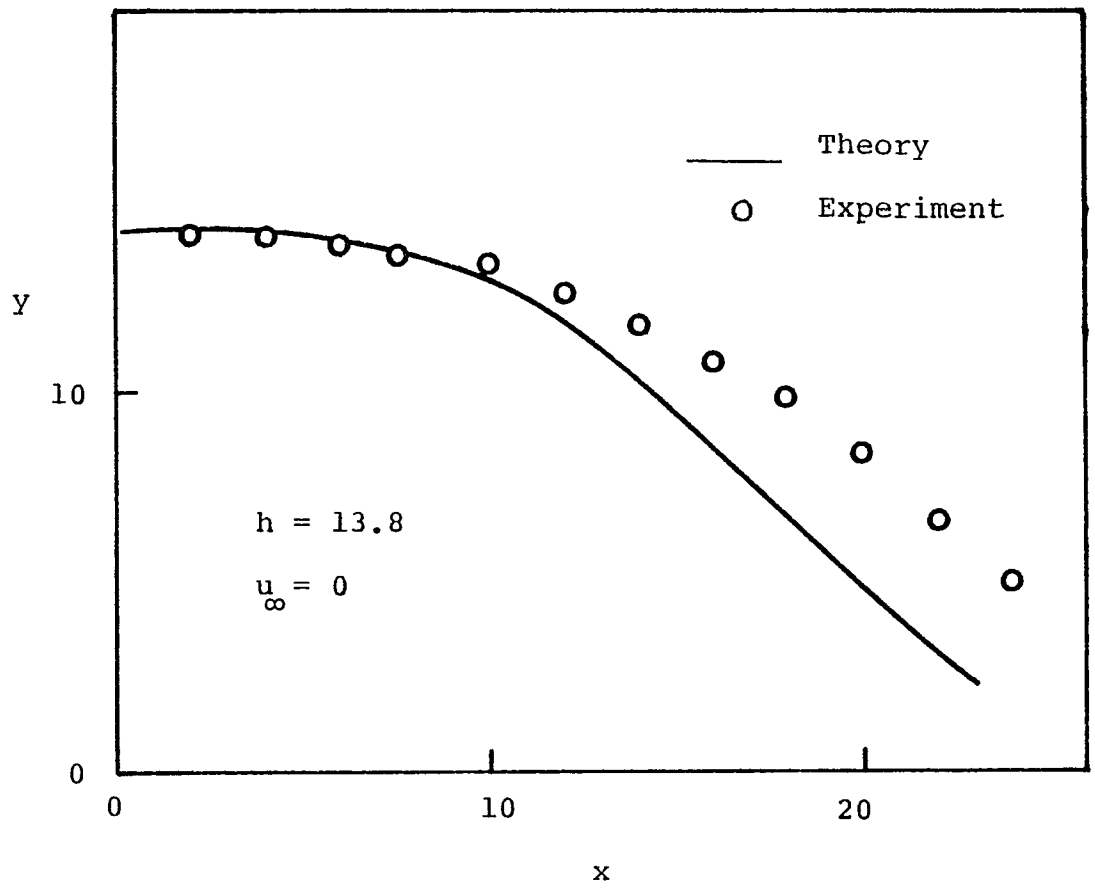

Figure 34. Jet Trajectory in the Pre-attachment of an Offset Jet (h=13.8)

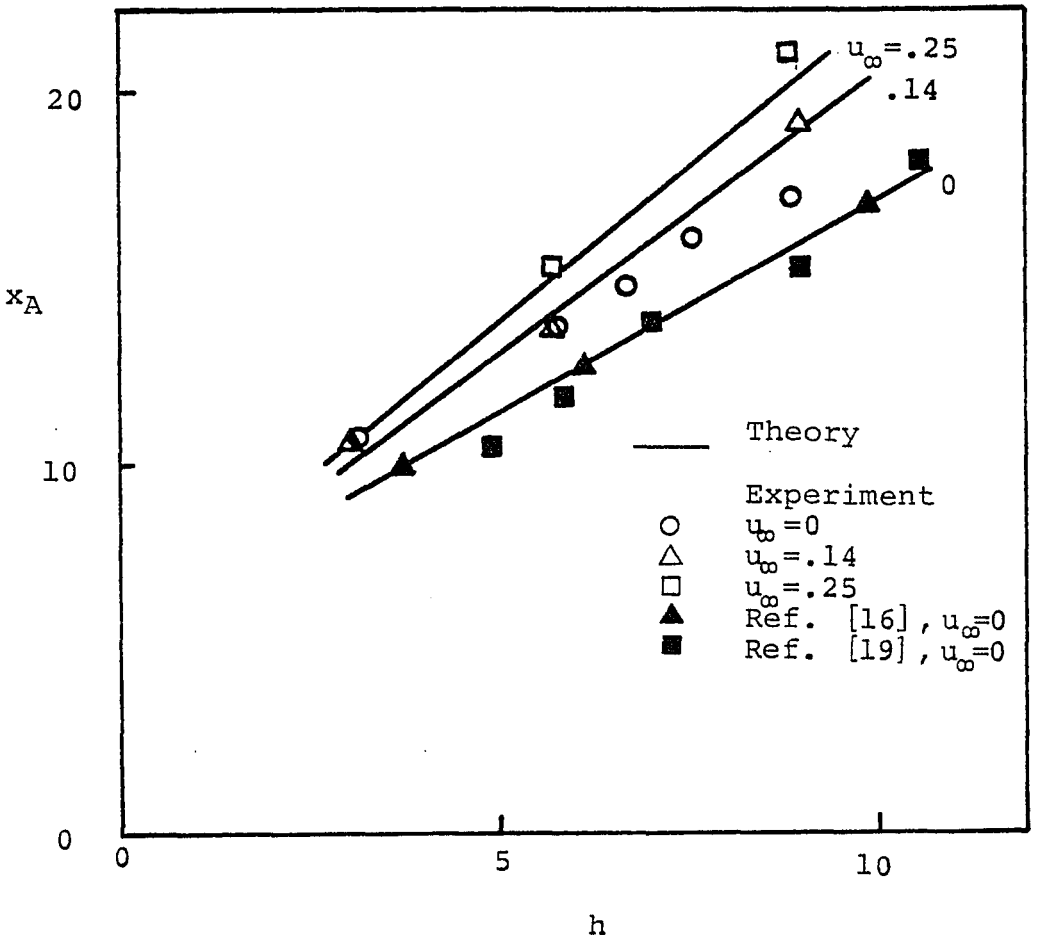

Figure 35. Variation in the Re-attachment Length of Two-Dimensional Offset Jets

the experimental point of re-attachment is defined as the point of maximum wall pressure. Also shown are the experimental data of Bourque and Newman [16] and of Sawyer [19]. The lower theoretical prediction may be due to the assumed polynomial shape of the trajectory. A higher order polynomial may give better results.

Although the theory does not predict the pressure distribution inside the recirculation region, it does give the solution for the base pressure P_b, or the effective pressure difference perpendicular to the jet axis. This variation is shown in Figure 36 for an offset parameter of 12.5. Also shown is the pressure difference across the jet taken from Bourque and Newman's [16] approximate pressure contours. Although agreement for the maximum pressure is good, the higher negative pressure predicted by the theory is due to the fact that the jet attaches too early.

b. Maximum Wall Pressure

Theoretical predictions for the maximum wall pressure, or pressure coefficient c_p, are shown in Figure 37 for various values of free stream velocity. This is the pressure that occurs just as the jet impinges onto the wall. Sawyer's [19] data for the maximum pressure is also shown. Agreement with experimental data is good. It should be noted that previous solutions of this type of jet-boundary interaction problem using a constant radius of curva-

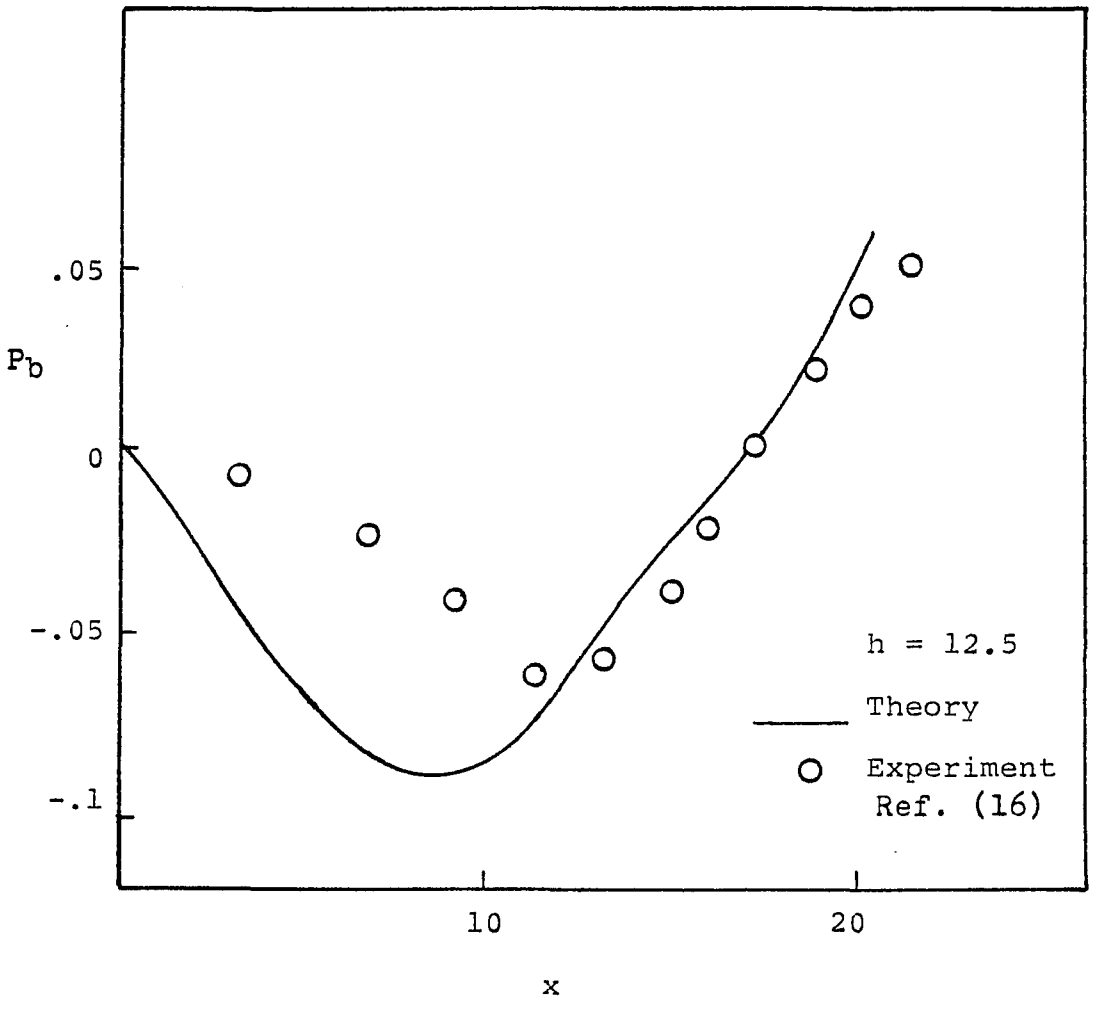

Figure 36. Variation in the Re-attachment Region Base Pressure

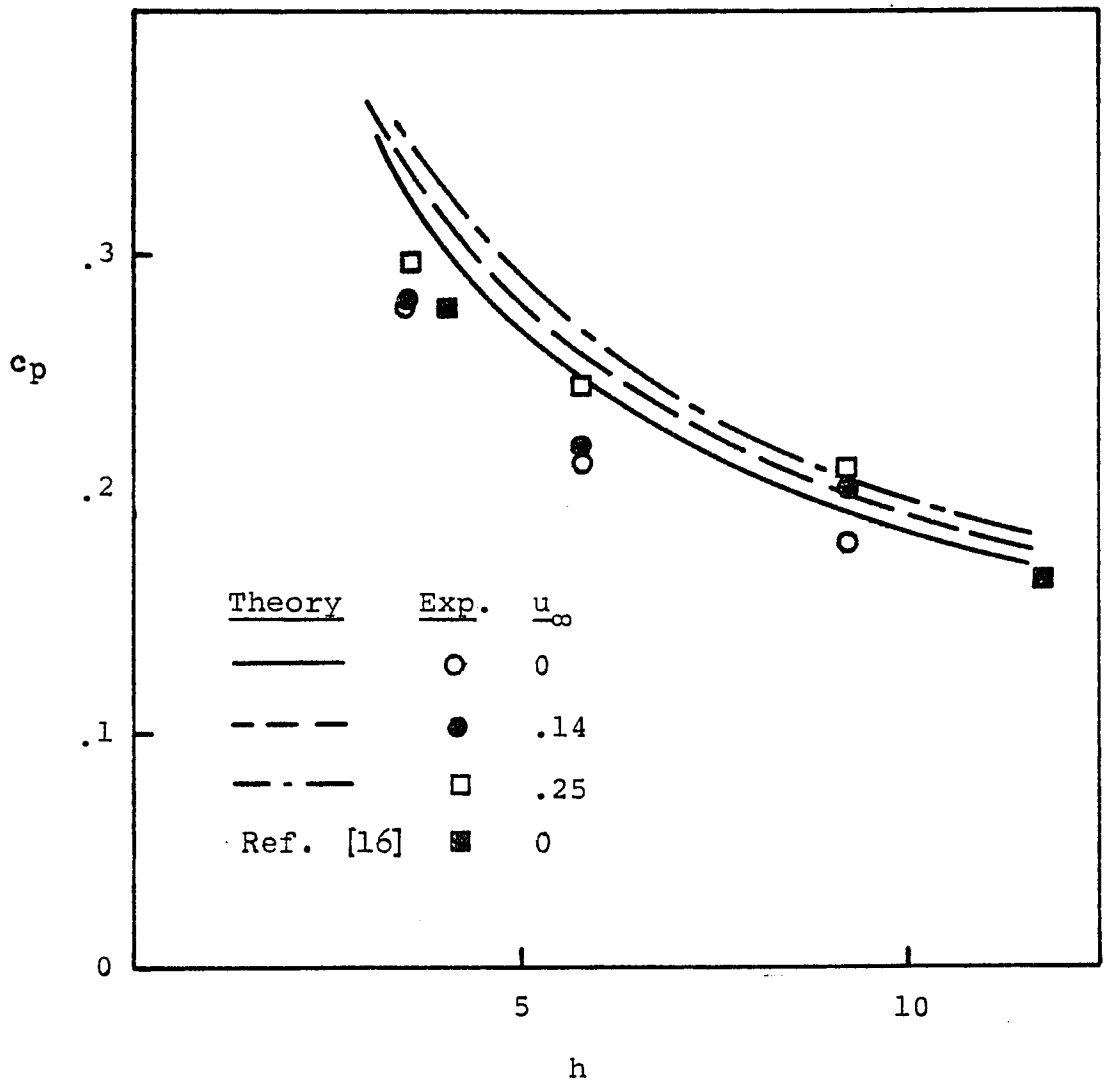

Figure 37. Maximum Wall Pressure of Two-Dimensional Offset Jets

ture assumption were unable to predict the maximum wall pressure [18, 19, 25].

c. Velocity Profiles

Sample experimental jet velocity profiles in the pre-attachment region are shown in Figure 38. Figure 39 shows similar velocity profiles, at the same value of the offset parameter, and with a free stream velocity of .14. It is apparent that the free stream does not affect the velocity distribution in the lower half of the jet.

4. Velocity Distribution

Theoretical predictions of the maximum axial velocity as a function of offset parameter are shown in Figure 40 for various offset heights in the absence of free stream. Close inspection of this figure reveals a change in slope of the velocity decay curve just prior to jet-attachment. This corresponds to the change in the sign of the pressure gradient of $d\bar{P}/dX_3$ soon after the jet is issued. The jet first enters a region of decreasing pressure which tends to slow down the velocity decay. For this reason, too, the zone of flow establishment is longer than for a free jet. However, the base pressure soon begins to increase, causing a more rapid jet deceleration. This can be seen more clearly in Figure 41, where the velocity decay and wall pressure distribution are both shown.

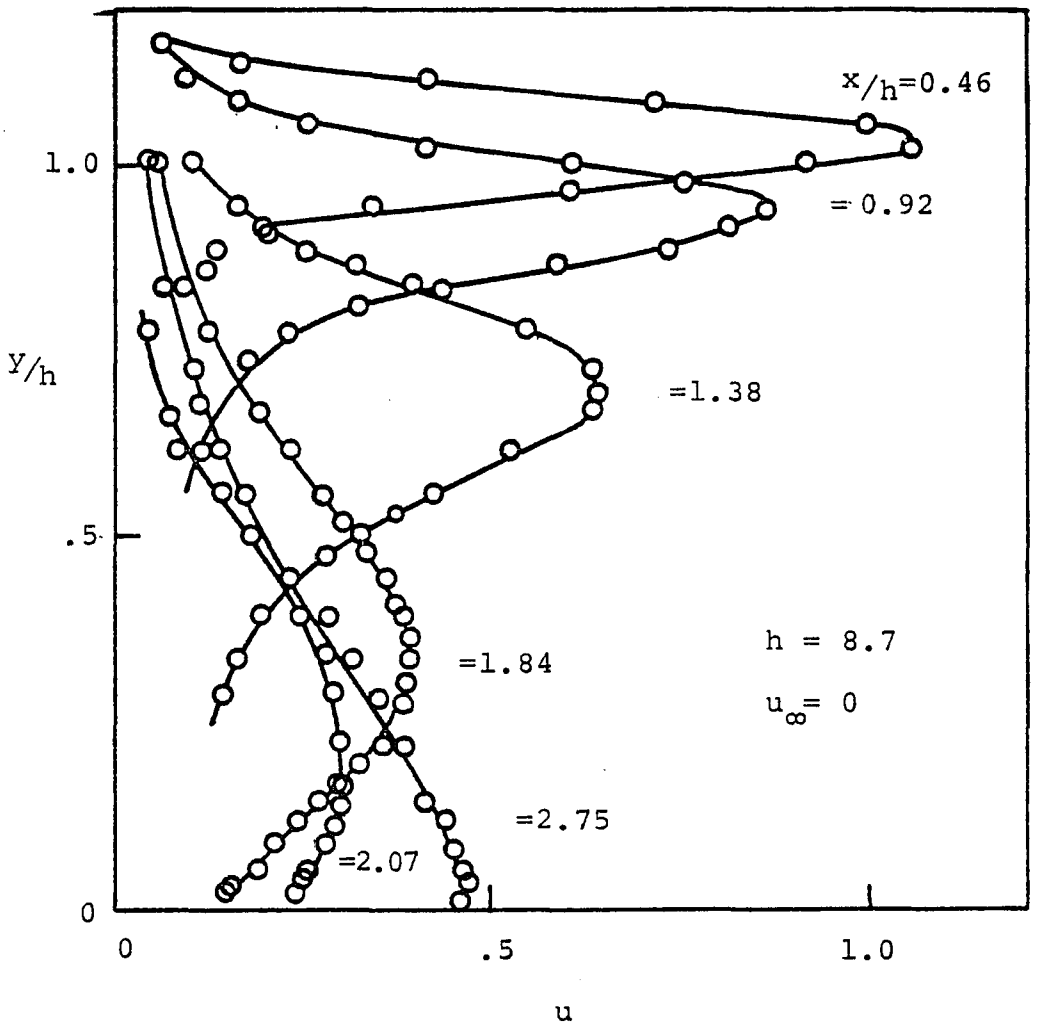

Figure 38. Velocity Profiles in the Pre-attachment Region of a Two-Dimensional Offset Jet

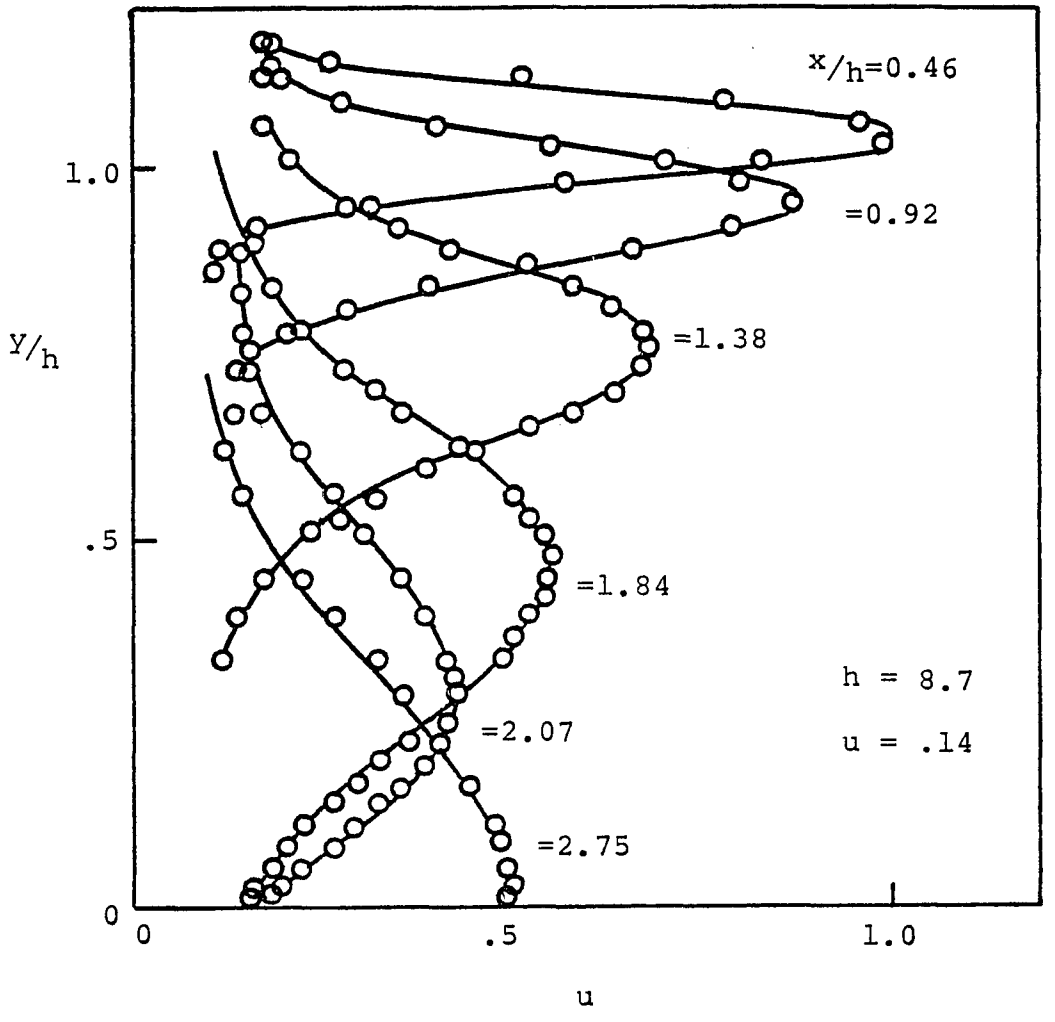

Figure 39. Velocity Profiles in the Pre-attachment Region of a Two-Dimensional Offset Jet in the Presence of a Free Stream

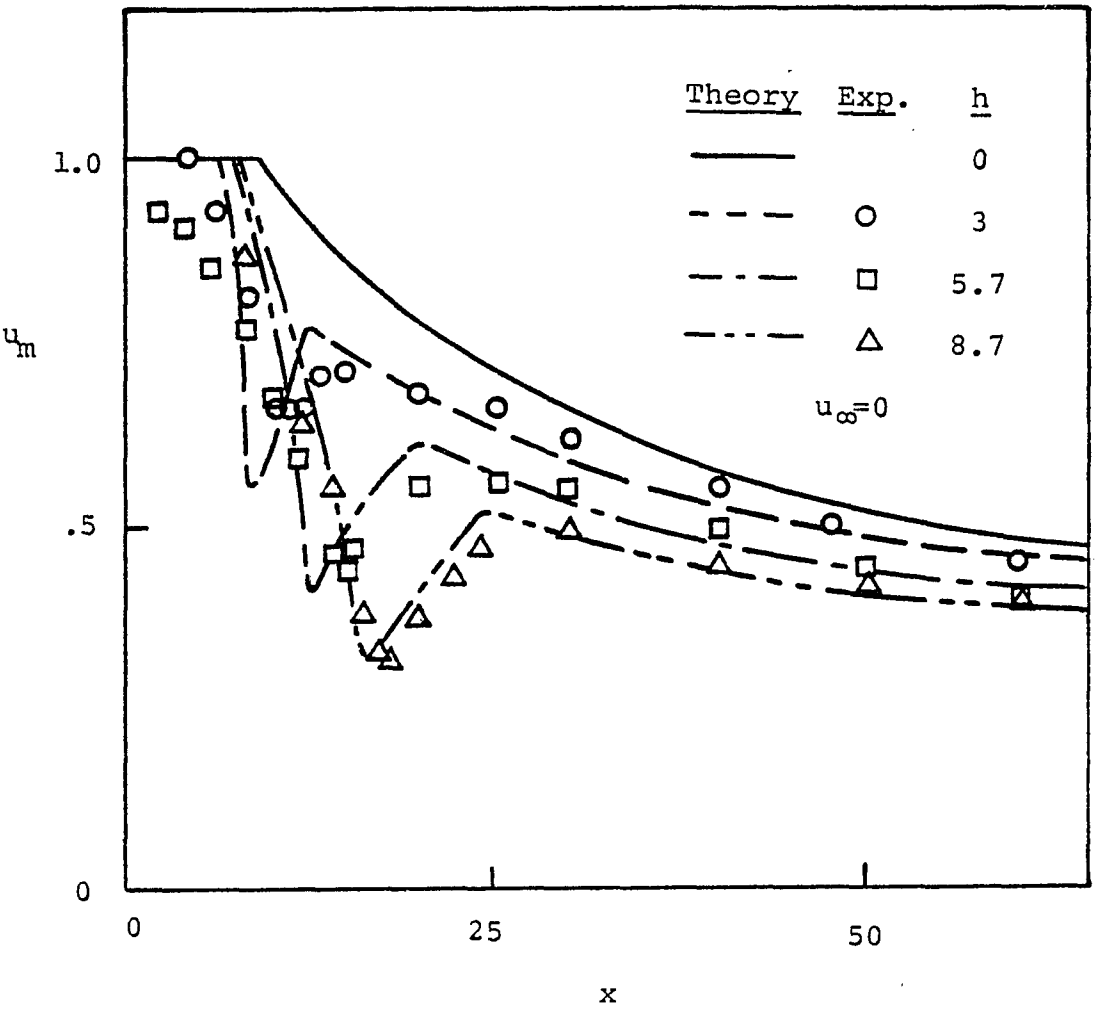

Figure 40. Maximum Axial Velocity Decay for a Two-Dimensional Offset Jet

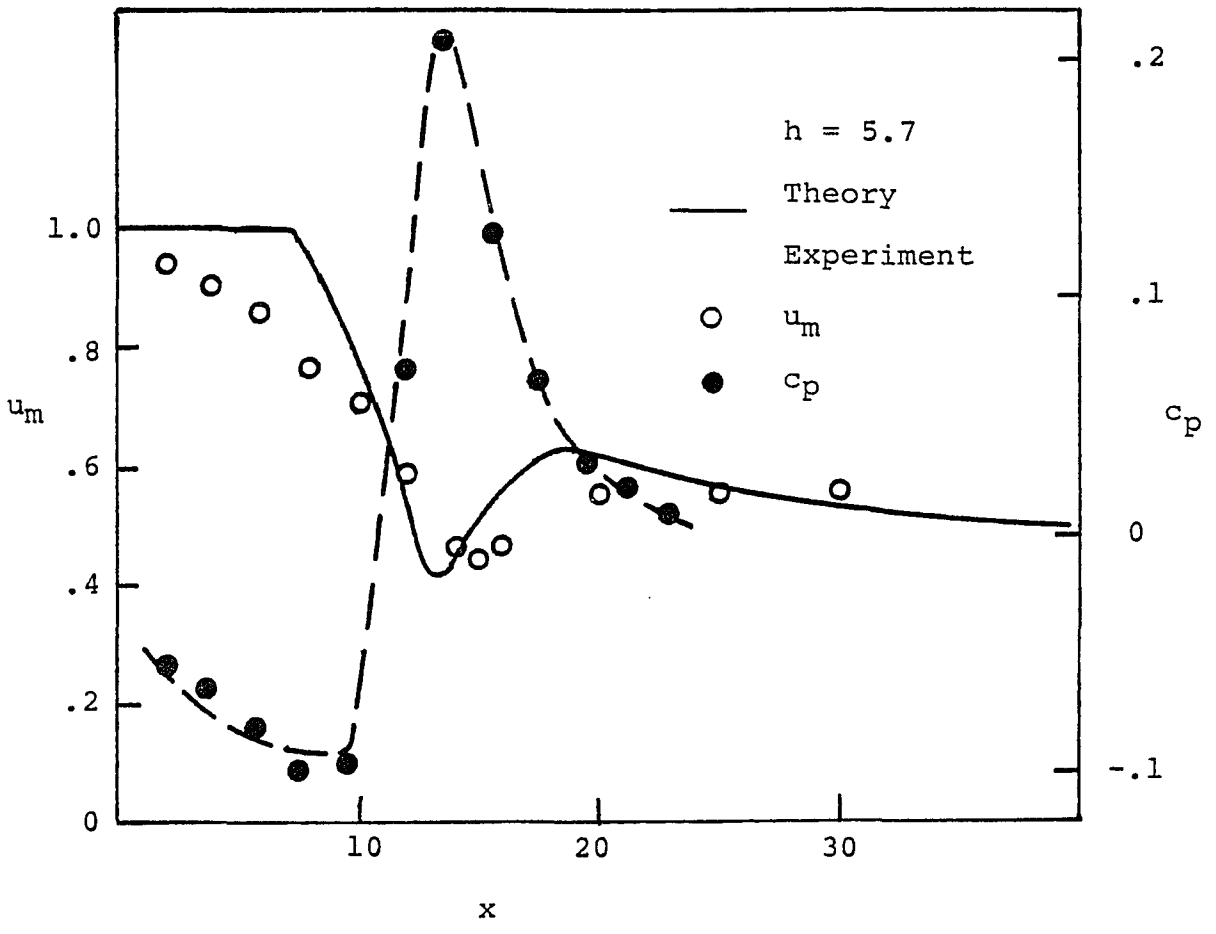

Figure 41. Comparison of the Velocity Decay and Wall Pressure for a Two-Dimensional Offset Jet

Following jet attachment, the maximum axial velocity increases until the jet reaches hydrostatic pressure levels. Eventually, in the wall jet region, all jets, regardless of offset parameter, seem to decay at the same rate.

Figures 42 - 44 show the variation of maximum axial velocity with free stream velocity for offset distances of 3.0, 5.7 and 8.7. Ambient motion does not greatly affect the maximum axial velocity in the pre-attachment and impingement regions. This is probably because there is only a small perturbation in the pressure field for low values of the free stream velocity ratio ($u_\infty < .3$), and the jet dynamics rather than the turbulent mixing govern the flow in these regions.

Comparisons with experimental data of the outer jet width for re-attached jets are shown in Figures 45 and 46. Agreement between theory and experiment is good. Note the decrease is the jet outer boundary in the impingement region due to the acceleration of the jet.

5. Temperature Field-: Experimental Results

a. Recirculation Temperature

The basic assumption in our derivation of the energy equation was that the temperature inside the recirculation region is constant. This is due, it was felt, to the efficient mixing in this region. In addition, the recirculation

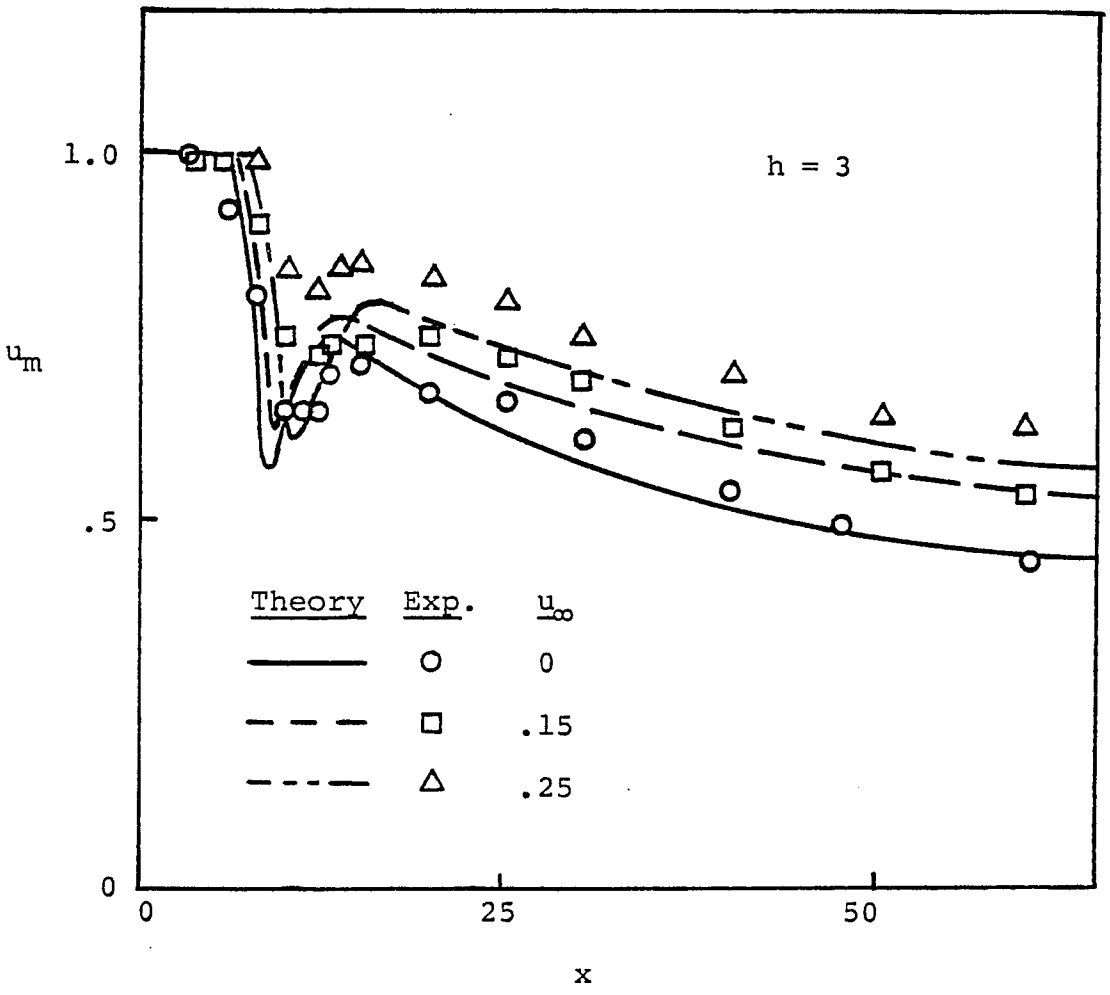

Figure 42. Maximum Axial Velocity Decay for a Two-Dimensional Coaxial Offset Jet (h=3.0)

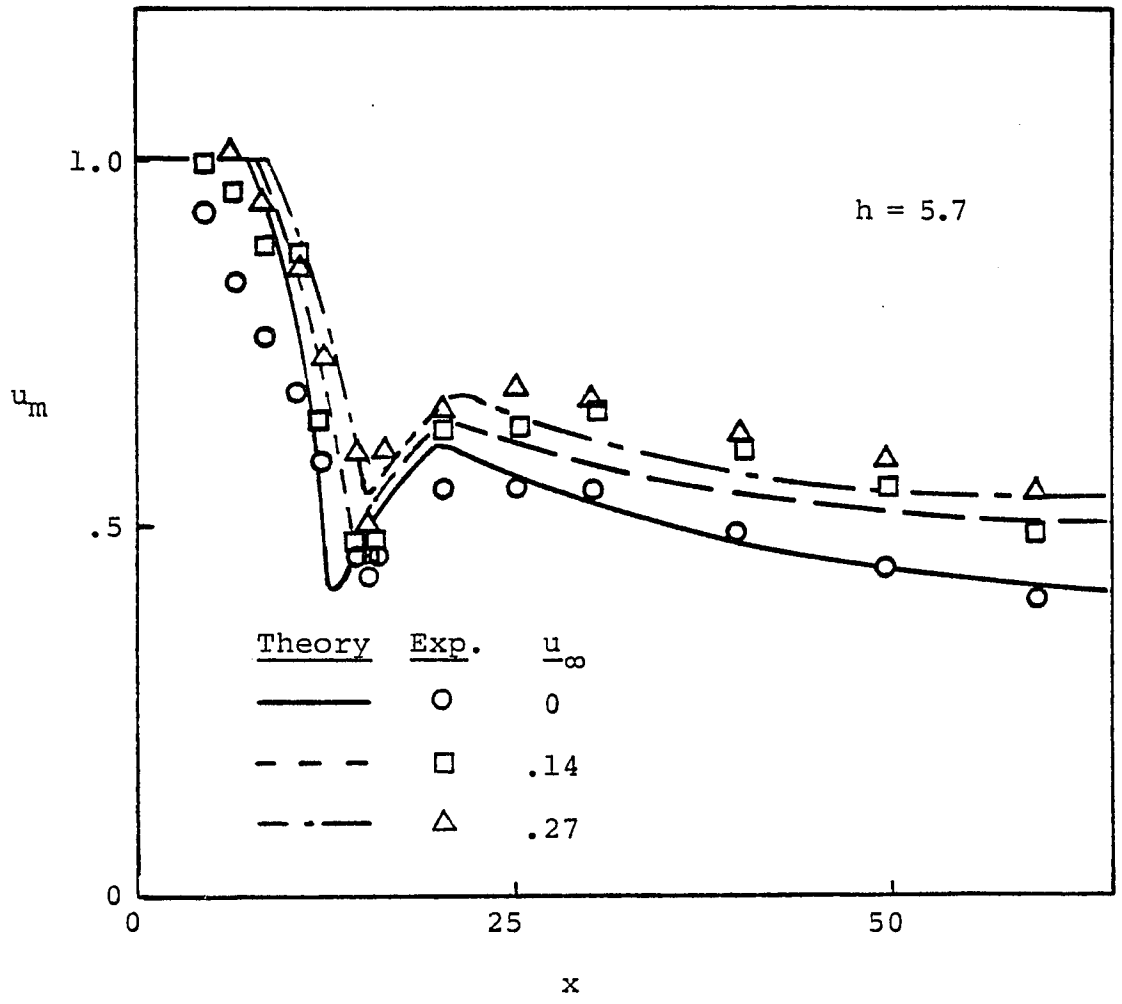

Figure 43. Maximum Axial Velocity Decay for a Two-Dimensional Coaxial Offset Jet (h=5.7)

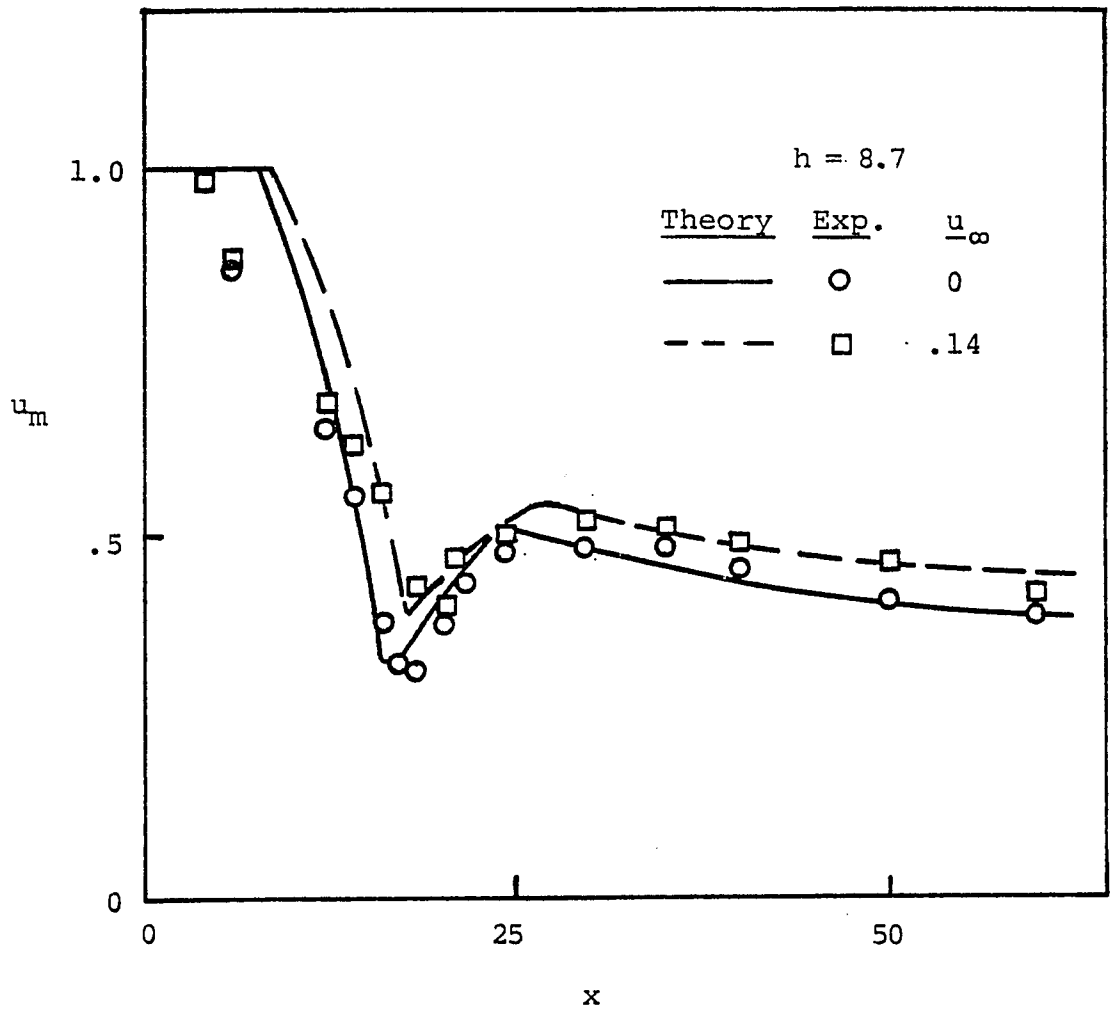

Figure 44. Maximum Axial Velocity Decay for a Two-Dimensional Coaxial Offset Jet (h=8.7)

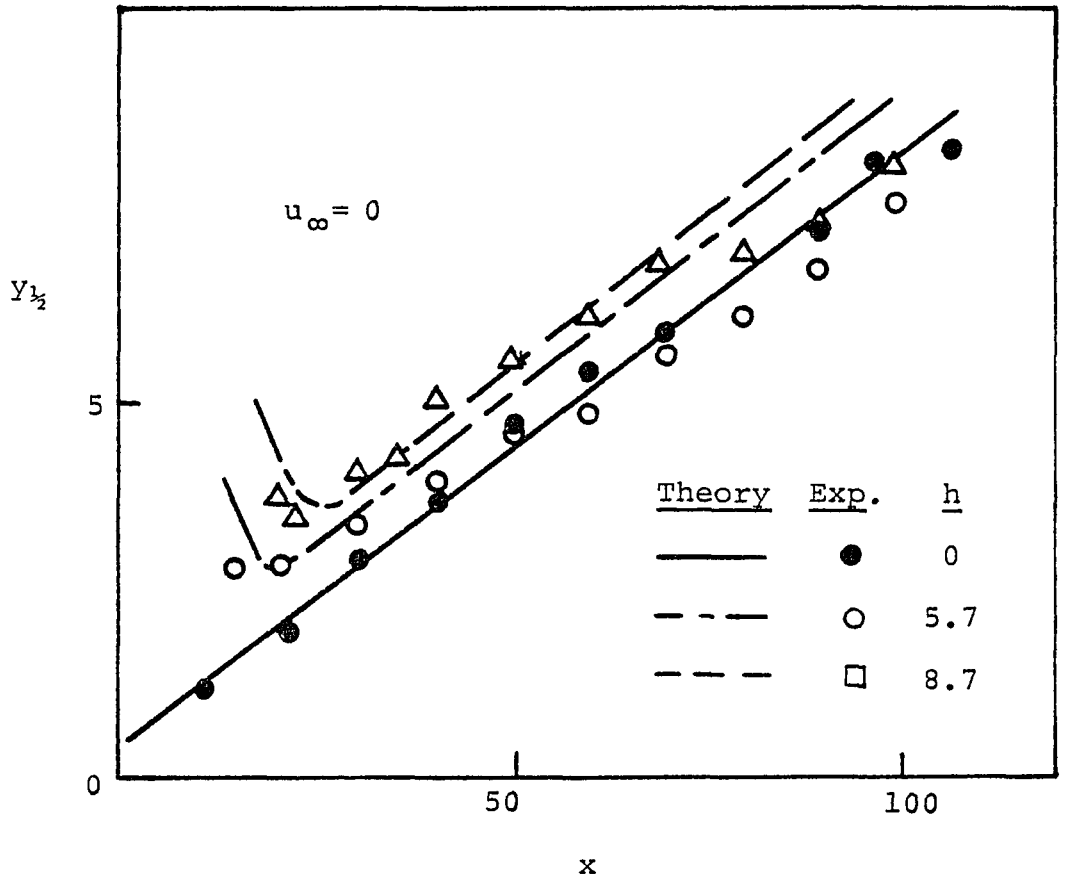

Figure 45. Jet Half-Width of a Two-Dimensional Offset Jet

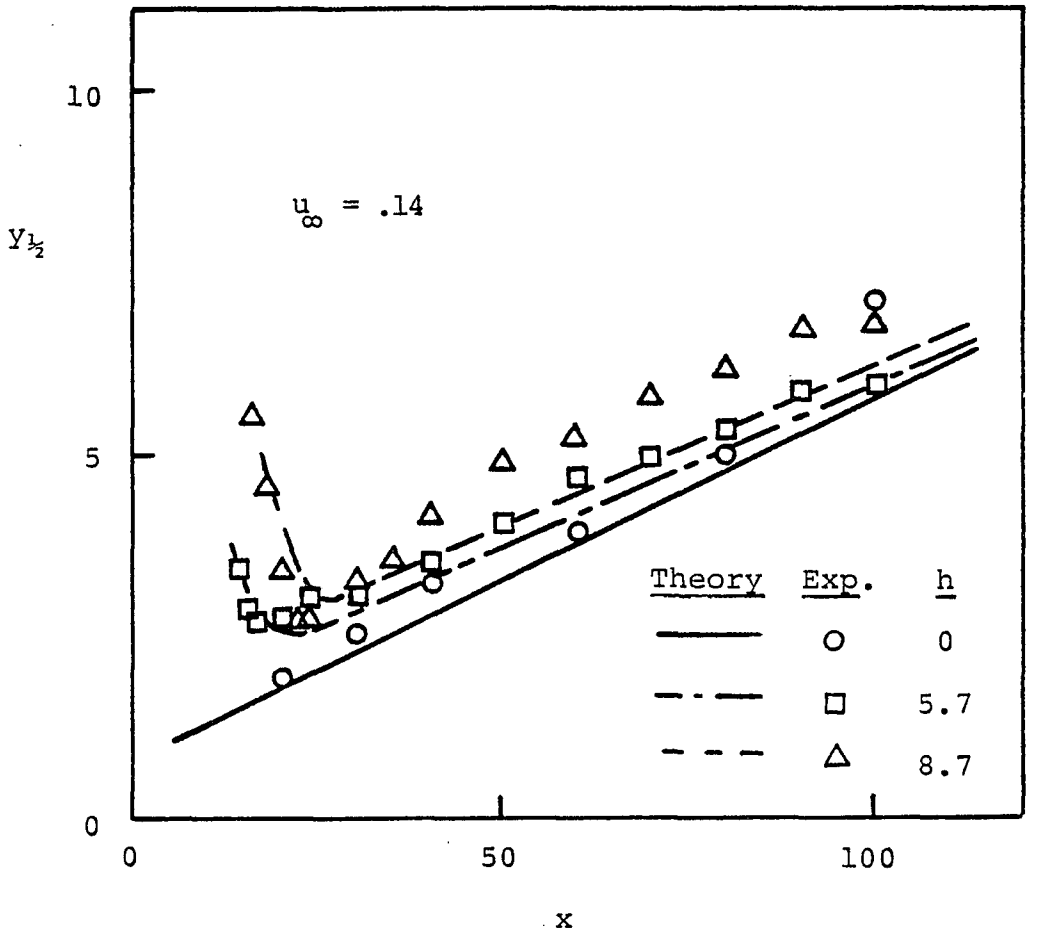

Figure 46. Jet Half-Width of a Two-Dimensional Coaxial Offset Jet

temperature was assumed equal to the maximum axial temperature of the jet at the inflection point in its trajectory. Figure 47 shows the temperature distribution in the pre-attachment region of a heated jet discharging into a stationary ambient. Figure 47 also shows the temperature distribution in the presence of a coaxial free stream. Also shown are the experimental jet axis and the approximate position of the dividing streamline as measured from peak RMS voltmeter readings. Both these figures illustrate the fact that the temperature distribution inside the recirculation region is uniform and approximately equal to the maximum axial temperature at the trajectory inflection point. This is where the fluid begins to return, or turn back, into the recirculation region.

b. Turbulent Schmidt Number

The value of the turbulent Schmidt number in the pre-attachment region was difficult to obtain experimentally. This is primarily due to the difficulty in obtaining the temperature profile in a plane perpendicular to the jet axis. In addition, because of its proximity to the discharge, the jet has not yet diffused sufficiently to permit accurate measurement of the jet half-width. This is especially true on the inner portion of the jet where maximum temperatures are almost equal to the recirculation temperature. This is illustrated in Figure 48, where sample temperature profiles

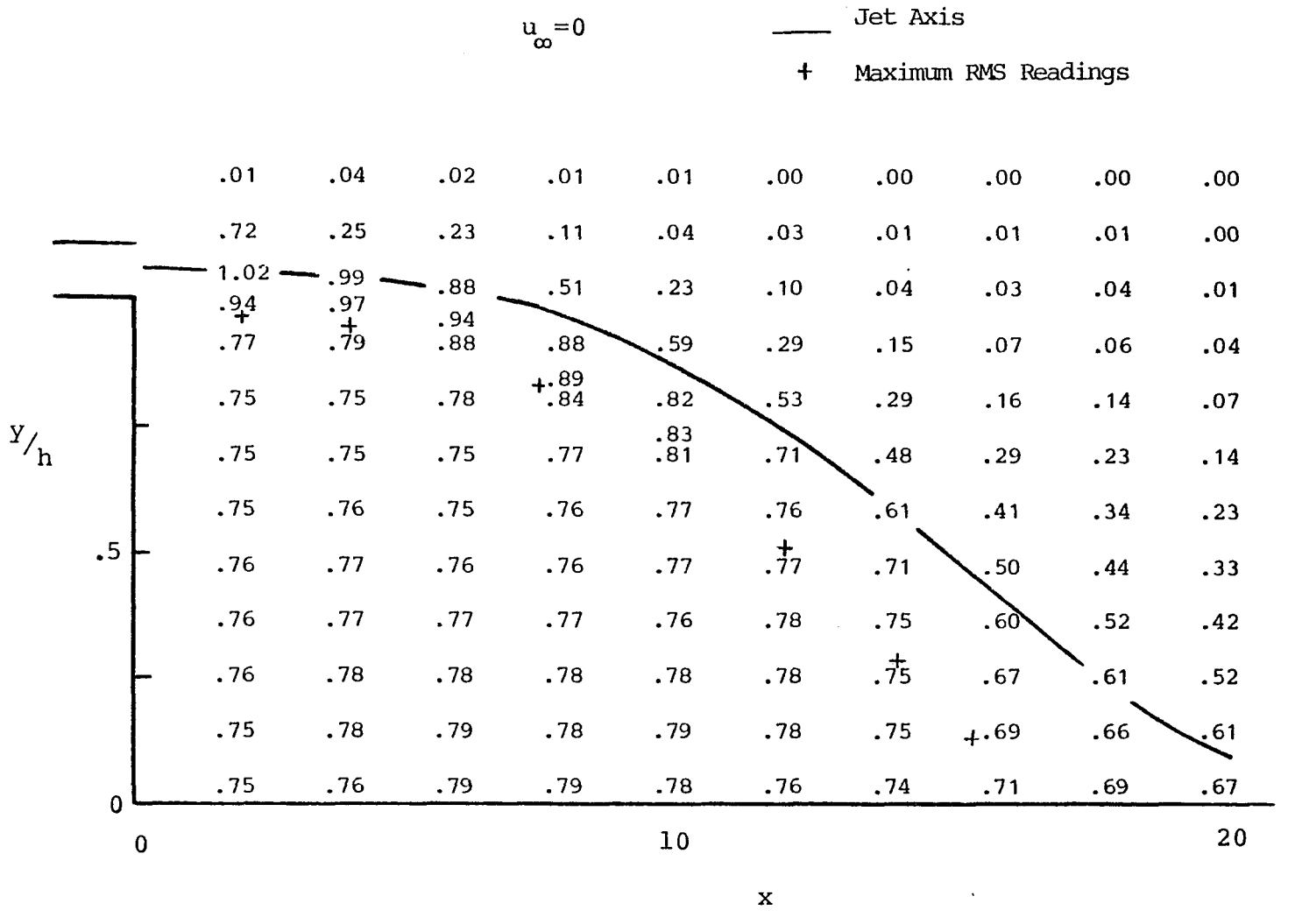

a) h=8.7

Figure 47. Temperature Distribution in a Two-Dimensional Heated Offset Jet

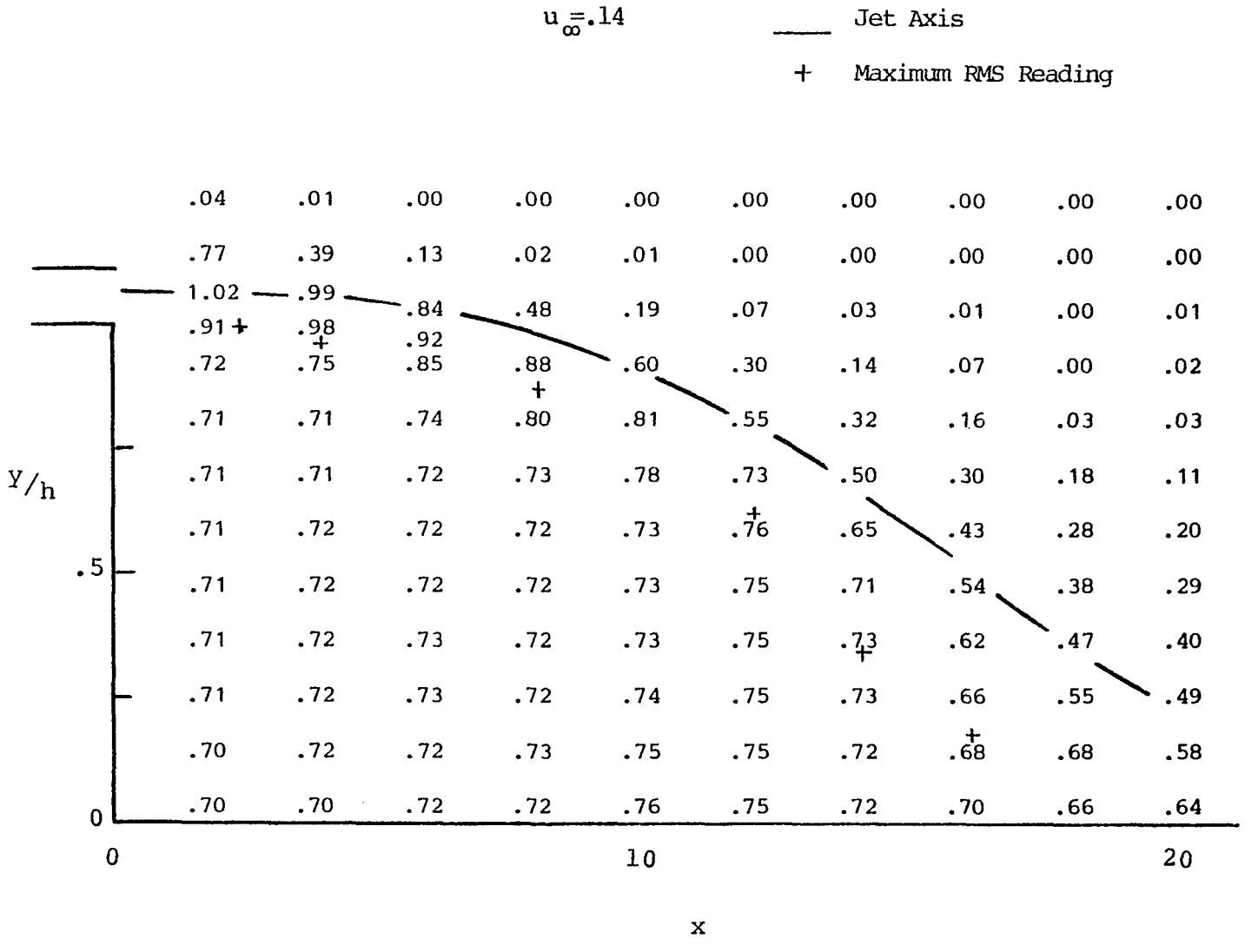

Figure 47a. Continued

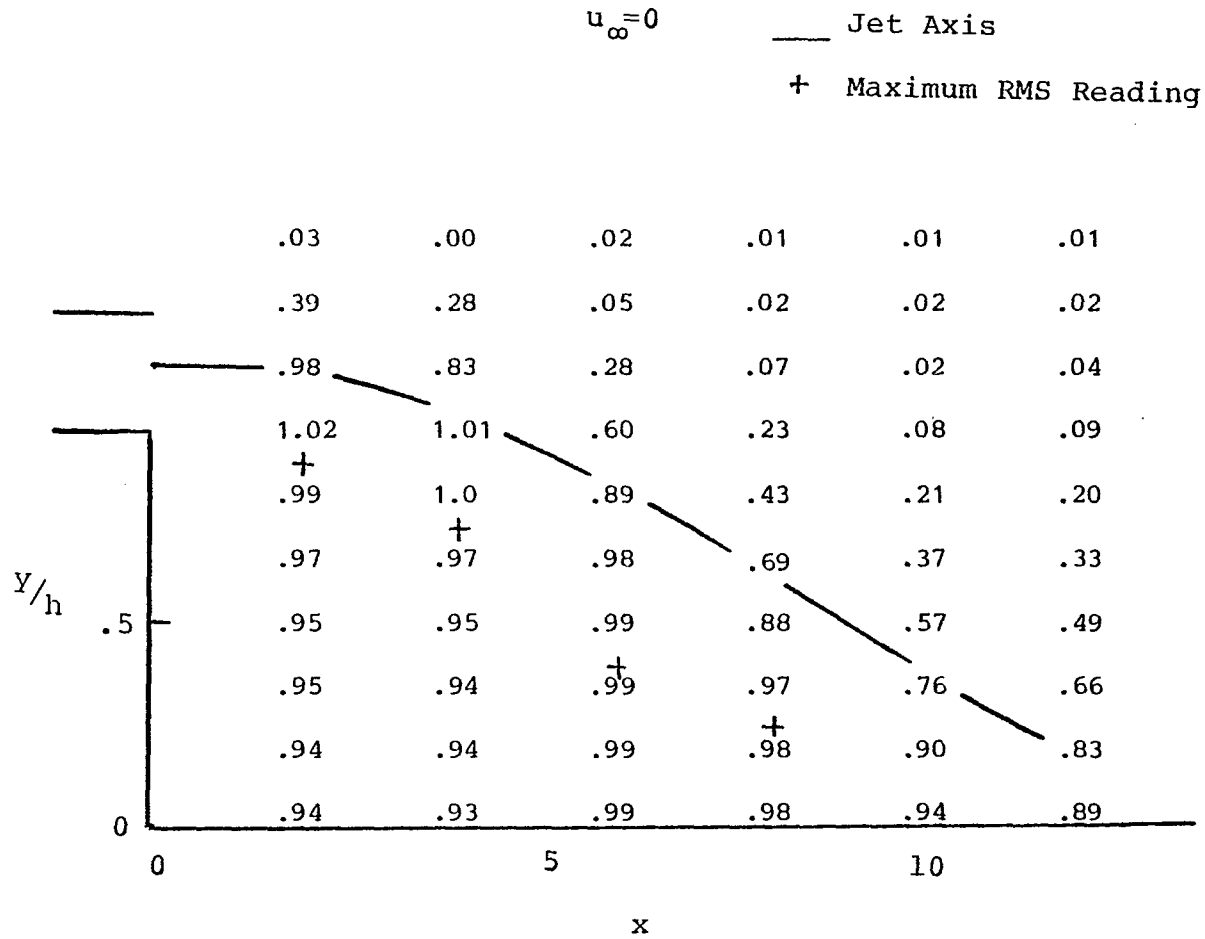

b) h = 3

Figure 47. Continued

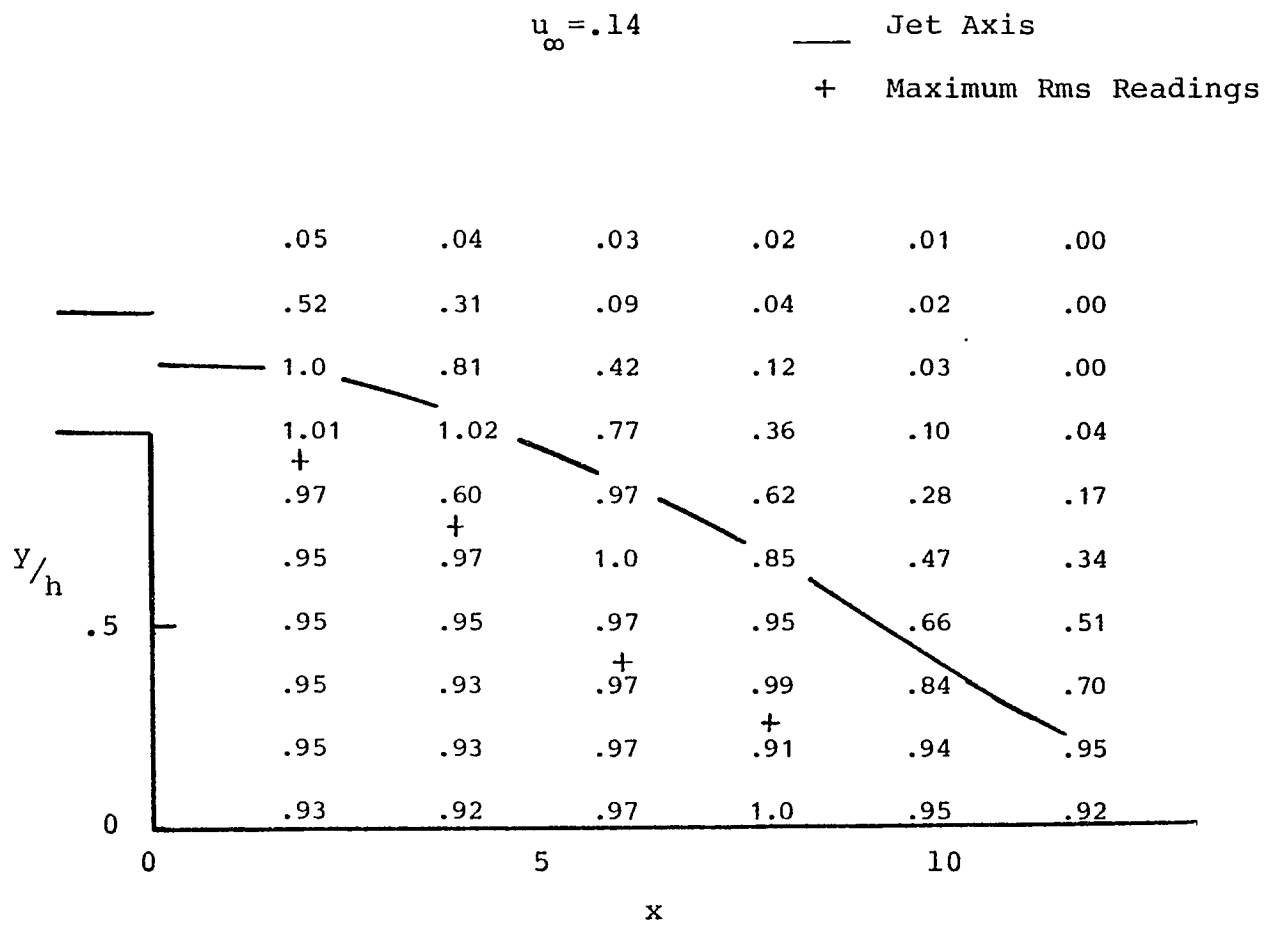

Figure 47b. Continued

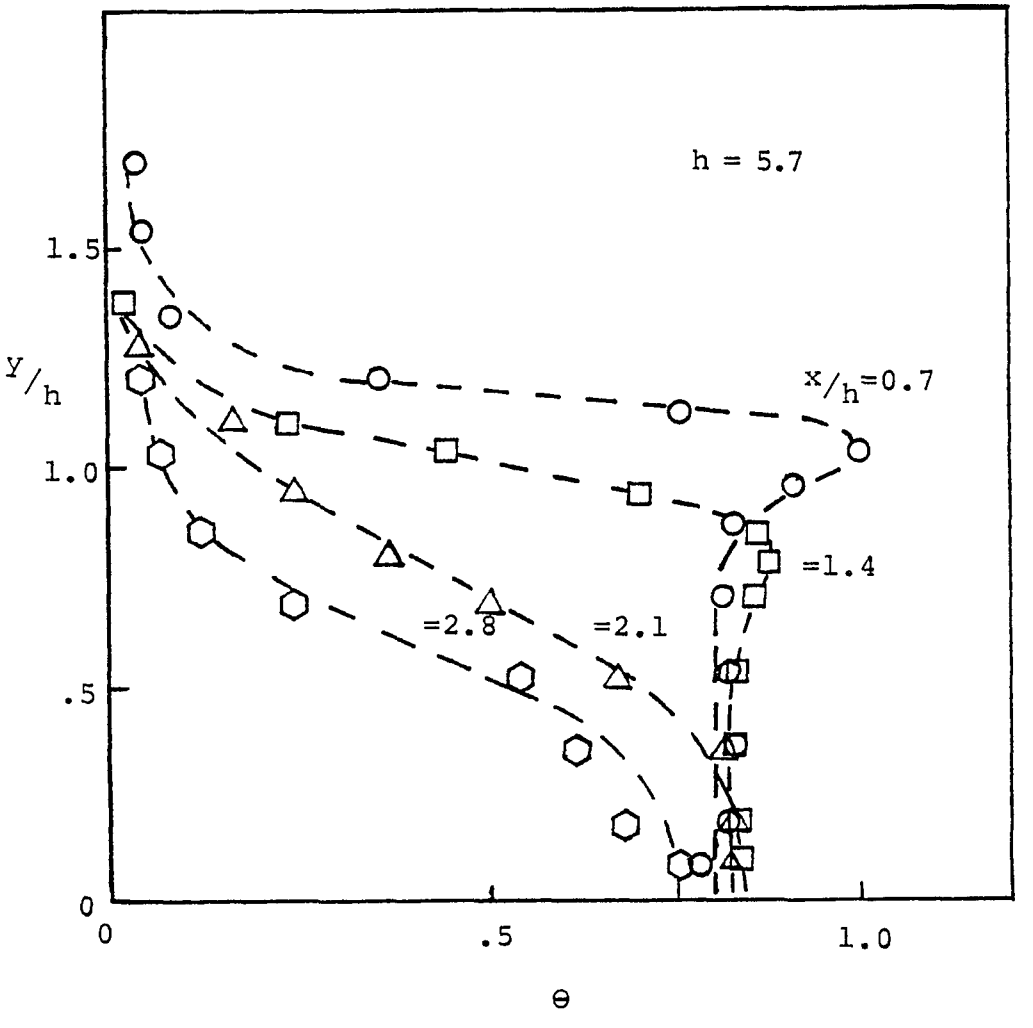

Figure 48. Experimental Temperature Profiles in the Pre-attachment Region of a Two-Dimensional Heated Offset Jet

in the vertical plane are shown for h = 5.7. Also note the general agreement with our assumed temperature profile.

Figure 49 shows a comparison between the velocity and temperature half-widths. The ratio of the slopes of the two widths is equivalent to the turbulent Schmidt number. This value of the turbulent Schmidt number is equal to the wall jet value of 1.15. However, unlike the wall jet, where both widths start out at the same value, for an offset jet the temperature width has a higher value at the beginning of the impingement region. This may be due to the fact that the value of the turbulent Schmidt number is slightly higher in the pre-attachment region. Using the wall jet value of λ leads to slightly higher values for the maximum axial temperature, θ_m.

Because of the difficulty of measuring the turbulent Schmidt number in the pre-attachment region, the wall jet value was used.

c. Maximum Axial Temperature Decay

Theoretical results for the maximum axial decay are compared with experimental data for various offset heights in Figure 50. Also shown is the maximum axial temperature decay for a wall jet. Comparison with experimental data is good. The effects of the offset heights are most noticable in the pre-attachment region. Eventually, the curves for different offset heights coalesce. Figures 51 and 52 illus-

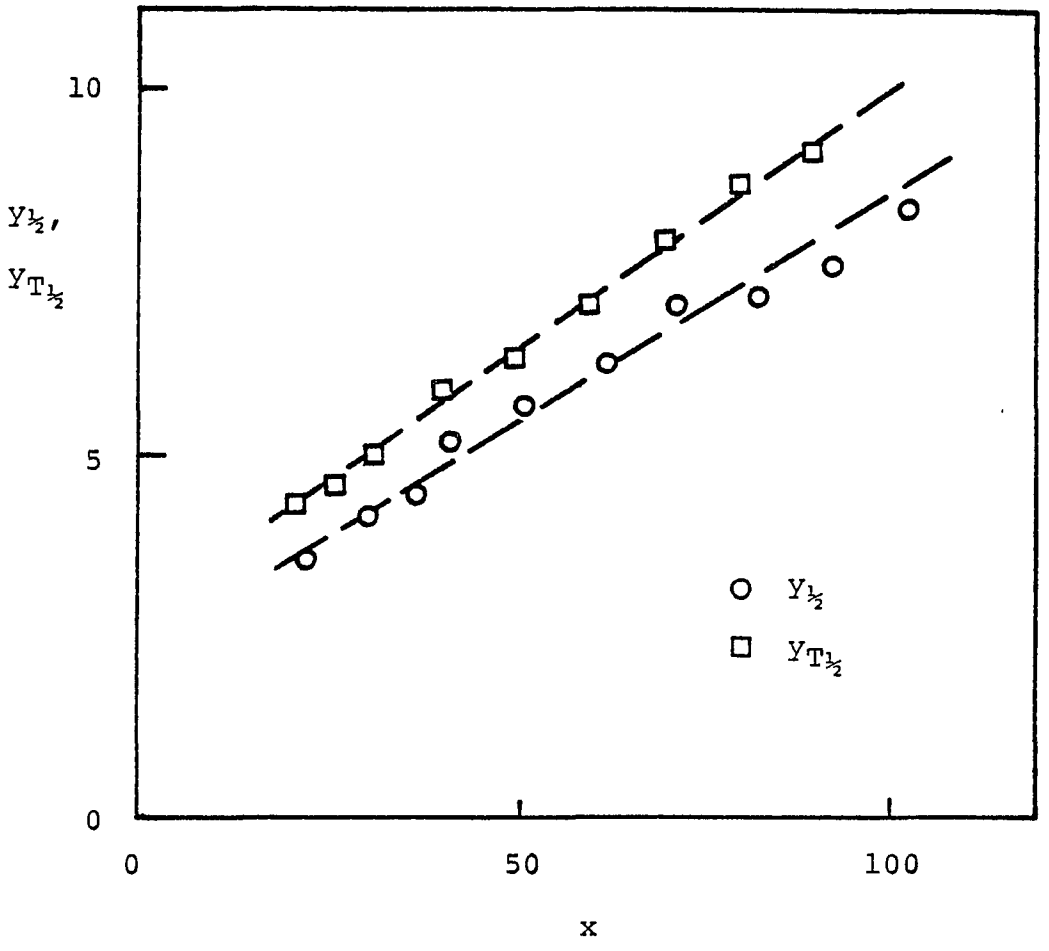

Figure 49. Velocity and Temperature Half-Widths in the Re-attached Regions of a Heated Two-Dimensional Offset Jet

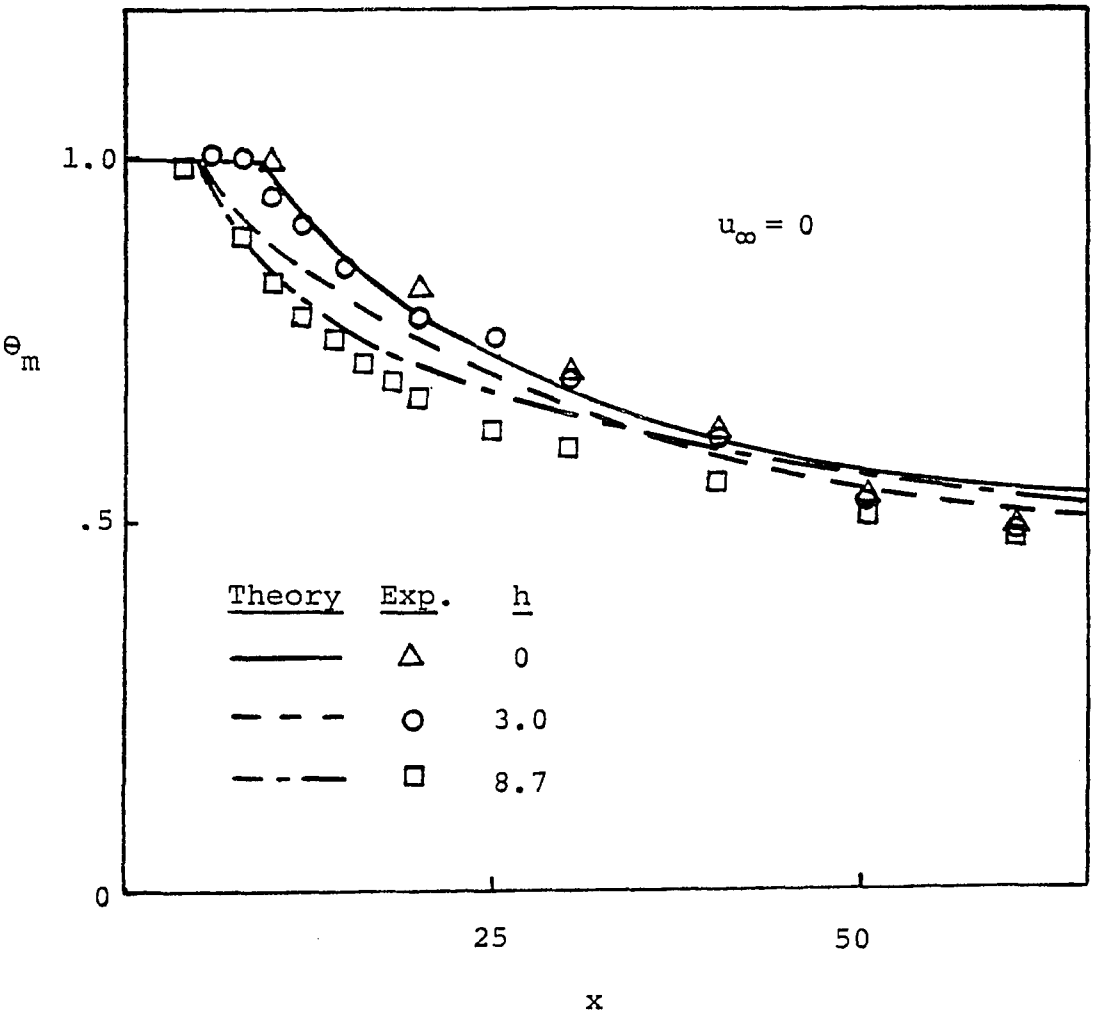

Figure 50. Maximum Axial Temperature Decay for a Two-Dimensional Heated Offset Jet

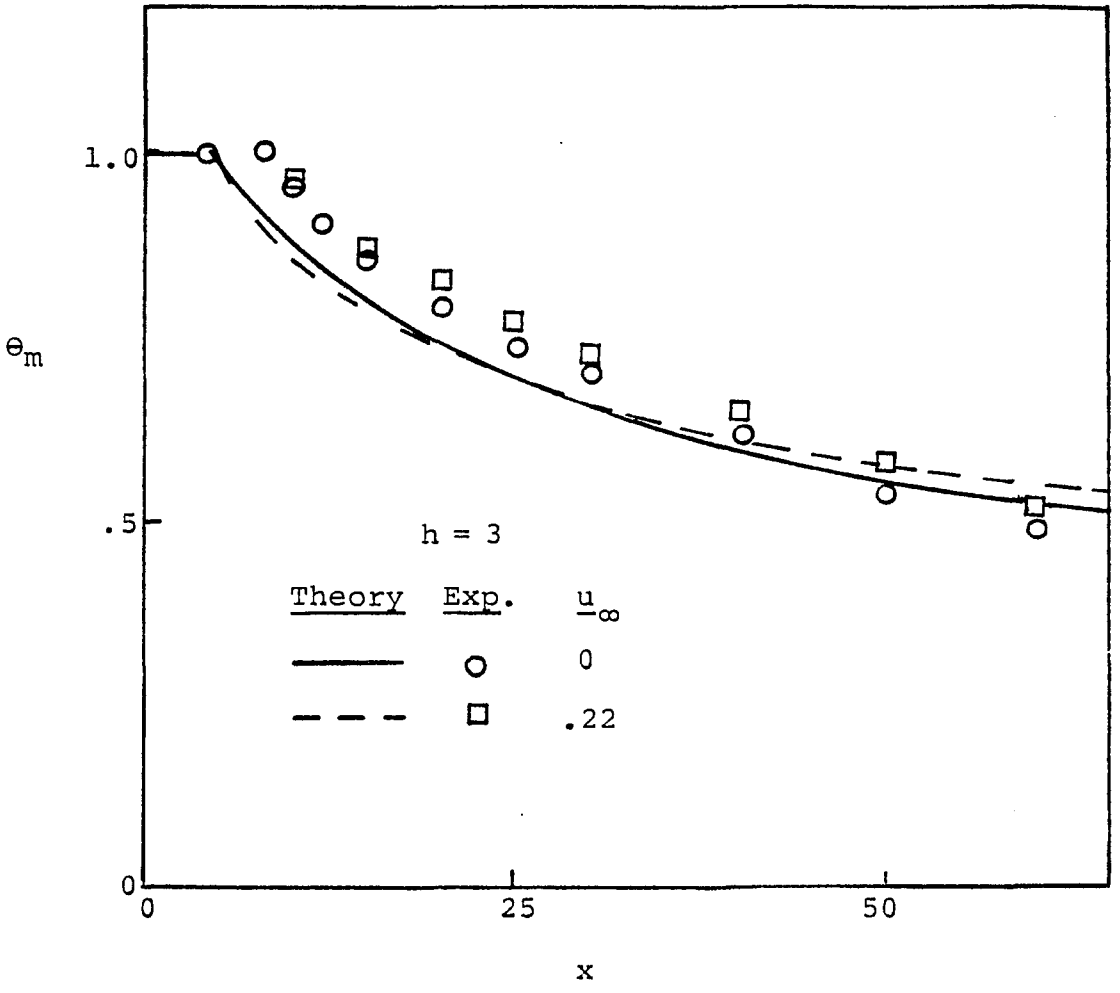

(a) h = 3

Figure 51. Maximum Axial Temperature Decay for a Two-Dimensional Heated Coaxial Offset Jet

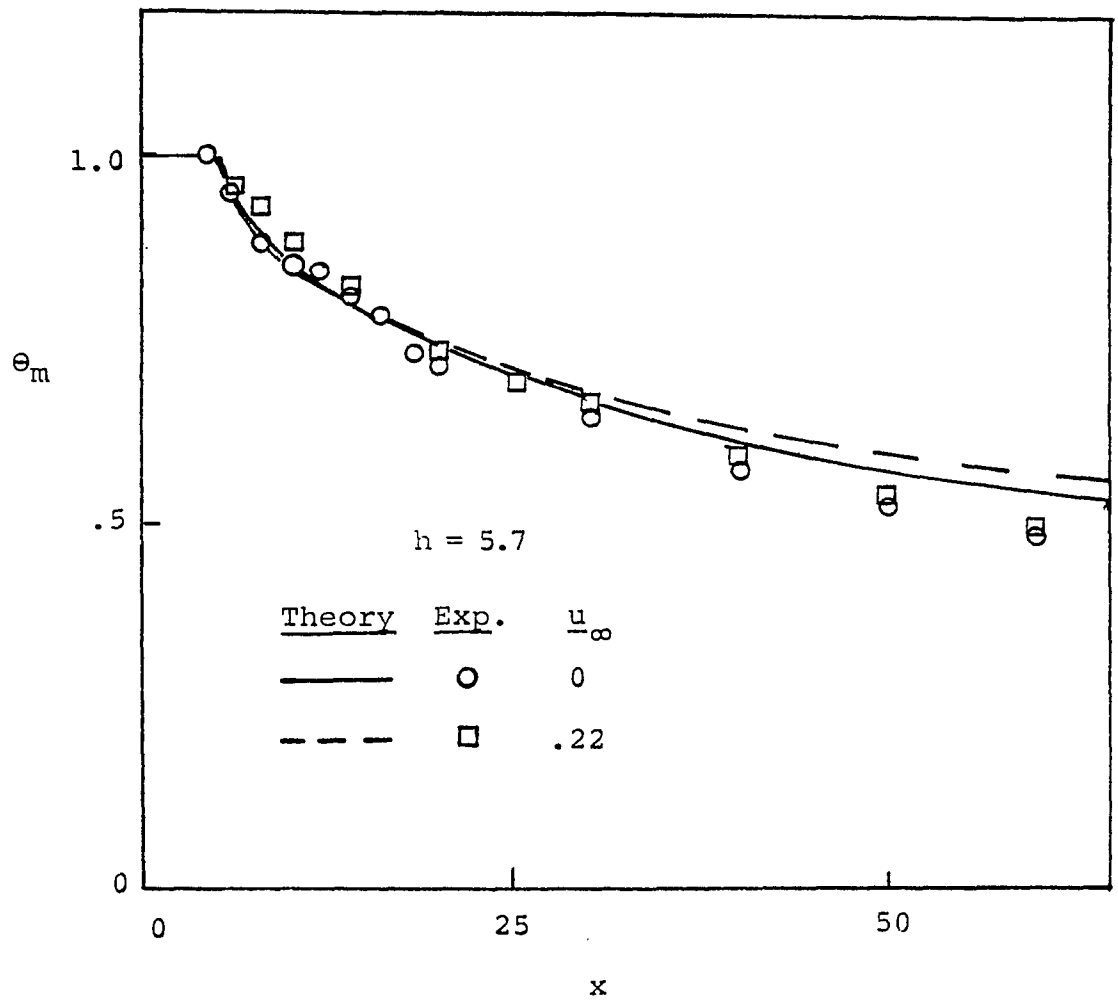

(b) h = 5.7

Figure 51. Continued

trate the effects of free stream on the maximum axial temperature decay. Apparently Θ_m is not affected by the presence of a free stream.

Figure 53 shows the comparison between theory and experiment of the recirculation temperature. Again, agreement is good. The experimental values of Θ_R were obtained by averaging measured values of temperature inside the recirculation region.

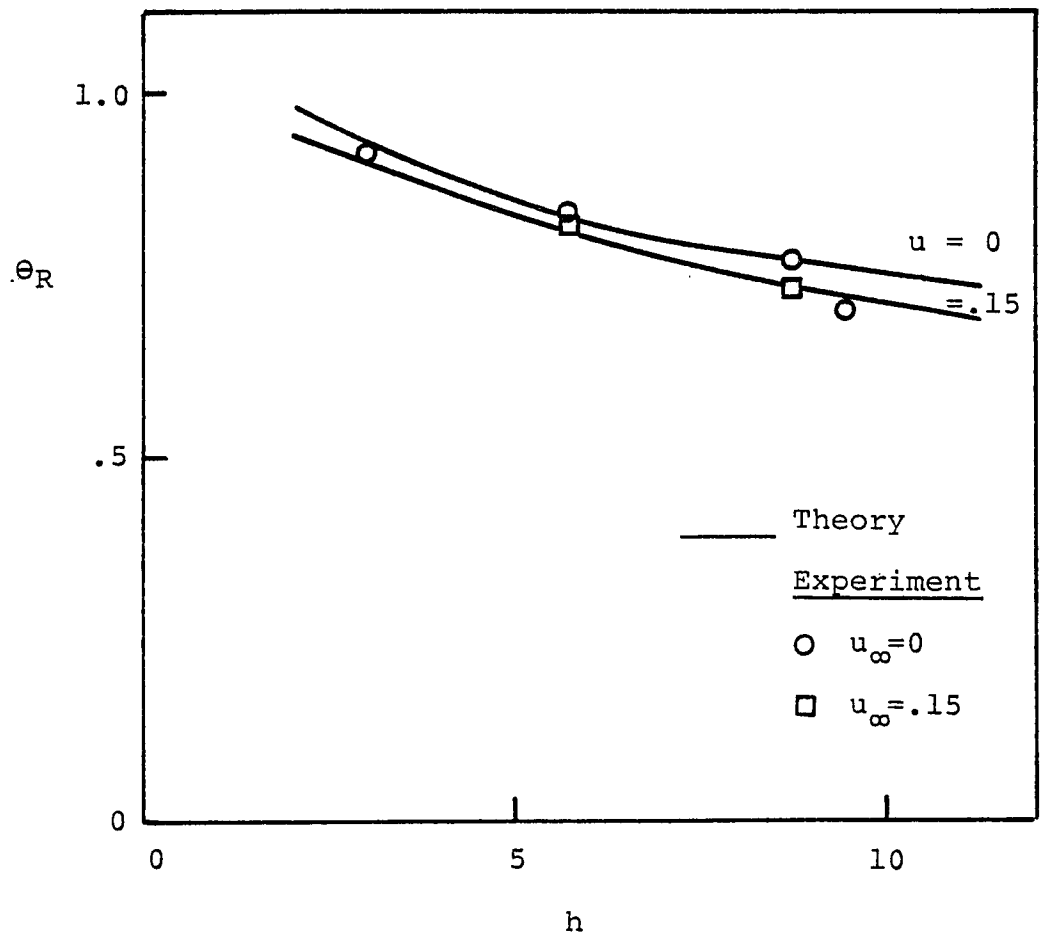

Figure 52. Recirculation Region Temperature for a Two-Dimensional Heated Offset Jet

VIII. Summary and Conclusions

The conclusions drawn from our theoretical and experimental studies may be summarized as follows:

A. Two-Dimensional Wall Jet

An integral-type solution, using an entrainment assumption, was employed to yield the velocity and temperature distribution of a two-dimensional heated wall jet. Agreement between theory and experiment, in general, is good. Experimental and theoretical results reveal that both the velocity and temperature distribution are sensitive to the free stream ratio, although this sensitivity is more pronounced for the velocity distribution.

Experimental data seems to verify the choice of a Gaussian temperature profile. Based on this assumed temperature profile, the value of the turbulent Schmidt number was measured as approximately 1.15. This value falls inside the range of measured values of the turbulent Schmidt number for two-dimensional heated free jets.

B. Jet-Boundary Interaction (Offset Jet)

1. Pre-attachment Region - Velocity Field

An integral solution utilizing an entrainment closure assumption was used to obtain the solution for the velocity and pressure fields of a two-dimensional jet discharging

offset from a solid-boundary. Besides the inclusion of a pressure term in the axial momentum equation, the integral conservation of mass and momentum equations, as well as the entrainment relationship and the velocity profile were similar to their free jet counterparts. The value of the entrainment coefficient was chosen midway between the limiting case of the free jet and wall jet.

The solution is unique in that base pressure as well as the local jet-axis radius of curvature were not held constant, thereby altering the velocity distribution from its free jet value. The addition of these new unknowns required the introduction of two closure equations in the form of two additional momentum relationships.

The horizontal momentum principle, applied locally at the point of re-attachment, was previously introduced by Bourque and Newman [16]. The vertical momentum principle, applied to a control volume enclosing the impingement region, is new and required specification of the surface pressure inside the impingement region. These relationships could not be applied directly in the stepwise numerical procedure because of their implicit nature, necessitating the use of an assumed jet-trajectory profile.

The introduction of ambient motion was accounted for by modifying thevelocity profile and entrainment relationship so as to account for the near-zero velocity inside the recirculation region.

In general, agreement with experimental data was good. The model accurately predicted the jet trajectory and axial maximum velocity decay for a wide range of offset heights and free stream values. Predictions of the maximum wall pressure and re-attachment length also compared well with experimental data.

Additional conclusions may be stated as follows:

a) Experimental data seems to confirm the choice of a Gaussian velocity profile in the pre-attachment region.

b) The introduction of a polynomial jet trajectory coupled with an iterative procedure provided a convenient and successful way of satisfying the two implicit momentum conditons at the point of re-attachment.

c) The free jet entrainment relationship could be used in an integral solution of the pre-attachment region of an offset jet. The solution was not sensitive to the value of the entrainment coefficient.

d) The theory does not agree as well with experimental data at high offset distances ($h > 12$). This is probably due to the choice of a fifth-order polynomial for the jet trajectory profile. It is likely that a higher order polynomial or perhaps another functional profile would improve the results at higher values of h.

e) The model as derived cannot be applied directly for very low offset values ($h < 2$). This is because jet attachment occurs in the jet's zone of flow establishment. This

complicates the solution because the velocity profile has not had a chance to become fully developed. However, at low offset heights, the velocity and temperature distributions do not differ significantly from their wall jet values.

f) The introduction of a moving ambient, at low values of free stream ($u_\infty < .3$), has minor effects on the jet characteristics in the pre-attachment region. However, the effects become more pronounced as the offset height increases.

2. Pre-attachment Region - Temperature Distribution

The jet integral equation was derived for the pre-attachment region of a two-dimensional offset jet. Both the energy equation and temperature profile were modified to account for the above ambient temperature inside the recirculation region. Results for maximum axial temperature decay and recirculation region temperature compared very well with experimental data. The following additional comments can be made:

a) The assumption of constant temperature inside the recirculation region was confirmed by experimental measurements. This temperature was roughly equal to the temperature of the fluid returned by the jet into the recirculation region.

b) Experimental data generally confirmed the form of our modified Gaussian temperature profile.

c) Though measurements of the turbulent Schmidt number were not made for the offset jet, values of the jet width

in the re-attached portion of the jet indicate that the value may be somewhat higher than that of a wall jet.

d) The temperature inside the recirculation region was found to decrease as free stream velocity increased. This is due to the fact that ambient motion tends to delay jet attachment.

3. Impingement Region

The wall pressure in the impingement region was found to resemble the wall pressure of an impinging jet. This led to the introduction of a Gaussian-shaped wall pressure profile. The pressure spread parameter was determined empirically, and was found to be independent of either offset height or free stream motion.

Except for the pressure term, the integral equations for conservation of mass, momentum and energy resemble those of a wall jet. Agreement with experimental data in this region and the subsequent wall jet region is good.

c. Recommendations for Future Research

The theoretical approach should be adapted to other two-dimensional jet-boundary interaction problems. For example, the problem of a jet discharging at an arbitrary angle to a solid boundary or that of "ventilated" jets where, entrainment of secondary flow between the jet and the boundary is possible, might be considered.

In addition, there is the need for a large-scale experimental and theoretical investigation of the more general three-dimensional jet-boundary interaction problem. Experimental data will help ascertain the range of applicability of the two-dimensional model. Though it is unlikely that the model can be directly applied to the far more complex three-dimensional jet-boundary problem, its importance as a limiting case is significant. The solution demonstrates the successful application of an integral-type solution coupled with an entrainment assumption to a jet-boundary interaction problem without introducing unrealistic assumptions regarding base pressure and velocity decay.

Appendix A

Determination of the Re-attachment Point

The position of the dividing or re-attaching streamline may be obtained at any location inside the pre-attachment region employing equation (19). This equation is obtained by applying conservation of mass between the jet axis and the dividing streamline. Substituting the velocity profile for the pre-attachment region (43a) we obtain the following implicit solution for b_R.

$$erf\left(b_R/b\right) = \frac{1}{\sqrt{\pi}\, u_m b} \qquad \text{(A-1)}$$

At any point in the pre-attachment region, once we have solved for b and u_m, we can obtain the value of b_R.

Application of equation (A-1) near the point of re-attachment, however, may be incorrect. This is because a Gaussian velocity profile was used, thus implying a non-zero velocity at the point or re-attachment which is in reality a stagnation point. This problem does not occur in the solution of the governing integral equations, since only the integrated value of mass, momentum and energy are important, and using the Gaussian profile is the best means of attaining these values for both sides of the dividing streamline. In addition, because of the small axial distances involved, the

application of the no-slip boundary condition as the jet impinges on the boundary is of no great consequence. However, when solving equation (19) for b_R at the point of re-attachment, because the distance between the jet axis and dividing streamline diverge in order to conserve mass as a portion of the fluid stagnates, a more relatistic profile must be used.

The stagnation condition can be satisfied by assuming a polynomial velocity profile of the following form:

$$u = a_0 + a_1 x_1 + a_2 x_1^2 + a_3 x_1^3 \quad , \quad 0 > x_1 > -b_R \qquad \text{(A-2)}$$

The constants can be determined from the following boundary conditions:

$$u(0) = u_m$$

$$\frac{du}{dx_1}(0) = 0$$

$$\frac{d^2u}{dx_1}(0) = 0 \qquad \text{(A-3)}$$

and

$$u(-b_R) = 0$$

The first three boundary conditions satisfy the Gaussian profile too. Substituting conditions (A-3) into (A-2), we obtain:

$$u = u_m \left[1 + (x_1/b_R)^3\right] \qquad \text{(A-4)}$$

Substituting equation (A-4) into equation (19), we have:

$$b_R = \frac{2}{3 u_m} \qquad \text{(A-5)}$$

Equation (A-5) represents the re-attaching condition. When the distance between the jet axis and the boundary along the x_1-axis is equal to this value, we can consider the jet to have re-attached (see Figure A-1).

Once the point of re-attachment is known, the re-attachment angle γ can be approximated by assuming the dividing streamline follows a straight line from the jet trajectory inflection, where the velocity is still Gaussian shaped, and the value of b_R is given by equation (A-1) to the point of re-attachment which is only slightly downstream.

Figure A-2 shows a comparison between experimental and theoretical trajectories and dividing streamlines at h=3 and 8.7. The experimental dividing streamline is represented by maximum RMS readings.

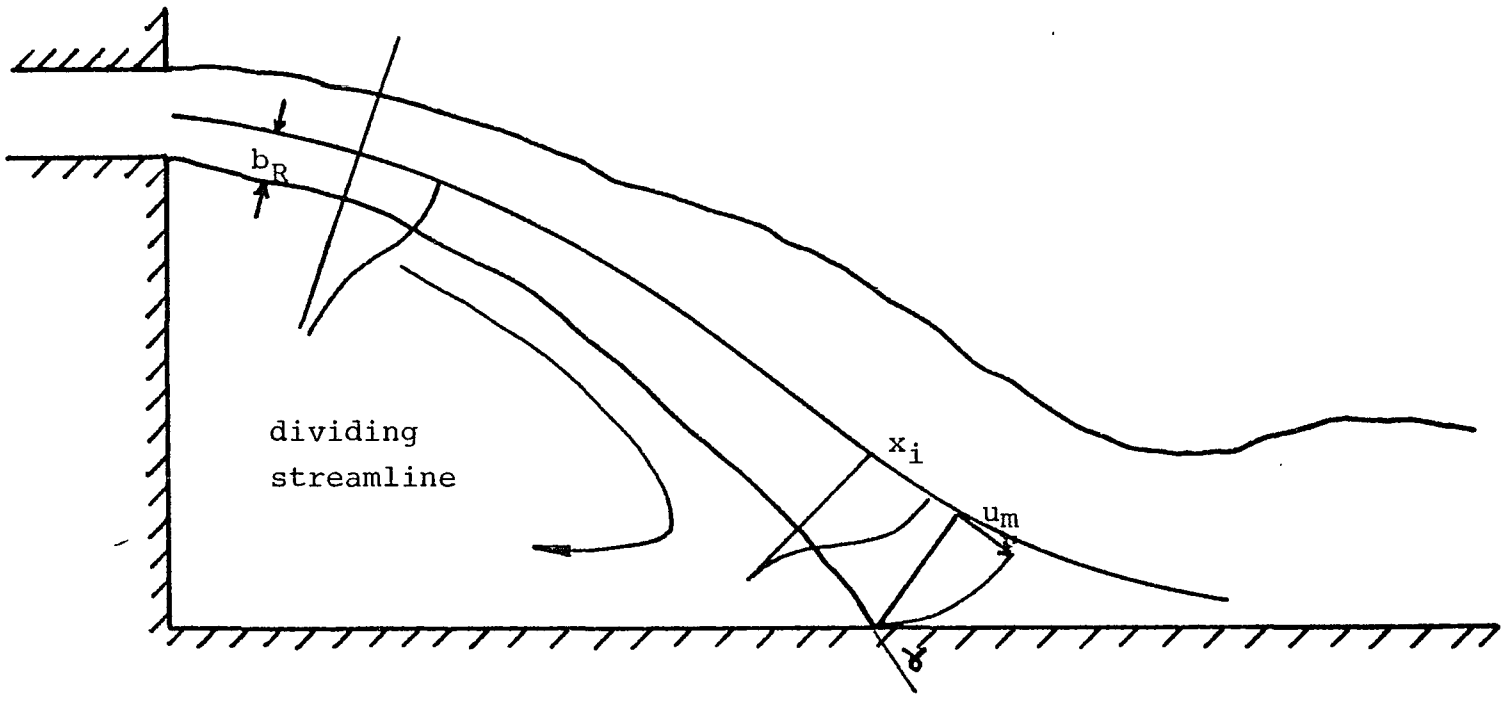

Figure A-1. Schematic of Jet Re-attachment

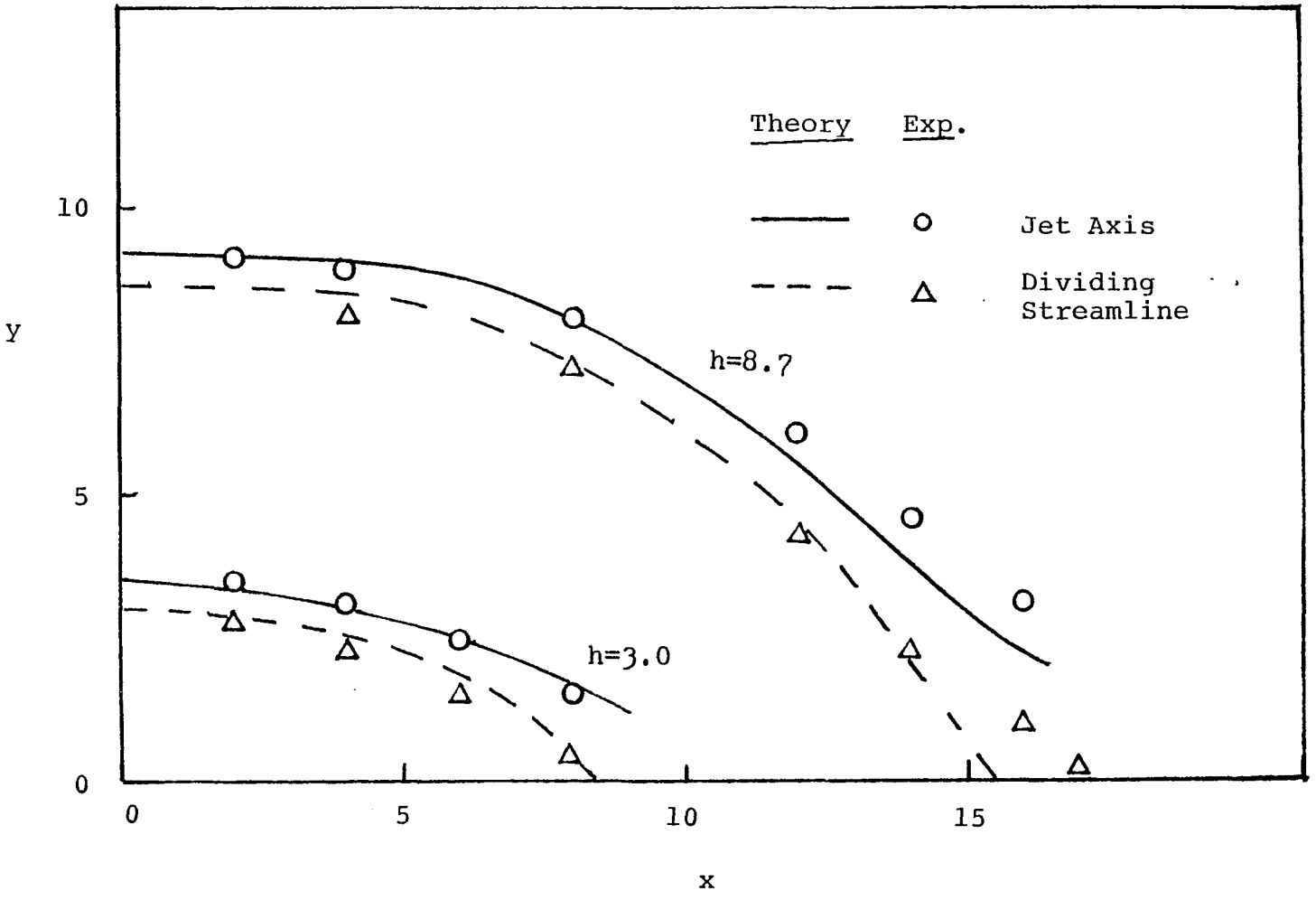

Figure A-2. Jet Trajectory and Dividing Streamline for an Offset Jet

Appendix B - BUOYANCY EFFECTS

Before attempting to solve a thermal discharge problem, it is necessary to determine whether or not buoyancy effects will be important. This is especially true for jet-boundary interaction, where buoyancy may significantly affect the jet trajectory. If buoyancy effects are important, the governing integral equations would have to be formulated accordingly.

Buoyancy effects are gauged by the densimetric Froude number, which is defined by:

$$Fr = \frac{u_o^*}{\sqrt{\frac{\rho_\infty - \rho_o}{\rho_\infty} g d}} \qquad \text{(B-1)}$$

If buoyancy does play an important role in two-dimensional jet-boundary interaction, one would expect experimental data to show significant variation as the Froude number is lowered.

However, due to the two-dimensional behavior of the jet, buoyancy effects are expected to be negligible. Previous experiments [56] on two-dimensional water jets discharged perpendicularly from the bottom of a moving water stream showed that the jet trajectory does not change appreciably with discharge temperature. This is due to the fact that in a two-dimensional jet, the cold ambient fluid cannot pass around the jet and exert a buoyant force on it.

The same is also true for a two-dimensional offset jet. For the jet-boundary interaction problem, as long as the fluid maintains its jet structure, buoyancy would not play a major role.

Surface pressure measurements at two different Froude numbers were compared to illustrate this point. Although the pressure values for the low Froude number are not very accurate, due to the extremely low velocities and pressures, they clearly show that the point of maximum pressure, which represents the re-attachment of the jet, is not affected by variations in the Froude number.

Once the jet re-attaches, it resembles a wall jet. For a wall jet, too, there was no perceptible variation in jet behavior over the range of Froude numbers used in our experiment. This is again due to the fact that cooler ambient air cannot get around the jet and lift it off the wall. Therefore, as long as the jet retains its momentum, it will have a tendency to hug the boundary. Smoke tracer tests failed to indicate any detachment of the jet from the wall for fairly low Froude numbers (Fr $\approx$ 10).

For extremely low Froude numbers, where the jet potential energy is the same order of magnitude as the kinetic energy, there is a likelihood of buoyancy induced jet instability causing a disintegration of the jet structure. This case was not considered.

It should be emphasized that for three-dimensional

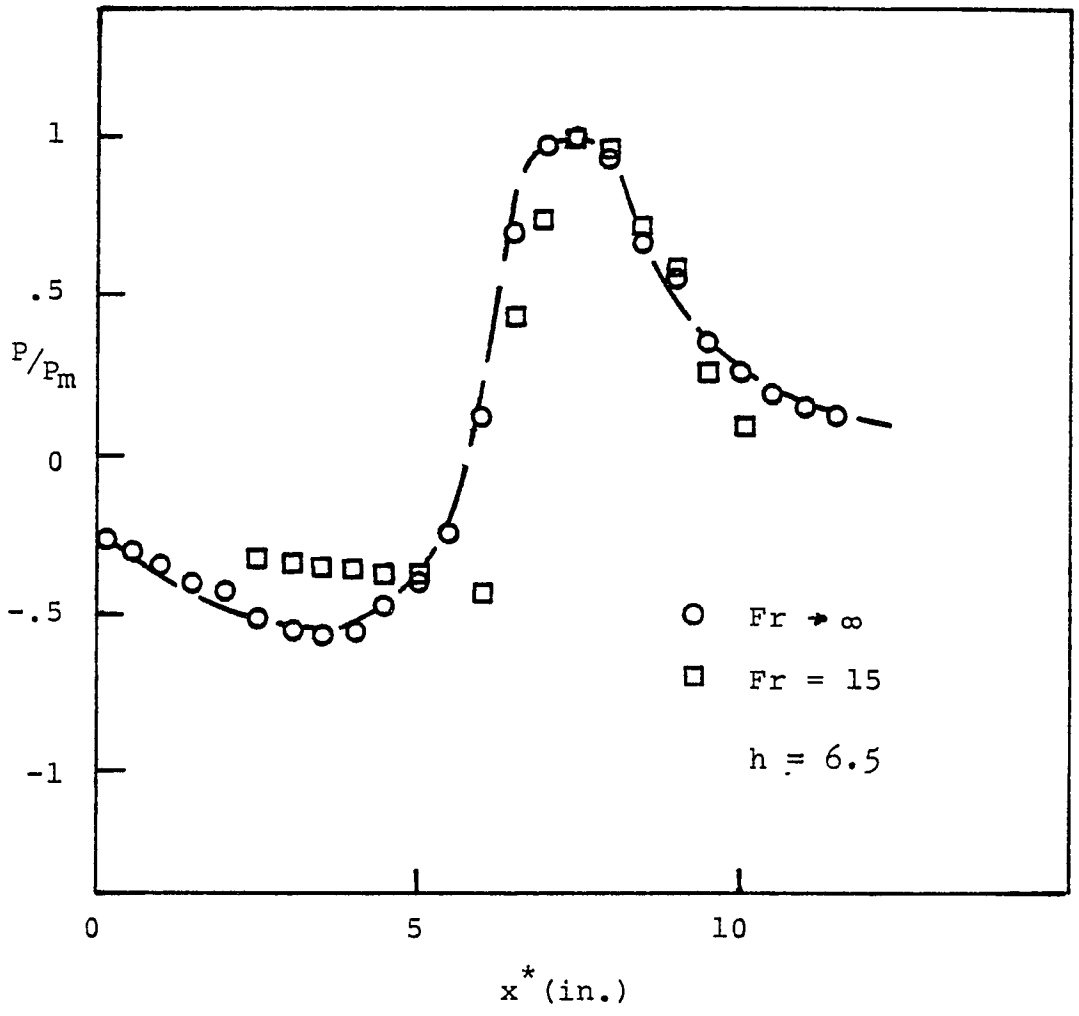

Figure B-1. Normalized Wall Pressure for a Two-Dimensional Heated Offset Jet

jet-boundary interaction, buoyancy will play a more prominent role. This is because the entire entrainment mechanism is different. There exists a possibility of entraining cooler ambient fluid between the jet and the boundary, which will give rise to a buoyancy force on the jet. This, in turn, may delay or entirely prevent attachment of the jet to the boundary.

APPENDIX C-CLOSURE ASSUMPTIONS

In applying the model for the solution of the velocity field in the pre-attachment region of a two-dimensional offset jet it became necessary to introduce an assumed trajectory profile to provide closure of the governing equations. Two momentum equations (53) and (56) are introduced as boundary conditions to help determine the shape of the jet trajectory.

The first of these boundary conditions is an horizontal momentum equation applied to a control volume surrounding the re-attachment point (see Figure 10). Local pressure variations on the control volume surface are neglected. This momentum relationship balances the momentum flowing downstream, following re-attachment, with the momentum returned into the re-circulation region. These momentums are evaluated by assuming that the momentum above and below the jet remain the same as the jet divides and flows along the wall. This momentum equation was taken from Bourque and Newman [16] and adjusted for our model so as to account for local variation of jet momentum in the pre-attachment region. In Bourque and Newman's model the jet momentum was assumed to be constant thereby simplifying this relationship and eliminating the need for any additional closure assumptions.

The second boundary condition is obtained by applying conservation of vertical momentum on a control volume covering the impingement region (see Figure 11). This boundary condition makes use of the wall pressure distribution in the impingement region.

Though the vertical momentum boundary condition is straightforward and requires only the specification of the wall pressure distribution in the impingement region, the horizontal momentum relation requires additional implicit assumptions regarding the pressure distribution near the point of re-attachment and the way the jet divides, which appear arbitrary and may be unrealistic. Equation (53) as written implies that the net pressure force on the control volume boundary is zero. This may be true since there is some symmetry in the pressure distribution around the re-attachment point, where the pressure is maximum. Figure 29 shows this to be true. However, the assumption that the jet divides in such a way so that the momentum of the intial reversed flow and the flow downstream of re-attachment are similar to the momentum above and below the dividing streamline is arbitrary and may be unrealistic for large pressure variations in the control volume.

In an effort to measure the effects of this assumption on our trajectory profile we will introduce a substitute horizontal momentum boundary condition. For the control volume shown in Figure C-1, neglecting frictional effects, conservation of horizontal momentum gives:

$$J_{w.j} - J_d = F_{r.w.} \qquad \text{(C-1)}$$

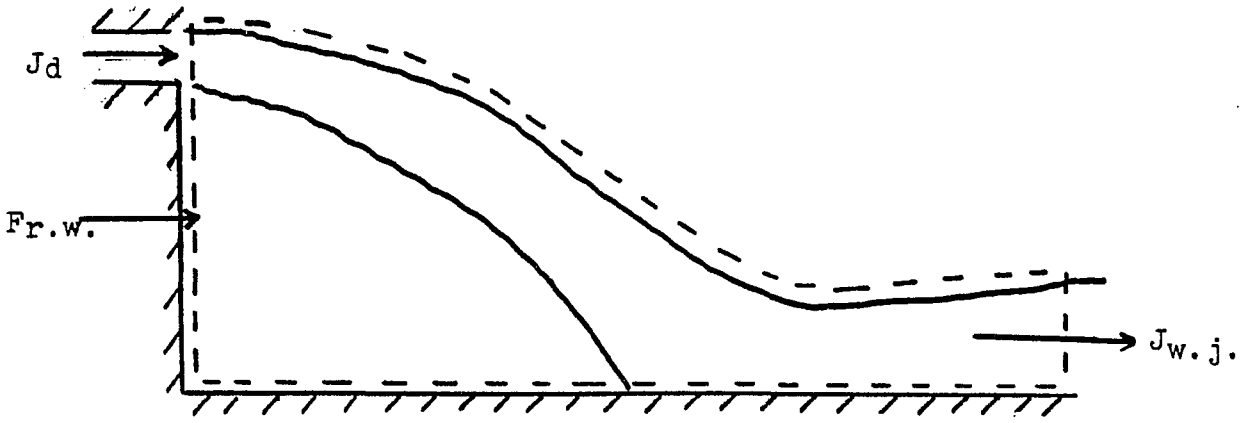

Figure C-1. Horizontal Momentum Condition

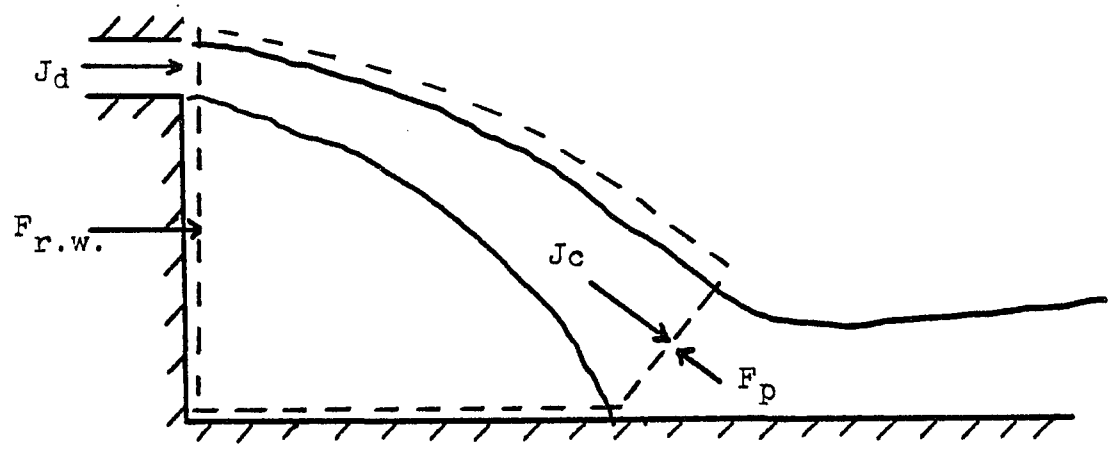

Figure C-2. Conservation of Horizontal Momentum for a Control Volume Covering the Pre-attachment Region.

where J_d is the momentum at the jet discharge and is equal to unity, $F_{r.w.}$ is the pressure force on the rearward facing step and $J_{w.j.}$ is the jet momentum at the end of the impingement region, where the pressure is at hydrostatic levels. This equation alone cannot be used as a boundary condition since $F_{r.w.}$ is unknown. We solve for $F_{r.w.}$ by applying conservation of horizontal momentum on the control volume shown in Figure C-2:

$$J_c \cos\phi - J_d = F_{r.w.} - F_p \cos\phi \qquad \text{(C-2)}$$

Equations (C-1) and (C-2) are used together as an implicit boundary condition in place of equation (54). Except that now the iterative procedure has to be extended to the impingement region. Unlike equation (54) these substitute equations can only be readily applied to the case of zero free stream.

Substitution of equations (C-1) and (C-2) into our numerical program for offset heights of h=3, 5.7 and 8.7 did not show any significant variation in results (see Table C-1). The solution of equations (C-1) and (C-2) for $P_{r.w.}$, the pressure on the rearward facing step, are compared with experimental data for h=5.7 in Figure C-3, where:

$$P_{r.w} = F_{r.w}/h \qquad \text{(C-3)}$$

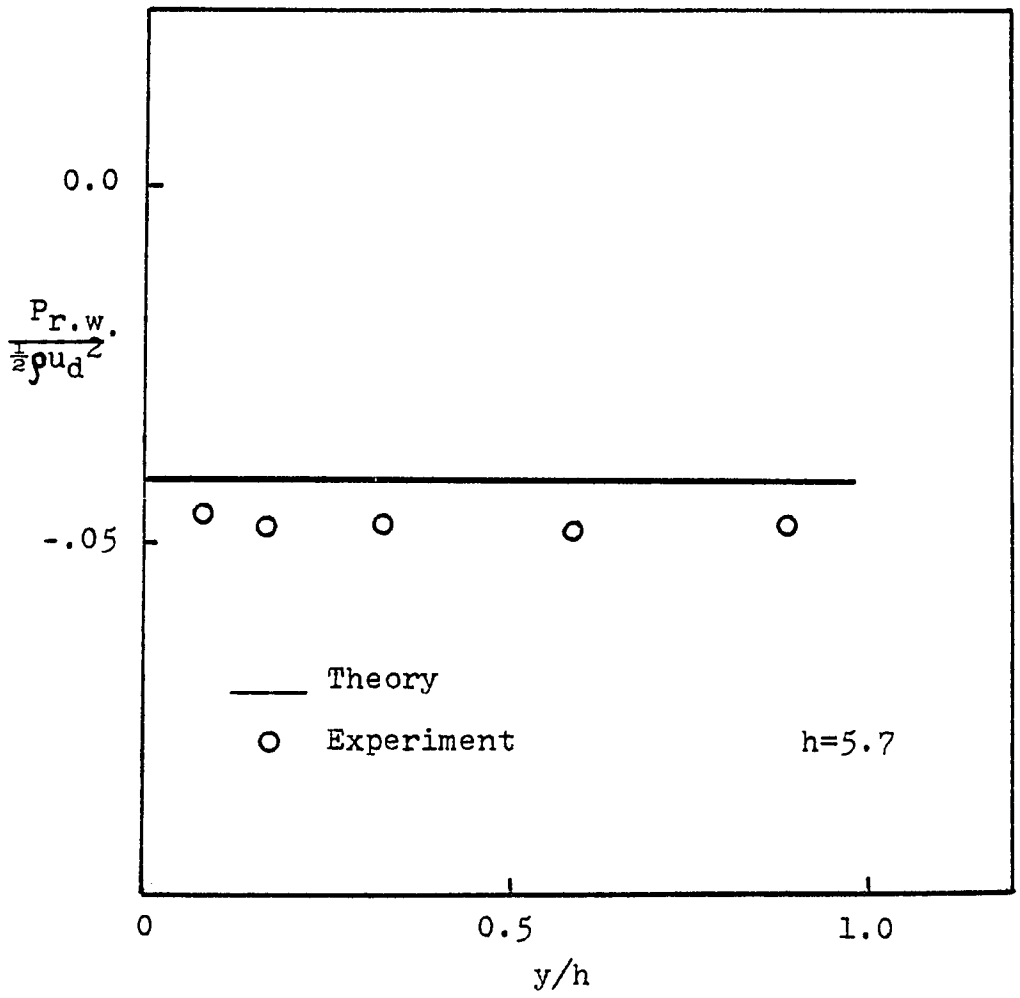

Figure C-3. Pressure disribution on the Rearward Facing Step

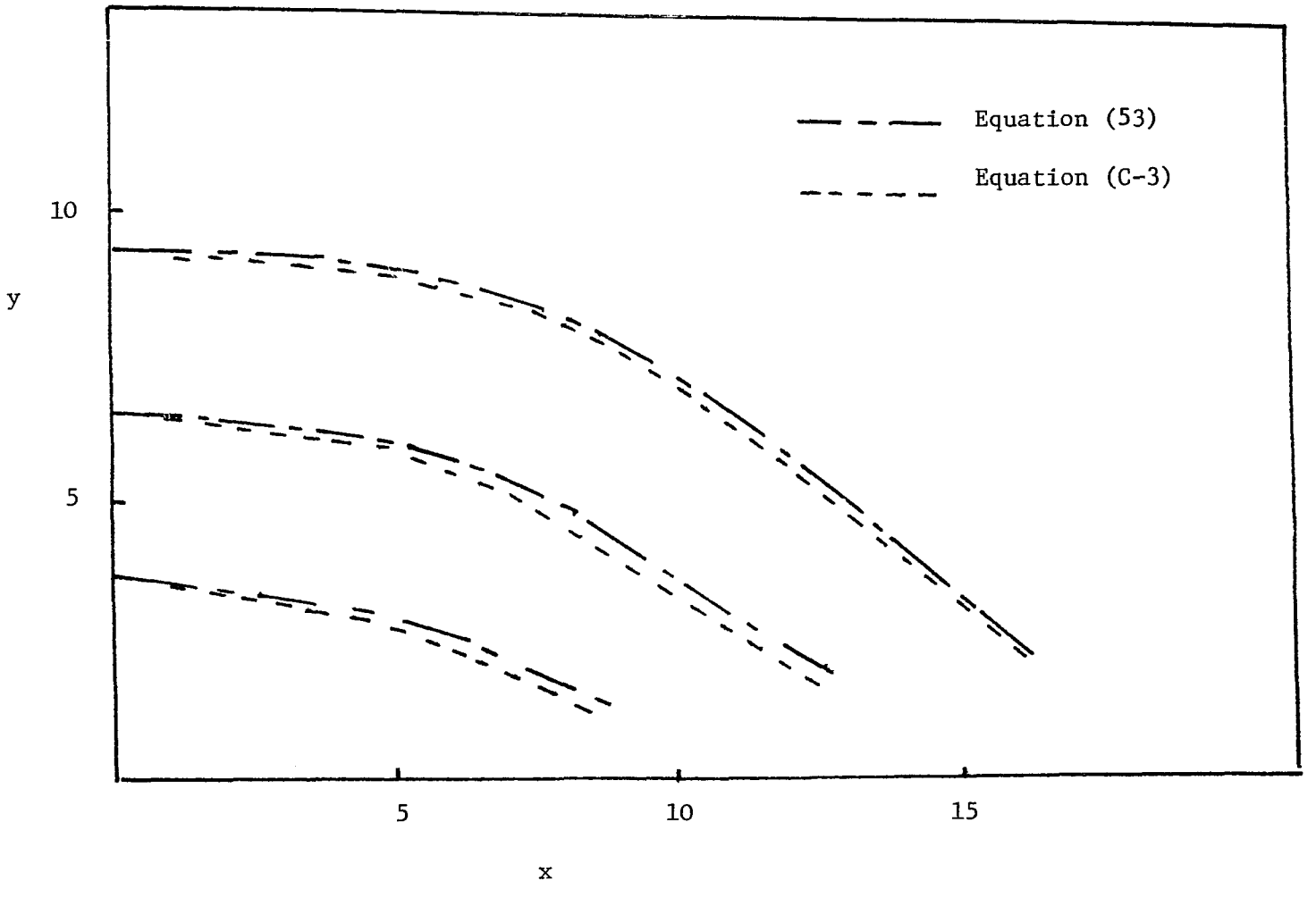

Figure C-4. Comparison of Jet Trajectories

Comparison with experimental data is very good.

By obtaining similar results with the substitute horizontal boundary condition we have demonstrated that application of equations (53) and (54), though approximate and to some extent arbitrary, still results in an accurate jet trajectory. This is probably true since any approximations in the boundary conditions will cause only a slight variation in the trajectory. This is usually the case with most integral method solutions.

References

1. Doddiah, D., M. L. Albertson and R. Thomas, "Scour from Jets," Proceedings, Minnesota International Hydraulics Convention, Minneapolis, Minnesota, September 1-4, (1953).

2. Policastro, A. J., "Thermal Discharges into Lakes and Cooling Ponds," Center for Environmental Studies, Argonne National Laboratory, (1973).

3. Tollmien, W. "Berechnung Turbulenter Ausbrertungsvorgänge," ZAMM 6, (1929).

4. Albertson, M. L., Y. B. Dai, R. A. Jensen, and H. Rouse, "Diffusion of Submerged Jets," ASCE Trans. 115, (1950)

5. Morton, B. R., G. I. Taylor, and J. S. Turner, "Turbulent Gravitational Convection from Maintained and Instantaneous Sources, " Proc. Roy. Soc. London, A234, (1956).

6. Jirka, G., and D. R. F. Harleman, "Heat Dissipation from Power Plants," M.I.T. Parsons Laboratory for Water Resources and Hydrodynamics, Technical Report No. 206, (1975).

7. Fan, L.-N., and N. H. Brooks, "Numerical Solutions of Turbulent Buoyant Jet Problems," W. M. Keck Laboratory for Hydraulics and Water Resources, California Institute of Technology, Pasadena, California, Report No. KH-R-18, (1969).

8. Anwar, H. O., "Behavior of Buoyant Jet in Calm Fluid," ASCE J. of Hydraulics Div., 91, HY 4, (1965).

9. Rouse, H., C. S. Yih, and H. W. Humphreys, "Gravitational Convection from a Boundary Source," Tellus, 4, (1952).

10. Priestley, C. H. B., and F. K. Ball, "Continuous Convection from an Isolated Source of Heat," Quar. J. Roy. Meteorol. Soc,. 81, (1956).

11. Fox, D. G., "Forced Plume in a Stratified Fluid," J. Geophys Res. 75(33), (1970).

12. Hirst, E. A., "Analysis of Round, Turbulent, Buoyant Jets Dishcarged to Flowing Stratified Ambients," Oak Ridge National Laboratory, ORNL-4685, (1971).

13. Jirka, G., and D. R. F. Harleman, "The Mechanics of Submerged Multiport Diffusers for Buoyant Discharges in Shallow Water," M.I.T. Parsons Laboratory for Water Resources and Hydrodynamics, Technical Report No. 169, (1973).

14. Jiji, L. M. and J. Hoch, "Submerged Thermal Discharges," Department of Mechanical Engineering, The City College of The City University of New York, Report No. 101 (1975).

15. Jiji, L. M. and J. Hoch, "Analysis of the Zone of Flow Establishment for Buoyant Turbulent Jets in Cross Flow," International Center for Heat and Mass Transfer, Dubrovnik, Yugoslavia, (September 1976).

16. Bourque, C. and B. G. Newman, "Reattachment of a Two-Dimensional Incompressible Jet to an Adjacent Flat Plate," Aeronautical Quarterly, 11, (1960).

17. Görtler, H., "Berechnung von Aufgaben der Freien Turbulenz auf Grund Eines Neuen Naherugsansatzes," Zertschrift fur angowandte Mathematik and Machanik, 22 (1942).

18. Bourque, C., "Reattachment of a Two-Dimensional Jet to an Adjacent Flat Plate," Advances in Fluidics, Fluidics Symposium, Chicago, (1967).

19. Sawyer, R. A., "The Flow Due to a Two-Dimensional Jet Issuing Parallel to a Flat Plate," J. of Fluid Mechanics, 9, (1963).

20. Prandtl, L., "Influence of Stabilizing Forces on Turbulence," Vortrage vas dem Gebeite der Aerodynamik und verwandte Gebiete, Aachen (1929).

21. Newman, B. G., "The Deflection of Plane Jets by Adjacent Boundaries Coanda Effect," Boundary Layer and Flow Control, p. 232. London, Pergamon Press (1961).

22. Sawyer, R. A., "Two-Dimensional Reattaching Jet Flows Including the Effect of Curvature on Entrainment," J. of Fluid Mechanics, 17, (1963).

23. Marsters, G. F., "Interaction of Two-Plane Parallel Jets", AIAA Journal, 15 (1977).

24. Bourque, C. and P. Rougier, "Annular Jet Reattachment," Transactions of the ASME, 2, (1973-4).

25. Rajaratnam, N. and K. Subramanya, "Plane Turbulent Reattached Wall Jets," ASCE J. of Hydraulics Div., 94, HY1, (1968).

26. Forthmann, E., "Turbulent Jet Expansion," N. A. C. A. TM-789, (1936).

27. Glauert, M. B., "The Wall Jet," J. of Fluid Mechanics, 1, (1956).

28. Sigalla, A., "Measurements of Skin Friction in a Plane Turbulent Wall Jet," J. Royal Aero., Soc., 62, (1958).

29. Myers, G. E. Schauer, J. J. and R. H. Eustis, "Plane Turbulent Wall Jet Flow Development and Friction Factor," Journal of Basic Engineering, Trans., ASME, 85, (1963).

30. Schwarz, W. H. and W. P. Cosart, "The Two-Dimensional Turbulent Wall Jet," J. of Fluid Mech., 10, (1961).

31. Kruka, V. and S. Eskinazi, "The Wall Jet in a Moving Stream," J. Fluid Mech., 20, (1964).

32. Spalding, E., "A Unified Theory of Friction, Heat Transfer, and Mass Transfer in the Turbulent Boundary Layer and Wall Jet," Aero, Res. Counc. Rep. No. 25,925, (1964).

33. Escudier, M. P. and W. B. Nicol, "The Entrainment Function in Turbulent Boundary Layer and Wall Jet Calculations," J. Fluid Mech., 25, (1966).

34. Rajaratnam, N., "Turbulent Jets," Elsevier Scien. Publishing, Canada (1976).

35. Townsend, A. A., "The Structure of Turbulent Shear Flow," Cambridge Univ. Press, England, 2nd Ed., (1976).

36. Seban, R. A. and L. H. Back, "Velocity and Temperature Profiles in a Wall Jet," Int. J. Heat and Mass Transfer, 3, (1961).

37. Sacks, S., J. E. A. John, and C. H. Marks, "Interaction of a Three-Dimensional Fluid Jet with a Nearby Wall Boundary," Proc. of Thermal Pollution Analysis Conf., Virginia Polytechnic Inst. and State University, (1974).

38. Sforza, P. M. and G. Herbst, "A Study of Three-Dimensional; Incompressible, Turbulent Wall Jets," AIAA J., 8, (1970).

39. Trentacoste, N., and P. Sforza, "Further Experimental Results for Three-Dimensional Free Jets," AIAA Journal 5, (1967).

40. Sforza, P. M. and W. Stasi, "Heated Three-Dimensional Turbulent Jets," ASME Paper No. 77-WA/HT-27, Presented at the Winter Annual Meeting, Atlanta, Georgia, November 27-December 2, 1977.

41. Yevidjevich, V. M., "Diffusion of Slot Jets with Finite Orifice Length-Width Ratios," Hydraul. Pap., 2, Colorado State University, Fort Collins, (1966).

42. Sfier, A. A., "The Velocity and Temperature Fields of Rectangular Jets," Int. J. Heat Mass Transfer, 19, (1976).

43. Narian, J. P., "Momentum Flux Development from Three-Dimensional Free Jets," J. of Fluids Engineering, Trans. ASME, 98, (1976).

44. Abraham, G., "Jet Diffusion in a Stagnant Ambient Fluid," Delft Hydraulics Laboratory, Publ. No. 29 (1963).

45. Davies, E., Keffer, J. F. and W. D. Baines, "Spread of a Heated Plane Turbulent Jet," Physics of Fluids, 18, (1975).

46. Schichting, H., "Boundary Layer Theory," 6th Edition, McGraw-Hill Publishing Co., New York, (1968).

47. Kreyszig, E., "Advanced Engineering Mathematics," 3rd Edition, John Wiley and Sons, Inc., New York (1972).

48. Beltaos, S. and N. Rajaratnam, "Plane Turbulent Impinging Jets," J. of Hydraulic Research, 11, (1973).

49. Wolfshtein, M., "Some Solutions of the Plane Turbulent Impinging Jets," J. of Basic Engineering, Trans. ASME, 92, (1970).

50. Beltaos, S. "Oblique Impingement of Plane Turbulent Jets," ASCE J. of the Hydraulics Division, 102, HY9(1976).

51. Sexton, D. E., "A Simple Wind Tunnel for Studying Air-Flow Around Buildings," Architect and Building News, (1968).

52. Tandowski, B., "Near Field Pollution Due to Emissions from Short Stacks on Buildings," Ph.D. Dissertation, Mechanical Engineering Department, The City University of New York, (1977).

53. Holman, J. P., "Experimental Methods for Engineers," McGraw-Hill Book Co., New York, (1971).

54. Parkhurst, R. C. and D. W. Holder, "Wind Tunnel Technique," Sir Isaac Pitman and Sons, London, (1952).

55. Schwind, R. G., "The Three-Dimensional Boundary Layer Near a Strut," Gas Turbulence Laboratory Report No. 67, M.I.T., Cambridge, Mass., (1962).

56. Patton, A. J., F. L. Test, and W. M. Hagist, "An Experimental Investigation of a Heated Two-Dimensional Water Jet Discharged Into A Moving Stream," ASME Journal of Heat Transfer, Vol. 96, (1974).

NOMENCLATURE

a_0, a_1, a_2 a_3, a_4, a_5	jet trajectory profile constants
b	dimensionless measure of jet spread
$b_{pl/2}$	pressure profile half-width, see Figure 13
b_T	dimensionless measure of thermal jet spread
b_R	dimensionless distance from the dividing streamline to jet axis
c	specific heat
c_f	skin friction coefficient,
c_p	pressure coefficient , $\frac{P_o^* - p^*}{\frac{1}{2}\rho u_d^{*2}}$
d	discharge width
F_p	pressure force on control volume shown in Figure 11
F_w	pressure force on wall in Impingement Region
$F_{r.w.}$	pressure force on the rearward facing step, see Figure C-1
Fr	Densimetric Froude Number, defined in Equation (B-1)
g	gravitational force
h	dimensionless offset height
H	distance from the jet to boundary in an impinging jet, see Figure 13
J	jet momentum at re-attachment
J_a	downstream jet momentum at re-attachment
J_b	reversed jet momentum at re-attachment
J_c	jet momentum above dividing streamline
$J_{w.j.}$	wall jet momentum, see Figure C-1
P	dimensionless pressure
P_b	dimensionless base pressure
P_m	dimensionless maximum wall pressure

Q_e	dimensionless volumetric mass entrained
r	dimensionless radius of curvature
Re_d	Reynolds number,
T	temperature
T_R^*	dimensional recirculation temperature
T_∞^*	dimensional ambient temperature
u	dimensionless axial velocity
u_c	centerline velocity of a free jet
u_m	dimensionless maximum axial velocity
u_∞	dimensionless free stream velocity
V_∞	free stream velocity in boundary layer flow
w	dimensionless jet width
X	horizontal coordinate of an impinging jet shown in Figure 13
x	dimensionless horizontal cartesian coordinate, see Figures 7 and 8
x_A	reattachment point, see Figure 8
x_1, x_2, x_3	dimensionless jet coordinates in pre-attachment region, see Figure 8
y	dimensionless vertical cartesian coordinate, see Figures 7 and 8
$y_{1/2}$	jet half-width, value of y at which $\frac{u-u_\infty}{u_m-u_\infty} = \frac{1}{2}$
α	entrainment coefficient
β	pressure spread parameter
γ	angle at which the dividing streamline intersects the solid boundary
δ	dimensionless thickness of inner layer for a wall jet
θ	dimensionless temperature

θ_m	dimensionless maximum temperature
θ_R	dimensionless temperature in the recirculation region
λ	turbulent Schmidt number
Λ	quantity defined in equation (71)
ν	kinematic viscosity
ϕ	jet inclination angle in the pre-attachment region, defined in Figure 8
τ_o	wall shearing stress

Superscripts

*	dimensional quantity

Subscripts

1/2	lccation where velocity or temperature is one-half the maximum value
d	discharge
m	maximum
o	quantity evaluated at end of zfe
R	recirculation
T	thermal
∞	ambient quantity